3D TORO-POLOIDAL IMPLANTABLE DEVICE FOR THE CONTROLLED DELIVERY OF RIVAROXABAN

SIMPHIWE VALENTIA MAVUSO

A thesis submitted to the Faculty of Health Sciences, University of the Witwatersrand, in fulfilment of the requirements for the degree of
Doctor of Philosophy

Supervisors:

Professor Yahya Essop Choonara

Professor Pradeep Kumar

Associate Professor Thashree Marimuthu

University of the Witwatersrand, Department of Pharmacy and Pharmacology, Johannesburg, South Africa

2023

DECLARATION

I**,** Simphiwe Valentia Mavuso, declare that this thesis is my own work except where specifically indicated in the text for outsource analysis. It has been submitted for the degree of Doctor of Philosophy in the Faculty of Health Sciences at the University of the Witwatersrand, Johannesburg, South Africa. It has not been submitted before for any degree or examination at this or any other University.

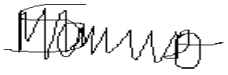

Signature

Signed this 17th day of January 2023

ANIMAL ETHICS DECLARATION

I, Simphiwe Valentia Mavuso, hereby confirm the study entitled "*In-vivo* study of a 3D toropoloidal, implantable device for the controlled delivery of rivaroxaban in New Zealand White Albino rabbits" was approved by the animal Ethics Screening Committee (AESC) of the University of the Witwatersrand with Ethics Clearance Number 2021/08/08C (Certificate in Appendix A and AESC M&Es in **Appendix B, C** and **D**).

RESEARCH OUTPUTS

Publication drafts emanating from PhD research

1. Simphiwe Mavuso, Thashree Marimuthu, Pradeep Kumar, Viness Pillay, Yahya E. Choonara*. A Review on 3D Printed microstructures, their geometry and biological performance in drug delivery (To be submitted to Drug Delivery and Translational Research) (**Appendix E**).

2. Simphiwe Mavuso, Thashree Marimuthu, Pradeep Kumar, Viness Pillay, Yahya E. Choonara*. 3D Toro-Poloidal Implantable Device for Controlled Delivery of Rivaroxaban (To be submitted to the International Journal of Pharmaceutics) (**Appendix F**).

3. Simphiwe Mavuso, Thashree Marimuthu, Pradeep Kumar, Viness Pillay, Yahya E. Choonara*. *In-vivo* study of a 3D toro-poloidal implantable device for the controlled delivery of rivaroxaban on New Zealand White Albino rabbits (To be submitted to the Journal of Pharmaceutical Sciences) (**Appendix G**).

ABSTRACT

Implantable drug delivery devices offer many benefits over other routes of drug delivery. Most significantly, the potential of reducing systematic side-effects and improving patient compliance as drugs are delivered in lesser doses over an extended period. The present work was focused on designing a novel polymeric blend through a judicious combination of polymers. Polymeric material was used for the fabrication of implantable drug delivery devices (IDDDs) with varying geometrical considerations viz. torus and cylinder for the controlled delivery of a model antithrombotic agent, rivaroxaban (RXB). RXB is an antithrombotic drug used primarily for the prevention of stroke and systemic embolism in the general population of patients with thromboembolic disorders. Even though RXB is often a preferred anti-thrombotic it is associated with some degree of gastrointestinal (GI) bleeding, which is the most common extracranial haemorrhagic complication in patients on oral RXB. This 3D implant formulated is expected to offer an alternative route bypassing the gut, more convenient and safer for RXB delivery especially during long-term use, this device may be widely applied over a range of diseases requiring long-term use of a specific drug. A polyurethane (PU), polyethylene glycol (PEG) and Poly (lactic-co-glycolic acid) (PLGA) blend was used to load the RXB, while hydroxypropyl methylcellulose (HPMC) was used as a supporting material due to its gelation properties. Extrusion and compression-based methods were both utilised for the formulation of the 3D toro-poloidal (RXB loaded PU-PEG-PLGA/HPMC) implantable devices. The RXB loaded PU-PEG-PLGA/HPMC was then characterised using different physicochemical methods such as Fourier-Transform infrared (FTIR) spectroscopy, powder X-ray diffraction (PXRD) and differential scanning calorimetry (DSC), Thermogravimetric analysis (TGA) studies, all revealing the chemical and compatibility of the formulated components. For comparison 3D porous and non-porous donut shaped implants were also fabricated using compression method. Lastly *in-vitro* Factor Xa (FXa) assay*, in-vitro* release profiles, cytotoxicity, and *in-vivo* drug release studies using New Zealand White Albino rabbits were carried out. The 3D toro-poloidal implantable devices were successfully formulated and characterised using FTIR, PXRD, DSC and TGA, where analysis confirmed the formation of the RXB loaded and HPMC/PU-PEG-PLGA blends, also evident is that the individual structures of the innate polymers were only blended and not altered. Cytotoxicity studies using MTT assay showed no toxicity signs and the FXa activity increased with the increase in RXB concentration. The porous RXB showed much more drug released compared to the non-porous, while both geometries showed controlled sustainable drug release profiles suitable for delivery of potent drugs applied in small doses such as the RXB. The cylinder released the RXB at a constant rate while the donut released the RXB at a consistently increasing rate, both within the therapeutic range. The devices were observed to be having a biphasic release pattern, where an initial burst release was followed by a controlled extended drug release, with an initial burst release and a sustained release from 72 h to day 49. Approximately 97% and 89 % RXB was released on day 49 for donut implants, while only 61.3 % and 66.1 % of the RXB was released from the cylinder, the release was from compressed and extruded 3D implants, respectively. In both the *in-vivo* and in-vitro RXB release profiles the conventional oral RXB had a bioavailability lower by ±40% and ±32% for *in-vitro* and *in-vivo,* respectively, compared to the toro-poloidal 3D implant devices. Correlation of the cytotoxicity and RXB release studies was seen with the *in-vitro* relative to the *in-vivo* studies. In conclusion, the 3D toro-poloidal, 3D RXB loaded PU-PEG-PLGA/HPMC implant, has a great potential for personalised medicine, as these devices can be modified into different geometries with different release properties, suitable for both systematic and local drug delivery while avoiding the gut system.

ACKNOWLEDGEMENTS

Foremost I would like to thank the almighty God with whom all was possible, His guidance, sustenance and unconditional love made me come to this far.

Then I would like to thank my family, my mother Busisiwe Gladys Mamba deserves a special mention, for her everlasting care, prayers, encouragement, support, and gentle love, even words fail to express my indebtedness to her. Thank you for supporting every decision I have made, your confidence and fighting spirit has shaped and pushed me beyond limits. To my late grandmother, the angels couldn't wait to have you back, but this is also for you with all the inseparable support and prayers. To my other grandmother, aunts, uncles, siblings and cousins thank you for being supportive and believing in me pushed me beyond limits. To my son Kgosietsile Nkhabelane thank you for being the sweetest angel one could ever ask for, from the moment you were conceived to the time you were born, you were such an understating baby, I love you beyond measures, Mkhabel'omkhulu. To my life partner and Nkhabelane family, thank you for your support, understanding, praying with and for me, loving and caring for me, I thank God that you came into my life.

I want to express my heartfelt gratitude to the late Prof Viness Pillay for granting me the opportunity to be part of Wits Advanced Drug Delivery Platform (WADDP), I have had extraordinary experiences throughout this work. To Prof. Yahya E. Choonara thank you for all the advice, your critique and views on my research, working with you has been such a great honour. To Prof. Thashree Marimuthu and Prof. Pradeep Kumar, thank you for your selfless, unwavering assistance, mentoring and supervision from the beginning to the completion of this program.

To the head of department Prof. Choonara and the rest of the pharmacy and pharmacology department staff, thank you making my stay in the department worth a while. To the technical stuff Mr Sello Ramarumo, Bafana, Kleinbooi and Tshidi, thank you for all the support. To the post-doctorates thank you for your contribution into my project, special thanks to Dr Philemon who assisted me with my *in-vitro* cytotoxicity studies. To the Wits Research Animal Facility (WRAF), with special thanks to Dr Kim, Amelia, Mduduzi and Mashudu thank you for the support, advice, and assistance throughout my *in-vivo* studies.

I would also like to thank all my friends who have been my extended family for the past few years thank you for being with me throughout the bad and good moments in my life, especially for pulling up with all my different personalities, I love you all.

To National Research Foundation and the University of the Witwatersrand thank you for the financial assistant.

Lastly, I would like to express my apology that I could not mention everyone personally, thank you to everyone who had an input to the successful realization of this thesis, I appreciate and love you all.

God was, is and will forever be in complete control

DEDICATION

This thesis is dedicated to my superhero my mother, Busisiwe Gladys Mamba.
Thank you for your endearing love and support.

TABLE OF CONTENTS

LIST OF ABBREVIATIONS

3D	Three Dimensional
3T3	Embryo Fibroblasts
APAs	Anticoagulants or antiplatelet agents
CAD	Computer aided design
CV	Cell viability
DDS	Drug delivery systems
DCM	Dichloromethane
DMSO	Dimethyl sulfoxide
DSC	Differential Scanning Calorimeter
EXT	Extrusion
FDA	Food and Drug Administration
FDM	Fused Deposition Modelling
FOBT	Faecal Occult Blood Test
FTIR	Fourier-transform infrared spectroscopy
FXa	Factor X activated
GIT	Gastrointestinal tract
H	Hour (s)
H&E	Hematoxylin and eosin
HPMC	Hydroxypropyl methylcellulose
LGIC	Ligand-gated ion channel
Min	Minute (s)
MB	Methylene blue
NaCl	Sodium Chloride
PBS	Phosphate-buffered saline
PC	Polycarbonate
PCL	Polycaprolactam
PEG	Polyethylene glycol
PEI	Polyetherimide
PLA	Polylactic acid
PCL	Polycaprolactone
PVA	Polyvinyl alcohol
PLA	Poly-(lactic acid)
PLGA	Poly (D,L-lactide-co-glycolide)

PLLA	Poly-L-lactic acid
PSU	Polysulfone
PU	Polyurethane
R^2	Correlation coefficient
RXB	Rivaroxaban
SA/V	Surface area/volume
SEM	Scanning electron microscopy
SLA	Stereolithography
SLS	Selective Laser Sintering
STL	StereoLithography
TA	Texture Analyser
THF	Tetrahydrofuran
TGA	Thermogravimetric analysis
UV-Vis	Ultraviolet–visible
WRAF	Wits Research Animal Facility
XRD	X-ray diffraction

LIST OF EQUATIONS

LIST OF FIGURES

LIST OF TABLES

CHAPTER ONE
INTRODUCTION AND BACKGROUND

1.1 BACKGROUND OF STUDY

Thromboembolic disorders are regarded as potential life-threatening diseases that can result in severe cardiovascular complications (Abouhussein et al., 2019; Lancet, 2015). Three common clinical indications of thromboembolic disorders are a past or recent history of venous thrombo-embolism (including Deep Venous Thrombosis (DVT) and pulmonary embolism), current Atrial Fibrillation (AF), arterial thromboembolism, and the presence of a mechanical heart valve which carries the risk of arterial thromboembolism (Duggan, Scott and Plosker, 2009; Mueck et al., 2011). All of these clinical indications can manifest into high death rates if left untreated (Schafer et al., 2003), and they require chronic antithrombotic therapy which calls for consistent and daily drug administration.

First line therapy for these disorders usually involves administration of anticoagulants as a treatment plan and prophylaxis for the prevention of thromboembolism in patients that fall into medium or high-risk categories. Most patients are managed through the administration of oral warfarin or an antiplatelet drug, or a newer anticoagulant agent such as oral rivaroxaban (RXB). Despite the prevalent use of antithrombotic drugs, there are still challenges in the management of medication in patients requiring antithrombotic therapy, resulting in poor patient compliance (Abdou et al., 2016). Some of these challenges are linked to patient motivation and related to concerns over the side-effects of these drugs, or patient capability e.g., stroke patients who may have cognitive and physical impairments. Nevertheless, the oral route of administration of antithrombotic drugs such as RXB is widely used in many patients (Ageno et al., 2016; Chan et al 2015), despite its high reliance on patient compliance.

Vitamin K antagonists have been the predominant anticoagulants for clinical use for decades, with demonstrated proficiency compared to other formulations (Cloney et al., 2018). However, with a number of limitations such as drug-drug interactions, unpredictable pharmacodynamic responses (Krothapalli and Bhave, 2014; Lewalter et al., 2014) routine monitoring of coagulation and the necessity for monitored dose adjustment (Lewalter et al., 2014; Mueck et al., 2014). These oral anticoagulants instigated an on-going search for more efficacious and safer anticoagulants,

resulting in the development of direct oral anticoagulants that specifically target a single coagulation factor such as Factor Xa or thrombin (Mueck et al., 2014). According to Paikin and co-workers (2012) oral rivaroxaban (RXB) became an attractive alternative compared to other investigated antithrombotic agents, as several studies proved that oral RXB to be more efficacious (Krothapalli and Bhave, 2014; Lewalter et al., 2014). RXB directly inhibits both free and clot-bound Factor Xa and prevents the formation of new clots and the extension of existing clots (Turpie, 2014; Curto, 2017; Antoniou and Amara, 2018). It has been broadly used for the primary prevention of stroke and systemic embolism in the general population of patients with thromboembolic disorders (Laube et al., 2012). Even though RXB is preferred over other anticoagulants it is associated with some degree of gastrointestinal (GI) bleeding, which is the most common extracranial haemorrhagic complication in patients on oral RXB (Ammar et al., 2006; Lewalter et al., 2014). In South Africa, pharmacological prophylactic anticoagulation is often under-prescribed, which has led to increased and unacceptable rates of morbidity and mortality (Jacobson et al., 2013). Additionally, due to cost next generative antithrombotic like RXB is not freely accessible.

To overcome the adverse effect associated with RXB use, the use of a drug eluting implant is alternative drug delivery approach. Furthermore, it has been shown that the shape of the implant can be tailored to give predictable and controlled release. In a local context this implant will furthermore benefit patients who need more efficacious RXB treatments. Hence in this study, a 3D toro-poloidal implantable device was formulated, offering an alternative route (bypassing the gut), a more convenient, accessible, safer and cost-efficient alternative for RXB delivery especially during long-term usage.

This project encompasses the application of a novel polymeric blend for the fabrication of 3D toro-poloidal implantable devices using different 3-Dimensional (3D) techniques for the development of a controlled delivery system. The 3D toro-poloidal implantable devices were loaded with RXB which served as a model antithrombotic drug, where the applicability of different geometries (cylindrical and donut shapes), different fabrication method viz. direct compression and extrusion methods as well as different formulation types such as porous and non-porous tablet devices were evaluated.

1.2 RATIONALE AND MOTIVATION

The 3D toro-poloidal implantable devices, herein refers to the design of implants with complex geometries. In geometrical terms, a torus that is described in this study is a circular and revolving surface that fills a 3D space (**Figure 1.1**.). Toroidal referring to the direction of fill which is co-planar to the circle and poloidal refers to the direction of the fill that is perpendicular to the circle. The poloidal direction follows a small circular ring around the surface, while the toroidal direction follows a large circular ring around the torus, encircling the central void. Therefore, it has been hyphenated as these are two separate direction vectors.

In this project two specific 3D architectures were formulated (cylindrical and donut) (**Figure 1.1.)**. The 3D toro-poloidal structured devices were achieved by means of a compression or an extrusion method, which were very cost efficient, faster, less material wastage compared to using the actual 3D technique (Alhnan et al., 2016; Amighi, 2016). These 3D devices are expected to overcome limitations such as batch-to-batch variability of drug-excipient blend during implant manufacture and inconsistent architecture of geometrically specific devices (Li et al., 2017). Meanwhile, the 3D device ensures feasibility of comprehending rapid, sustained, controlled and multiple drug delivery systems. The 3D approach tremendously surpasses in the area of personalized medicines, where by tailoring the geometry of the implant results in different release profiles. 3D devices offer a high productivity rate due to their fast-operating systems, and the ability to achieve higher drug-loading with precision especially for potent drugs applied in small doses such as RXB (Tagami et al., 2017). Therefore, 3D toro-poloidal, implants, have a great potential in controlling the delivery of encapsulated drug for personalized medicine purposes in drug delivery.

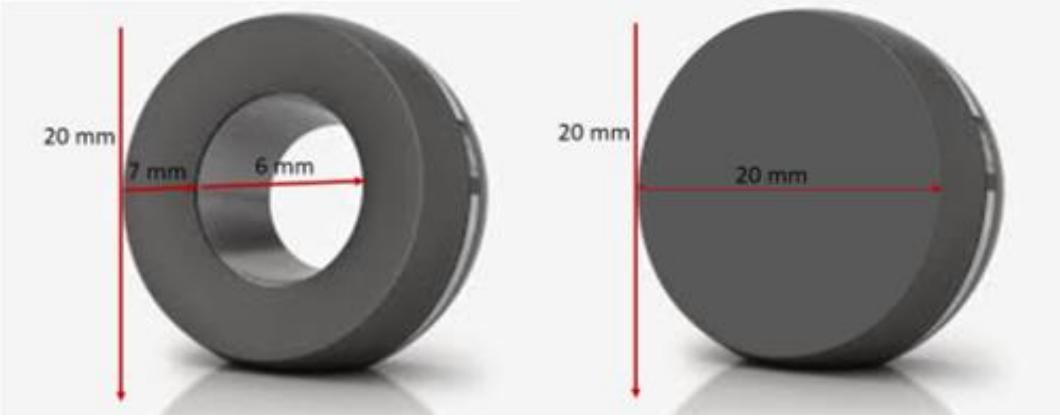

Figure.1.1. An outline of 3D toro-poloidal, implantable devices.

The device was formulated using biocompatible polymers, allowing for subcutaneous implantation on the buttocks, abdomen or upper arm under local anaesthetic, depending on the reason for implant it can also be used during surgery and inserted into the site to prevent thrombosis (i.e. hip replacement surgery*).* Controlled drug delivery can be realized through the shape of the 3D implantable device (Konta et al., 2017) and it has been previously demonstrated within the Wits Advanced Drug Delivery Platform (WADDP) research unit that a toro-poloidal or "donut" shaped type of an implant enables controlled drug delivery in the eye as opposed to conventional implants (Choonara et al., 2006). The toro-poloidal shape, illustrated in **Figure 1.1**, increases the surface area of the IDDD, resulting in controlled degradation and sustained drug release, which is ideal for chronic therapy, hence a 3D toro-poloidal shaped IDDD was investigated in this work. The donut 3D toro-poloidal, implant established controlled degradation (due to the different edges offered by the shape) resulting to sustained drug release ideal for conditions requiring chronic suppressive maintenance therapy. The overall dimensions of the device being approximately 20 mm x 20 mm x 7 mm as adapted from Fitzpatrick (2015) where an implant was designed for subcutaneous implantation into the buttocks, abdomen, or upper arm under local anaesthetic.

Implantable drug delivery systems have a number of advantages compared to oral drug delivery systems; advantages of implantable drug delivery systems are as follows:

(i) Localized drug delivery: Drug(s) are released in immediate vicinity of implant. Action may be diffusion, limited to the specific location of implantation.

(ii) Improved patient Compliance: Patient does not need to comply with repeated and timely intake of medication throughout the implantation period. Compliance is limited to one-time implantation (and potential removal in the case of non-biodegradable implants).

(iii) Minimized systemic side effects: Controlled release for extended periods of time and localized dosing possible at site of action; adverse effects away from site of action are minimized; peaks and valleys in plasma drug concentration from repeated intermediate release dosing are avoided.

(iv) Lower dose: Localized implantation of site-specific drugs can avoid first pass hepatic effects, thereby reducing dose required to ensure systemic bioavailability.

(v) Improved drug stability: Protection of drug undergoing rapid degradation in the gastrointestinal and hepatobiliary system.

(vi) Suitability over direct administration: Hospital stay or continuous monitoring by healthcare staff may not be required for chronic illnesses.

(vii) Facile termination of drug delivery: If allergic or other adverse reaction to drug is experienced, discontinuation of therapy by implant removal is possible.

1.3 AIM AND OBJECTIVES

This study aimed at designing a novel polymer blend through a judicious combination of controlled release and hydrophilic polymers for the fabrication of implantable drug delivery devices (IDDDs) with varying geometrical considerations viz. torus and cylinder for the controlled delivery of a model antithrombotic agent, RXB. The following objectives were considered:

1. Designing a novel polymeric blend for fabrication of 3D implantable drug delivery devices with geometrical varying drug release profiles and mechanisms.
2. Characterisation of key physicochemical and physicomechanical properties of the 3D implantable drug delivery device for controlled release kinetics.
3. Optimisation of the novel polymeric blend formulation for the precise preparation of two geometrical toro-poloidal 3D implantable drug delivery device using direct compression and extrusion methods.
4. Evaluation of the comparative degradation, porosity, and drug release, of the 3D implantable device in terms of geometrical properties.
5. Evaluation of the *in-vitro* cytotoxicity of the toro-poloidal 3D implantable device for preliminary establishment of biocompatibility.
6. Evaluation of the in-vitro Factor Xa (FXa*) assay* of the toro-poloidal 3D implantable device to verify the presence of the Factor Xa (FXa*)* inhibition effect of the RXB on the device*.*
7. Evaluation of the *in-vivo* drug release and biological performance of the toro-poloidal 3D implantable device in a New Zealand White Albino rabbit model.

1.4 NOVELTY OF THE STUDY

This research will make substantial contribution in the pharmaceutical society as it is the first report towards a more profound understanding on how 3D implants behave in the pre-clinical level. Below are the significant novelty points:

1. The novelty of the polymer combination, where the formulation was formulated using different polymers with distinctive properties and their characterization. The application of the novel blend of PU-PEG-PLGA/HPMC has been shown for the first time in this project.
2. The conceptualization of the toro-poloidal, 3D implantable device, formulation thereof using direct compression and extrusion techniques contributes to new research in the field

of polymeric blends for application in controlled delivery systems. This is the first time this approach is proposed for use as a 3D RXB loaded PU-PEG-PLGA/HPMC implant.

3. Based on the *in-vitro* release studies, this device may be a significant step forward as a 3D RXB loaded polymeric implant. This research is a first step towards a more profound understanding of how geometry influences drug release properties of an implant.
4. This is the first occasion this method has been investigated for the *in-vivo* release of RXB from a subcutaneous implantable device.

1.5 OVERVIEW OF THE THESIS

CHAPTER 1: In this chapter, the background, rationale and motivation of the study undertaken was delineated. The aim, objectives and novelty of the study were stated, as well as the graphic representation of the toro-poloidal, 3D implant.

CHAPTER 2: This chapter, provides a concise account of geometrical correlation properties of various 3D formulated products with their biological performances, wherein an appraisal of drug release from different 3D formulated microstructures, biocompatibilities, and their application in pharmaceutics was discussed.

CHAPTER 3: In this chapter, preliminary results emanating from the use of a 3D Bioplotter to fabricate the 3D toro-poloidal, implant were discussed.

CHAPTER 4: In this chapter the novel PU-PEG-PLGA/HPMC blend for the toro-poloidal, 3D RXB loaded polymeric implant was formulated and characterised. Different RXB loaded PU-PEG-PLGA/HPMC formulations were analysed and discussed.

CHAPTER 5: In this chapter, two 3D geometrical structures (cylinder and donut) were successfully formulated through the extrusion-based and direct compression techniques using the texture analyser and tableting machinery, respectively. *In-vitro* cytotoxicity and Factor Xa (FXa) assay activity studies were carried out using the RXB loaded PU-PEG-PLGA/HPMC to compare the different formulations. Lastly *in-vitro* extended drug release studies were also established in this chapter. The formulations were assessed to establish the nature of the RXB release and inhibition of the Factor Xa activity.

CHAPTER 6: In this chapter, the *in-vivo* drug delivery of the 3D toro-poloidal, devices was designed and carried out using New Zealand White Albino rabbits. Faecal Occult Blood Test (FOBT), histology and blood samples were harvested, analysed and discussed.

CHAPTER 7: This chapter presents concluding remarks, recommendations and future prospective of the study.

1.6 REFERENCES

Abouhussein, D.M., Bahaa El Din Mahmoud, D. and Mohammad F, E., 2019. Design of a liquid nano-sized drug delivery system with enhanced solubility of rivaroxaban for venous thromboembolism management in paediatric patients and emergency cases. Journal of Liposome Research, 29(4): 399-412.

Ageno, W., Mantovani, L.G., Haas, S., Kreutz, R., Monje, D., Schneider, J., Van Eickels, M., Gebel, M., Zell, E. and Turpie, A.G., 2016. Safety and effectiveness of oral rivaroxaban versus standard anticoagulation for the treatment of symptomatic deep-vein thrombosis (XALIA): an international, prospective, non-interventional study. The Lancet Haematology, 3(1): e12-e21.

Alhnan, M.A., Okwuosa, T.C., Sadia, M., Wan, K.W., Ahmed, W. and Arafat, B., 2016. Emergence of 3D printed dosage forms: opportunities and challenges. Pharmaceutical Research, 33(8): 1817-1832.

Ammar, H.O., Ghorab, M., El-Nahhas, S.A. and Kamel, R., 2006. Design of a transdermal delivery system for aspirin as an antithrombotic drug. International Journal of Pharmaceutics, 327(1-2): 81-88.

Antoniou, S. and Amara, W., 2016. Once-daily rivaroxaban for long-term stroke prevention in patients with atrial fibrillation. European Heart Journal Supplements, 18 (suppl_D): D7-D15.

Chan K.E., Edelman E.R., Wenger J.B., Thadhani R.I, Maddux F.W., 2015. Dabigatran and rivaroxaban use in atrial fibrillation patients on hemodialysis. Circulation, 17; 131(11):972-9.

Choonara, Y.E., Pillay, V., Carmichael, T. and Danckwerts, M.P., 2006. An *in-vitro* study of the design and development of a novel doughnut-shaped minitablet for intraocular implantation. International Journal of Pharmaceutics, 310(1-2): 15-24.

Cloney, M.B., Hopkins, B., Dhillon, E.S. and Dahdaleh, N.S., 2018. The timing of venous thromboembolic events after spine surgery: a single-center experience with 6869 consecutive

patients: Presented at the 2017 AANS/CNS Joint Section on Disorders of the Spine and Peripheral Nerves. Journal of Neurosurgery: Spine, 28(1): 88-95.

Curto, A., 2017. Management of patients taking rivaroxaban for dental treatments. European Journal of General Dentistry, 6(1): 1.

Duggan, S.T., Scott, L.J. and Plosker, G.L., 2009. Rivaroxaban. Drugs, 69(13): 1829-1851.

Fitzpatrick, D., 2015. Implantable drug delivery systems. Implantable Electronic Medical Devices, 139–157.

Jacobson, B.F., Louw, S., Mer, M., Schapkaitz, E., Buller, H., De Jong, P.R., Rowji, P., Adler, D., Beeton, A., Hsu, H.C., Wessels, P., Haas, S., 2013. Venous thromboembolism: prophylactic and therapeutic practice guideline: guideline. South African Medical Journal 103, 261-267.

Konta AA, García-Piña M, Serrano DR., 2017. Personalised 3D printed medicines: Which techniques and polymers are more successful? Bioengineering, 4(4):79.

Krothapalli S, Bhave PD., 2014. My Patient taking a novel oral Anticoagulant needs surgery, device implantation, or ablation. Journal Atrial Fibrillation, 7(3).

Laube, E.S., Yu, A., Gupta, D., Miao, Y., Samedy, P., Wills, J., Harnicar, S., Soff, G.A. and Mantha, S., 2017. Rivaroxaban for stroke prevention in patients with nonvalvular atrial fibrillation and active cancer. The American Journal Cardiology, 120(2): 213-217.

Lewalter T, Kanagaratnam P, Schmidt B, Rosenqvist M, Nielsen-Kudsk JE, Ibrahim R, Albers BA, Camm AJ., 2014. Ischaemic stroke prevention in patients with atrial fibrillation and high bleeding risk: opportunities and challenges for percutaneous left atrial appendage occlusion. Europace, 1;16 (5):626-30.

Li, Q., Guan, X., Cui, M., Zhu, Z., Chen, K., Wen, H., Jia, D., Hou, J., Xu, W., Yang, X. and Pan, W., 2018. Preparation and investigation of novel gastro-floating tablets with 3D extrusion-based printing. International Journal of Pharmaceutics, 535(1-2): 325-332.

Mueck, W., Lensing, A.W., Agnelli, G., Decousus, H., Prandoni, P. and Misselwitz, F., 2011. Rivaroxaban. Clinical Pharmacokinetics, 50(10): 675-686.

Paikin, J.S., Manolakos, J.J. and Eikelboom, J.W., 2012. Rivaroxaban for stroke prevention in atrial fibrillation: a critical review of the rocket AF trial. Expert Review of Cardiovascular Therapy, 10(8): 965-972.

Schafer, A.I., Levine, M.N., Konkle, B.A. and Kearon, C., 2003. Thrombotic disorders: diagnosis and treatment. ASH Education Program Book, 2003(1): 520-539.

Stewart SA, Domínguez-Robles J, Donnelly RF and Larrañeta E., 2018. Implantable polymeric drug delivery devices: Classification, manufacture, materials, and clinical applications. Polymers, 10(12):1379

Tagami, T., Fukushige, K., Ogawa, E., Hayashi, N. and Ozeki, T., 2017. 3D printing factors important for the fabrication of polyvinylalcohol filament-based tablets. Biological and Pharmaceutical Bulletin, 40(3): 357-364.

Turpie AG., 2014. Rivaroxaban as an oral anticoagulant for stroke prevention in atrial fibrillation. Therapeutics and Clinical Risk Management, 10:197.

CHAPTER TWO
A REVIEW ON 3D MICROSTRUCTURES, THEIR GEOMETRY AND BIOLOGICAL PERFORMANCE IN DRUG DELIVERY

2.1 INTRODUCTION

Three-dimensional printing (3DP) technology is a revolutionary technique for swift prototyping, wherein microstructures are built by depositing layers in a sequence generating 3D devices (Horst, 2018; Prasad and Smyth, 2016), where a microstructure is the structure of a prepared surface. The main benefits of 3D rely on the capability of 3D to produce unparalleled flexible, time-saving pharmaceutical and personalized pharmaceutical products with tailored sizes, geometries, dosages and release kinetics (Jassim-Jaboori and Oyewumi, 2015; Horst, 2018, Osouli-Bostanabad and Adibkia, 2018; Trenfield et al., 2018).

The most basic 3D printing set-up is based on the principle of using computer-aided drafting and programming technology to produce 3D objects by means of layering material onto a desired product (Goyanes et al., 2016; Osouli-Bostanabad and Adibkia, 2018; Maulvi et al., 2017; Jamróz et al., 2018). As 3D printers offers the ability to construct highly complex 3D architectures, a diversity of 3DP technologies have been developed to fabricate novel dosage forms, which are amongst the most renowned and distinct formulations nowadays (Park et al., 2018; Vithan et al., 2019).

Due to the numerous inherent benefits of 3DP over the conventional technologies, numerous printing methods have been developed capitalizing on the varying sources of energy, material, and other mechanical properties (Park et al., 2018). Among them, the mostly used in the pharmaceutical industry are inkjet-based 3DP, Stereolithography (SLA), extrusion-based Fused Deposition Modeling (FDM), Selective Laser Sintering (SLS), and Bioprinting have been applied in pharmaceutical context both academic researchers and industrial. (Horst, 2018; Osouli-Bostanabad and Adibkia, 2018). The outline of the properties of all 3DP technologies have been extensively studied and will not be covered in this review (Daly et al., 2015, Fina et al., 2017; Guo et al., 2017; Horst, 2018; Osouli-Bostanabad and Adibkia, 2018; Lamichhane et al., 2019).

The 3DP technologies allow for pharmaceutical products to be created in various peculiar geometries (size and shape of the 3D products), various microstructures with different geometries. The geometrical properties of pharmaceutical products are very important to consider when it comes to personalized medication, as they affect the overall biological performance of pharmaceutical products (Martinez et al., 2018: Goyanes et al., 2015). Furthermore, Ubaid and Mohamed (2019) also pointed out the importance of visual appearance of pharmaceuticals in adherence. There are two critical factors that affect the geometry of a 3D device: the selection of biomaterial and the fabrication method (Jammalamadaka and Tappa, 2018).

Biological performance is based on the properties of materials used to formulate the 3D printed devices, sometimes referred as biocompatibility, where the interaction of living systems with materials is measured based on two concepts: the response of the host which is the systemic and local response, other than the anticipated therapeutic response of living systems to the material and material response which is the response of the material to living systems (Barbucci, Lamponi, Magnani, 2000). The choice of material is a critical step in 3D printing as it can lead to devices with good mechanical properties, improved functionality, and customized 3D geometries (Ghilan et al., 2020). As biocompatibility is one of the most important traits for materials used in 3D printed devices for clinical use, much research has been done on modifying and creating new biomaterials for 3D printing and this review won't focus on the different biomaterials used in designing the different 3D printing geometries (Bandyopadhyay, Bose, and Das (2015); Chia and Wu (2015), Jammalamadaka and Tappa, 2018; Atala, 2020; Wasti and Adhikari, 2020, Wang and Yang, 2021).

Although 3D printing has exhibited promising outcomes in the pharmaceutical industry applications, the technology is still in the developing stage (Maulvi et al., 2017). Challenges include optimization of the process, selections of appropriate excipients, improving performance of device for versatile use, and to improve the 3D printed designs these drawbacks need to be addressed (Maulvi et al., 2017). The objective of this literature review is to give an overview/outline of the current correlation of the geometrical properties of pharmaceutical products with its biological performances and its drug release/dissolutions effects. Correlation of medicine drug release characteristics with their complex microstructures is one of the mostly explored novelty in this technology, according to Kotta, Nair and Alsabeelah (2018) a number of researchers have designed

formulations with various release profiles such as sustained and delayed release due to changes in polymers, densities and shape.

2.2. CORRELATION OF GEOMETRICAL PROPERTIES WITH BIOLOGICAL PERFORMANCE

3DP does not only offer a more convenient medicine manufacturing approach, but it also allows the fabrication of dosage forms in various geometries, which offer better precision, accuracy, affordability, and patient-specific dosages compared to conventional medicines (Jamróz et al., 2018; Trenfield et al., 2019, Mathew et al., 2020). Various medicine geometries correlate with dissolution, where geometry plays a major role in dissolution assessments to define drug release profiles, it was noted that 3D devices with a larger surface area/volume (SA/V) ratio resulted into faster drug release (Goyanes et al., 2015).

According to Nukala and co-workers (2019) a macroscopic dissolution study demonstrated that 3D-printed objects preliminary dissolve by erosion with the rate of erosion varying based on geometry (infill pattern), followed by solubilization of polymeric joints and then complete dissolution. This infill pattern principle is mostly important in personalized drug therapy, where patients require individualized drug release. Macroscopic dissolution studies have demonstrated that the geometrical shape of 3DP objects diminished proportionally which was in accordance with Hixon–Crowell, Korsmeyer–Peppas and Higuchi mathematical models of drug release (Khaled et al., 2018; Nukala et al., 2019). These models enhance the understanding of the release mechanism exhibited by various geometries (Khaled et al., 2018).

The Hixson-Crowell model defines the release from systems where there is a variation in SA and diameter of particles with time, presented with the following equation:

$$\mathbf{Q_0}^{\frac{1}{3}} - \mathbf{Q_t}^{\frac{1}{3}} = \mathbf{k_{HC}t}$$

Equation 2.1. Hixson-Crowell model

Where Q0 is the initial quantity of the drug in tablet, Qt is the quantity of drug released at a time t and kHC is the rate constant for Hixson-Crowell rate equation (Kalam et al., 2007; Singhvi and Singh (2011)).

Korsmeyer–Peppas model simply defines drug release from a polymeric system as different polymers are utilized in most 3PD products in pharmaceuticals, represented by the following equation:

$$\frac{\mathbf{M_t}}{\mathbf{M_\infty}} = \mathbf{kt^n}$$

Equation 2.2. Korsmeyer–Peppas model

Where Mt / M∞ is a portion of drug released at time t, k is the rate constant and n is the release exponent equation (Singhvi and Singh (2011); Kalam et al., 2007). The n value is used to describe various release mechanisms (Singhvi and Singh (2011)).

Higuchi model defines the release of a drug from an insoluble matrix as the square root of a time dependent progression, it is based on Fickian diffusion, presented as below:

$$\mathbf{M_t} = \mathbf{k_H t^{0.5}}$$

Equation 2.3. Higuchi model

Where k_H is the Higuchi rate constant (Singhvi and Singh (2011); Wójcik-Pastuszka et al., 2019). With these models, it is possible predict the control of drug release/dose on personalized basis, without the need for complex formulation mixtures, hence this geometry/SA principle simplifies the potential supply chain and quality of the 3DP products (Khaled et al., 2018).

For instance, the 3DP was used to fabricate tablets in different shapes, while the total SA of the tablets remained constant, drug release rates were in this subsequent order (starting from the slowest); cylinder ≤ sphere < cube< torus< pyramid, this order follows the SA/V ratio release of tablets, with the pyramid having the utmost value (Goyanes et al., 2015; Ubaid and Mohamed, 2019). This order directly correlates with the SA/V ratio, leading the researchers to conclude that the geometrical shape of a tablet undoubtedly influences its dissolution/drug release profile (Ubaid and Mohamed, 2019). In a study conducted by Goyanes and co-workers (2016) paracetamol tablets of diverse shapes with constant SA were formulated and studied. The fastest dissolution rates were attained from pyramid microstructure which has the greatest SA/V ratio whereas the spherical or cylindrical microstructures with lowermost SA/V ratio were characterized by the slowest dissolution ratio (Goyanes et al., 2018; Jamróz et al., 2018). The different fissures in between internal structures influenced the fragmentation and dissolution time, and it was concluded that

this design system could be an easier alternative for tablet disintegration application and to accelerate tablet breakdown (Jamróz et al., 2018).

In another study by Xu and co-workers (2019) three different tablet microstructural models (Cylinder, Horn and Reversed Horn) were designed in order to attain controllable drug release profiles, **Figure 2.1.** shows the different geometries with their matching release profiles

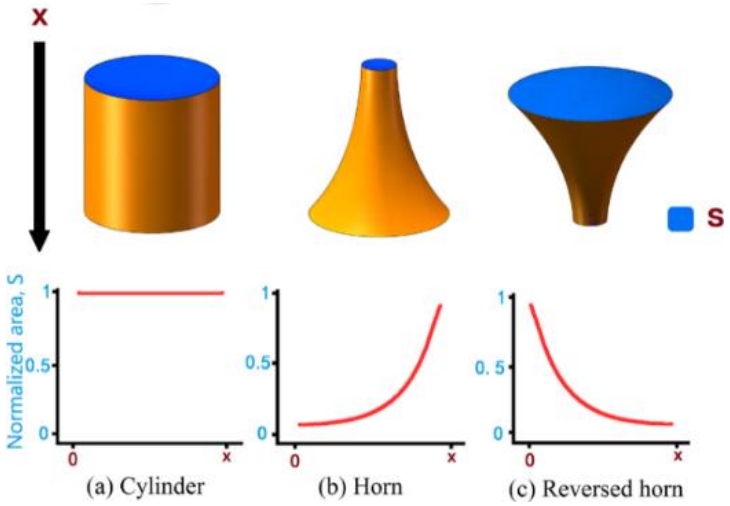

Figure 2.1. Three models of kernel tablets with different microstructures, the blue fragment represents the exposed area (the SA (S)) of the drug kernel. Adapted from with copyrights from from Xu et al. (2019).

This study demonstrated that the architectures of inner portion of the tablets had a significant effect on dissolution/drug release rate, as the drug release of all the models was positively linked to the changes of total SA. The SA of the exposed drug was constant, progressively increasing and gradually decreasing for Cylinder, Horn and R-Horn models, respectively as seen on **Figure 2.2.** The inner architecture was increasingly exposed with the decrease of the diameter of the tablet and the release rate was different due to the variation of SA of the inner architecture. This study is in agreement with other studies done by researchers such as Goyanes et al. (2015). Furthermore, Table 2.1. outlines more studies where the geometry and drug release/dissolution correlation had also been established. A brief correlation of geometrical properties with biological performance based on the different fabrication methods is also highlighted below. **Figure 2.2.** demonstrates the factors affecting the biological performance of 3D formulated devices in the pharmaceutical industry, which is the summary of all the main factors that influence the type of

drug release expected from any 3DP device. All the listed factors such as geometry, 3D fabrication method, degradation, biocompatibility, drug release mechanisms and microstructures affect the biological performance in various ways, the connection is highlighted in the overall chapter.

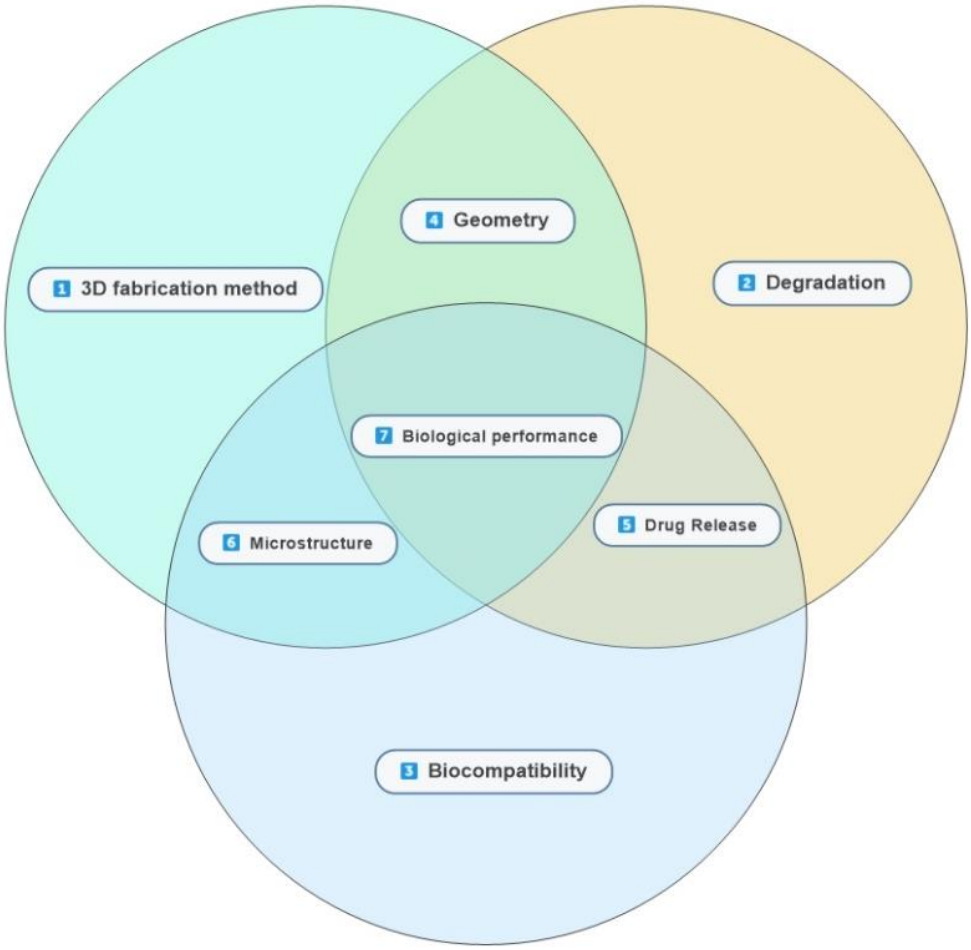

Figure 2.2. The summary of the factors affecting biological performance of 3D formulated devices in pharmaceutics.

2.2.1 Correlation of geometrical properties with biological performance for FDM fabricated 3D models

1. Based on **Table 2.1.** Drug release from these tablets was directly proportional to the SA/V, indicating the influence that geometrical shape has on drug release. Release rates were in this order: (starting from the slowest); cylinder ≤ sphere < cube< torus< pyramid.

2. The formulation with the thickest wall 2 mm showing a 100% infill density was selected as an optimized formulation due to its outstanding dissolution and drug release profile, as it had the largest SA/V.

3 The caplets were evaluated for hardness, disintegration and dissolution. The hexagon appeared to rapidly permeate and dissolved than the diamond, dissolving from surface to inside. In this case, it was concluded that, when the water interacted with the 3D micro-structure, the hydrophilic polymer (solid solution) dissolved gradually followed by the drug (solubilized state).

3. The results showed that the higher the density of the tablet was, the more sustained the drug was released and that the pliability of tablets was closely correlated to their densities. Overall, this study demonstrated the promising 3DP application in reducing the administration frequency and improving patients' compliance through the geometry manipulation of the products.

2.2.2 Correlation of geometrical properties with biological performance for Extrusion fabricated 3D models

1. Based on **Table 2.1.** The tablets displayed definite drug release profiles (including both immediate and sustained release) being controlled by their diverse geometries, and the dependency of dissolution/drug release on the SA/V ratio and the SA of the various tablets. 3D devices with greater SA/V ratios and SA had faster drug release. These results clearly demonstrated the potential of 3DP in creating novel unique pharmaceutical products, and further clinical opportunities.

2. The dissolution results exhibited dependency of dissolution on the SA/V ratio and the total SA of the tablet microstructures, such that tablets with greater SA/V ratios and total SA showed faster dissolution.

3. A good linear correlation between the theoretical volume and mass of the tablets was maintained, irrespective of the pattern used. Faster release behavior for drug was attained from the small-sized tablets due to their larger SA/mass ratio, proving geometric correlation with biological properties.

4. By changing the infill microstructure, the release mechanism was influenced, hence the drug release/ dissolution was described using the Korsmeyer-Peppas model and the mean dissolution time, respectively. Overall, the more infill resulted into faster drug release/ dissolution rates.

2.2.3 Correlation of geometrical properties with biological performance for SLS fabricated 3D models

Based on **Table 2.1.** The 3D tablets presented below proved that a constant SA/V ratio may be used to maintain dissolution performance and that dissolution may be modified for different individuals by using the SA/V ratio theory, as the dependency of the drug release kinetics on the geometric parameters of the 3DP microstructures was demonstrated.

Table 2.1. The presentation of various geometries with different biological performances

3D Technology	3D dosage form	Geometry of 3D dosage form	Ref.
FDM			
	Paracetamol-loaded filaments for oral administration.	Five different tablet geometries: cube, pyramid, cylinder, sphere and torus were printed.	Goyanes et al., 2015
	Tablets	Different geometrical tables were designed in terms of thickness (0.8, 1.2, 1.6, and 2.0 mm) and % density of the infill (50, 75, and 100)	Reddy Dumpa et al., 2020
	Caplets	Caplets were printed in hexagonal, and diamond infills in three different sizes.	Nukala et al., 2019
	tablets	Cylinder shaped tablets with different dimensions were studied.	Chai et al 2017
EXT 3D			
	tablets	Geometries (solid, ring, and mesh) from a similar paste-based formulation.	Khaled et al., 2019
	Tablets	Geometries (solid, ring, and mesh) from a similar paste-based formulation.	Wallacec, Yood and Robertsa, 2020
	Tablets	Three geometrical shapes (cylinder, oval and torus) were designed with various volumes	Cui et al., 2020
	Tablets	Tablet-like geometries were designed by changing the infill design of tablets	El Aita et al., 2020
SLS			
	Tablets (printlets)	A number of tablets with different geometries (torus, disc, cube, sphere and pyramid) with either similar SA or SA/V.	Martinez et al., 2018

2.3 ANALYSIS OF DRUG RELEASE FROM DIFFERENT 3D PRINTED MICROSTRUCTURES

Drug release from 3DP systems is greatly dependent on the overall design of the 3PD microstructures, thus the release profiles of 3DP may be tailored as per specific pharmaceutical expectations (Kempin et al., 2017). As the influence of 3PD microstructures on drug release may entirely differ within numerous designs a number of studies have been done to establish the different release profiles.

In a study done by Rowe and co-workers (2000) it was demonstrated that halving a single device into two units has the ability to incorporate different erosion and release mechanisms. **Figure 2.3.** displays the break-away mechanism, where the tablet was expected to break into two controlled sub units, a quicker dissolving region was also incorporated. This system clearly shows the potential for use of 3DP in designing complex release profiles by utilising compartments operating based on standard mechanisms such as diffusion and erosion.

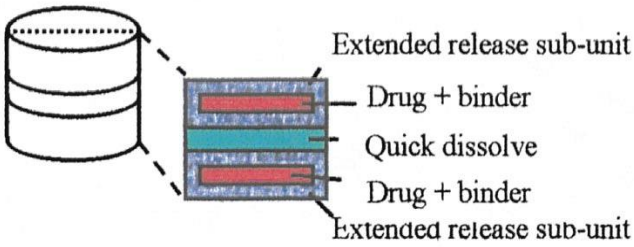

Figure 2.3. Depiction of a breakaway tablet. Adapted from Rowe et al., 2000 with permission.

Numerous reports in literature have directly interconnected the surge in dissolution rate/drug release to an increase in overall SA (increase in multi-units) as release is dependent on SA/V. However, Sadia and co-workers (2018) have further pointed out the impact of the channel length and its influence on drug release profiles. Where in a period of 30 min the use of 18-short channels, with a considerably lower SA/V ratio displayed more efficiency by gradually increasing *in-vitro* drug release in comparison with 9-long channels. **Figure 2.4.** shows how dissolution studies from three different designs (no channel (solid), long 9 channel, and short 18 channel) were compared at intervals of 5 min from zero to 30 min, using the USP II dissolution test at pH 1.2. It was concluded that the longer channels required sturdier hydraulic forces for medium to flow through the channels (Sadia et al., 2018), hence delayed drug release was displayed by the longer channels. The potential for 3DP channelled microstructures was clearly established in modifying the drug disintegration and release which could be utilised with individualised upcoming pharmaceutical products.

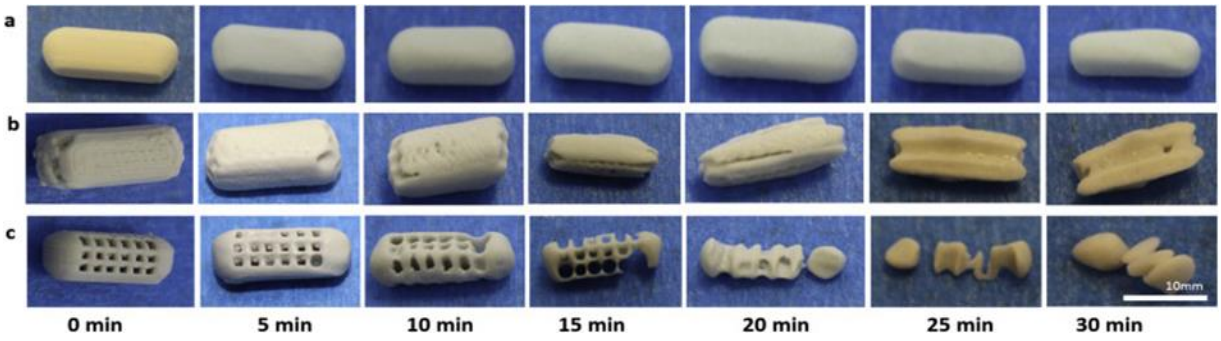

Figure 2.4. The dissolution of 3DP tablets based on the tablets design, the length and channel (a) design with no channel, (b) long 9, and (c) short 18 channel designs (Adapted from Sadia et al., 2018 with permission).

Drug release profiles from the dual-layered and multi-layered are one of the most interesting and auspicious devices for controlled drug release (**Figure 2.5**). The design of a multi-layered device enables the incorporation of more than one drug within the device and results have shown similar release profiles for all drugs with no effect on solubility. Hence it was concluded that this multilayer system may be effective for the release of various drugs with a similar release pattern or to deliver chemically incompatible drugs, as they can be isolated in separate segments of the device (Goyanes et al., 2015). In the dual-layered system, as expected drug released from the external layer resumes before the internal core. Due to the delayed release lag time from the internal core, this system may be useful in personalised extended drug delivery. In this dual system it was observed that specific drug release profiles may be achieved with modifications on both the external layer and internal core (Goyanes et al., 2015; Li Q et al., 2017).

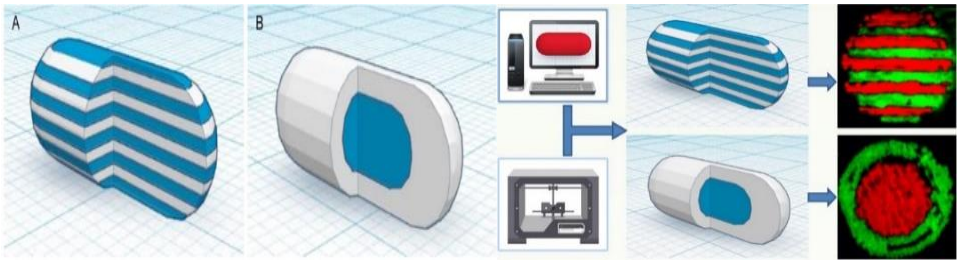

Figure 2.5. A representation of 3DP devices (a) sectioned multilayer and (b) sectioned dual-layered (reproduced with permission from Goyanes et al. (2015)).

The dissolution studies of duo-layered devices indicated the capability of designing 3DP devices displaying controlled drug release profiles by modifying the core microstructure of the devices (Li Q et al., 2017). Numerous drug release studies have been performed with data best suited by zero order, Higuchi, first order, and Korsmeyer–Peppas models, which were used to establish the kinetics of the drug released (Dash et al., 2010, Siepmann and Peppas, 2012; Li Q et al., 2017). This confirms that duo-tablet structural device can incorporate different drug concentrations to fulfil different desired purposes (Li Q et al., 2017) and the drug release dependent on both the core and external microstructures of the dual 3D printed devices.

2.4 BIOCOMPATIBILITY OF 3D PRINTED MICROSTRUCTURES

Even though 3D printing has been utilised to fabricate complex microstructures with different properties to suit personal needs of patients in pharmaceutical, no biocompatibility effects have been noted. All devices for Clinical use must be shown that they don't cause any unexpected, unjustifiable or unintentional adverse effects, hence biological risks must be evaluated for all 3D devices. In a study done by Chen and co-workers (2020) the method of hematoxylin and eosin (H&E) tissues staining was used to evaluate *in-vivo* efficacy of three types of microstructures. The results showed no significant inflammation and abnormal defects of the tissues surrounding the device after the administration for day 1 and 7. As shown in **Figure 2.6.**, the triangle, cross, and two-layer cake-like hydrogel microstructures were evaluated.

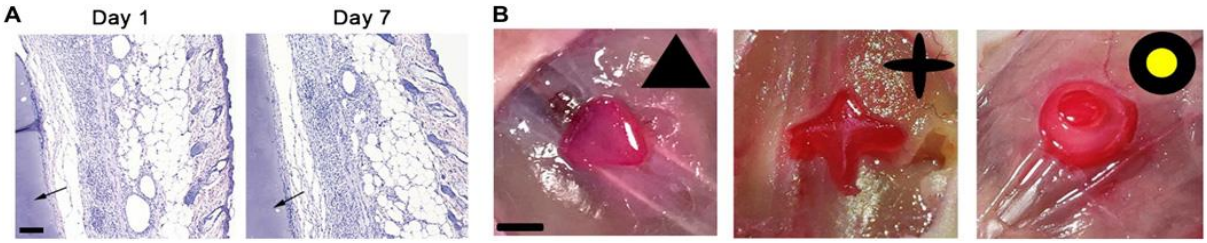

Figure 2.6. The H&E stain of the surrounding tissue after in-vivo 3DP microstructure exposure for day: (A) 1 and 7. The arrow denotes the printed microstructure. (B) In situ 3D fabricated triangle, cross, and two-layer cake-like microstructures (adapted with permission Chen et al., 2020).

Wang and co-workers (2020) implanted drug-loaded poly L-lactic acid (PLLA) implants microspheres into New Zealand white rabbits where no biocompatibility effects were observed throughout the experiment, and based on the histological H&E (**Figure 2.7**). It was concluded that the PLLA implants are bio-safe for implantation over extended period of time.

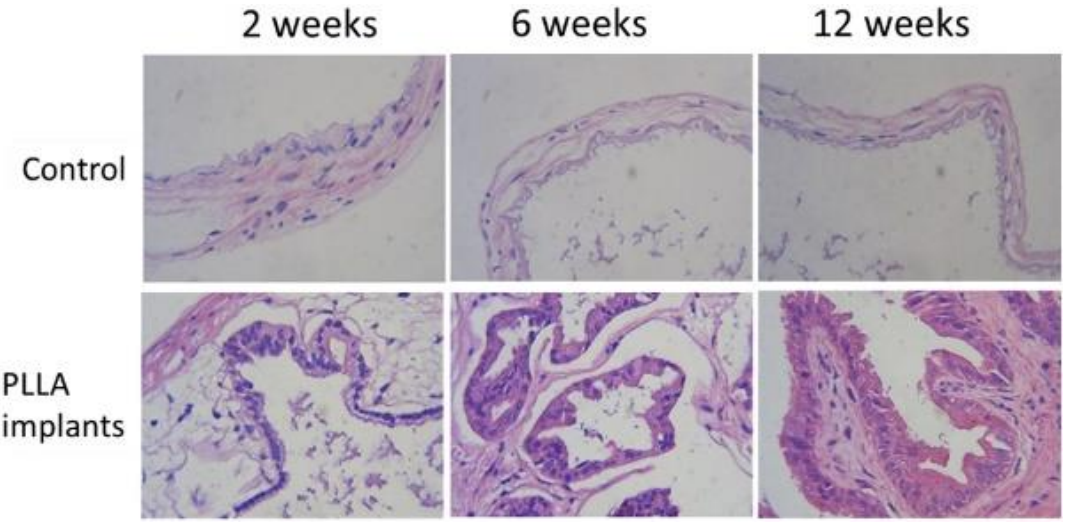

Figure 2.7. The H&E-stained histology of tissues around the implanting site of drug-loaded 3D microstructures-PLLA implants adapted with permission Wang et al., 2020).

Furthermore, another *in-vivo* study was done where a histology analysis was utilised to show no signs of necrosis nor reactions related to exaggerated inflammatory at any point of the study were detected after a 3DP microstructures was implanted (Barbeck et al., 2017). Based on case studies highlighted above it may be concluded that 3D microstructures are generally safe for drug release use in the pharmaceutical industry.

2.5 SELECTED PHARMACEUTICAL APPLICATION OF 3D PRINTED MICROSTRUCTURES

In 2015, the first 3D drug product (Spritam® (Levetiracetam)) was approved by the FDA, which unlocked a new novelty of 3D in the pharmaceutical industry (Norman et al., 2017). Briefly, this review highlights the pharmaceutical applications of 3D technology, indicating the potential 3D application holds in the commercial sector of pharmaceutics. The highlighted pharmaceutical 3D applications are presented on different geometric systems suitable for their specific applications, and this is relatively a progressing matter in the pharmaceutical industry.

2.5.1 Oral 3D application

In a study by Melocchi et al. (2015) oral capsules were manufactured through the combination of compartments resulting into a two-pulse release pattern for the purpose of product personalization and injection molding (**Figure 2.8.** (i)), a similar study was done by Maroni et al. (2017) where a multi-compartment capsular device with diverse thickness and composition for oral drug delivery was developed (**Figure 2.8.** (ii)). In 2014 3D fabricated oral tablets were formulated where the

release profiles were directly dependent on the percentage of the infill used for tablet printing, resulting in personal dependent doses/unit doses of medicine forms with personalised drug release profiles (Goyanes et al., 2014) (**Figure 2.8.** (iv)). Similarly, another recent study was done where 3D tablets were formulated into three different types of models (a) Cylinder, (b) Horn and (c) Reversed Horn. The potential for controllable release profiles of the three geometries was studied and correlation with biological performances observed (Xu et al., 2019) (**Figure 2.8.** (iii)).

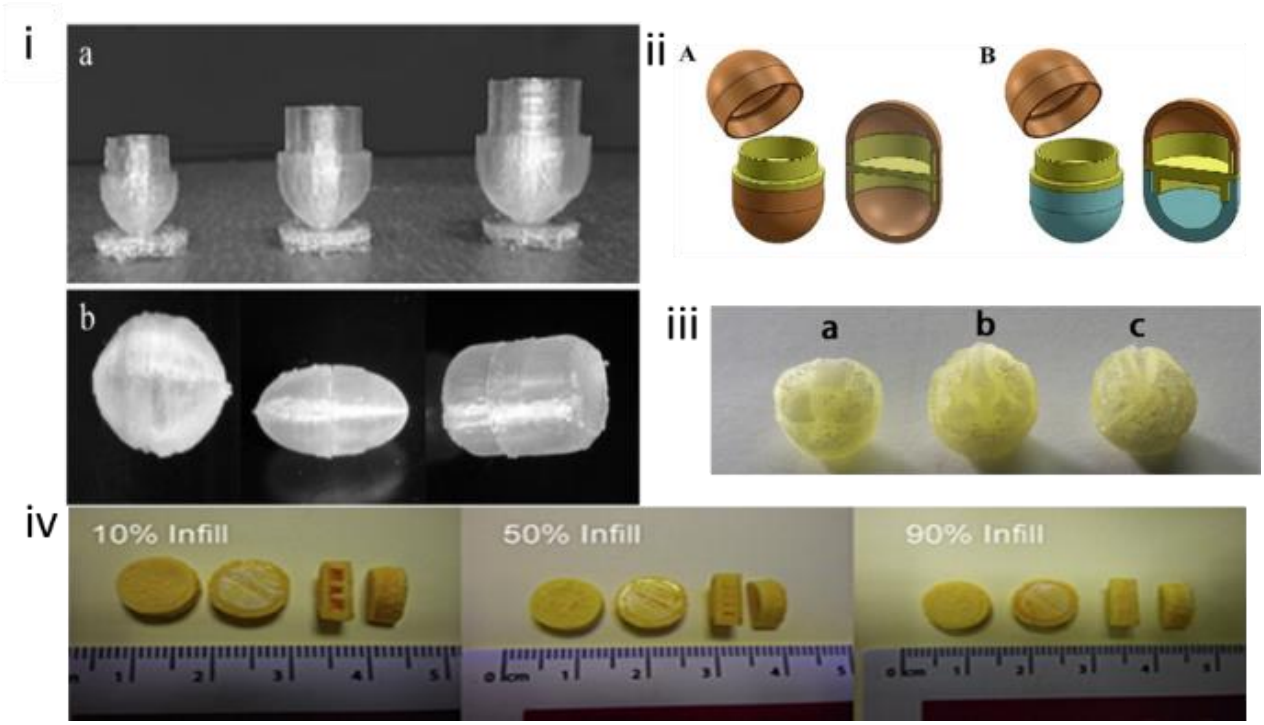

Figure 2.8. Physical photomicrographs and schematics representing (i) 3DP hollow microstructures (a) assembled capsular devices (b) with different size and shape. (ii) Cross-section and isometric views of capsular compartment devices either composed of halves with same (A) or different (B) thickness. (iii) 3DP tablet images of three different models. (a) Cylinder, (b) Horn, (c) R-Horn. (iv) Images of 3DP tablets as infill percentage function, showing top, base, internal and lateral views (Figures reproduced with permission from Maroni et al., 2017; Maroni et al., 2017; Xu et al., 2019; Goyanes et al., 2014, respectively).

2.5.2 Wound dressing 3D application

Recent studies have shown the application of 3D fabrication in hydrogel dressings and scaffolds, Cereceres et al. (2019) and Long et al. (2019), respectively. **Figure 2.9. (i)** shows the lattice microstructure and geometry programmed into a 3D printer, generating flexible macroporous and

microporous hydrogel dressings. **Figure 2.9 (ii**) shows scaffolds printed by a mechanical positive displacement dispensing system, the scaffolds also displayed good flexibility, skin self-adhesion, as well as good biological corelation with the design of the 3D wound dressing.

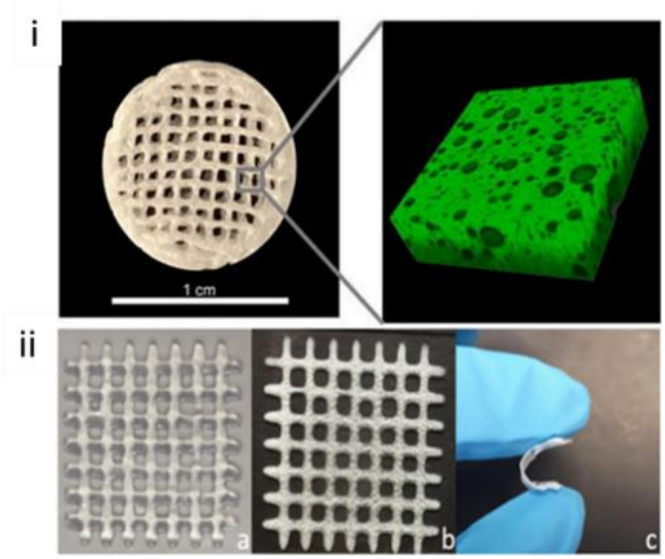

Figure 2.9. 3D structures showing (i) an image of a 3DP wound dressing hydrogel and its confocal emulsion image. (ii) 3DP hydrogel scaffold: a) from the printer, b) after lyophilisation and c) its flexibility (Reproduced with permission from Cereceres et al., 2019; Long et al., 2019, respectively).

2.5.3 Implants/patches application

Studies have shown the application of 3D technology in the fabrication of controlled release implantable devices (Holländer et al., 2016), where intrauterine system (IUS) filaments were invented for controlled release of implantable devices. Similarly, another study showed how porous hollow bullet-shaped implants may be formulated using a 3D printer system, where the drug dissolution/release from the implant was modified by altering various matrices, pore sizes and coating thickness (Yang et al., 2018).

Lastly, the application of 3D printing in patches was also considered in this review, where porous biodegradable patches demonstrated the ability to contain a high drug concentration for both dermal and intradermal drug delivery, as well as extended drug release. A number of studies were done where microneedles were fabricates as patches (Yi et al., 2016; Krieger et al., 2019; Economidou et al., 2019), resulting into superior skin penetration capacity compared to conventional formulated microneedles, **Figure 2.10.** (iii) shows as example of microneedle shaped patch.

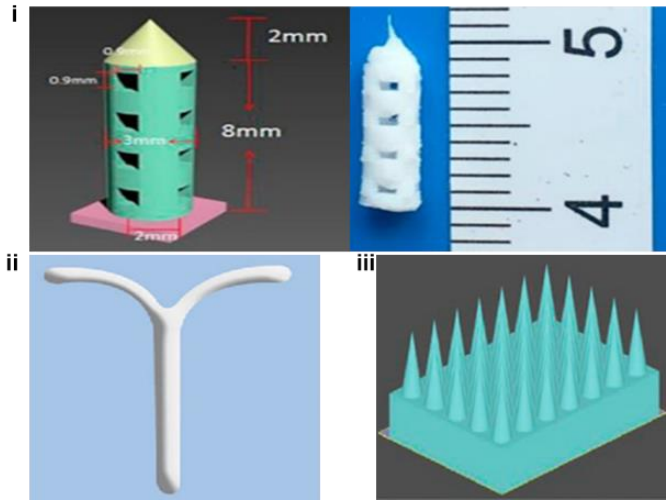

Figure 2.10. 3D implants/patches application where: (i) show the models of a hallow bullet implants with specific shown parameters of the implants were labelled. (ii) Drug incorporated IUS device (iii) Overview of microneedles shaped patch. (Reproduced with permission from Holländer et al., 2016; Yang et al., 2018, respectively).

2.5.4 3D-printed drug-eluting implants

3D-printed drug-eluting implants may be described as active implants with the potential to induce healing effects as an additional characteristic, they release the active ingredient in a controlled manner over a sustainable period of time (Zilberman et al., 2010). Drug eluting implants have unique properties compared to conventional implants as they provide site-specific, localised, as well as systematic drug delivery methods, making them useful for targeted drug delivery for instances such as oncology and cardiology (Domsta and Seidlitz, 2021). **Figure 2.11.** shows some of the previously reported 3D-printed drug-eluting implants in pharmaceuticals**.**

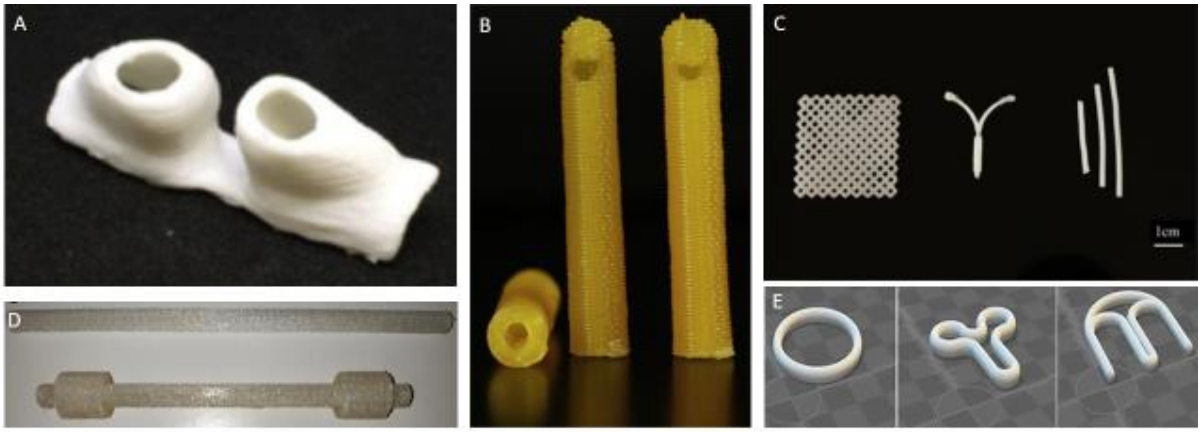

Figure 2.11. 3DP drug-eluting implants**,** (A) Bilateral nasal supports (adapted with copyright from Boyer et al., 2018), (B) drug loaded catheters (adapted with copyrights from Weisman et al., 2019), (C) hormone-eluting constructs (adapted with copyrights from Tappa et al., 2017), (D) Drug loaded anti-infective dialysis long catheters with and without integrated cuffs (adapted with copyrights from Mathew et al., 2019) and (E) hormone loaded vaginal rings in different shapes (adapted with copyrights from Fu et al., 2018).

2.6 PRESSURE ASSISTED 3D EXTRUDED DEVICES

Pressure assisted 3D extruded devices is whereby 3D models are formulated from material extruded via a syringe, the extruded material forms the desired geometry, that contains extruded layers (Pandey et al., 2020; Soleymani Eil Bakhtiari et al., 2021; Vaz and Kumar, 2021). See **Figure 2.12.** where the pressure applied to the syringe extrudes materials out via the depositing nozzle. Subsequently, the extruded material undergoes drying and solidification (Pandey et al., 2020), allowing sufficient physical strength for the obtained 3D model, with the drying process being one of the crucial steps affecting the final product, as the strength of the extruded layer has to be strong enough to avoid collapsing when succeeding layers are deposited on it (Chimate and Koc, 2014; Vaz and Kumar, 2021). The geometry of the devices may be manipulated to suit different desired personalised needs. In a study done by Mohammed and co-workers (2021) optimization of materials and pressure assisted printing process was achieved, where the choice of polymers with their solvents were converted into an extrudable paste. So far with the formulated pharmaceutical products the extrusion methods were being affected by printing pressure, printing speed, nozzle shape and size (Real, et al., 2020; Seoane-Viaño et al., 2021). Extruded formulations may be based on a pneumatic, mechanical or solenoid piston, with the major advantage of

extrusion-based 3D devices being the ability to avoid harsh temperatures during processing (Vaz and Kumar, 2021). **Table 2.2**. summarises some of the 3D devices formulated via extrusion.

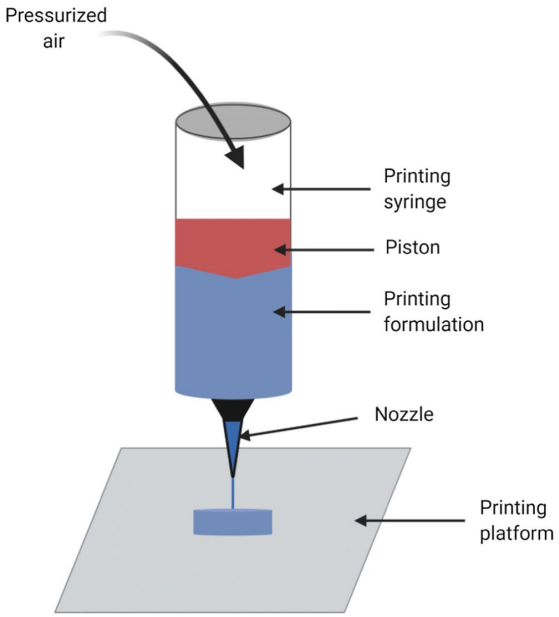

Figure 2.12. The formulation of 3D devices a pressure assisted method, adapted with permission from Vaz and Kumar, (2021).

Table 2.2. A summary of previous studies based on 3D extruded devices

Extruded 3D device	Formulation	Remarks	Ref.
3D drug-eluting implants: disc geometries	Extrudate filaments (extruded feedstock material) were used to formulate 3D-model geometries. The feed materials were extruded using a syringe where DSM Xplore micro compounder was utilised for pressurised air feed into the syringe.	Study demonstrated the potential of formulating personalized pharmaceutical products with controlled release using extruded material.	Water et al., 2015
Oral 3D shell cap	Extrusion of the optimized material was carried out through the 3D printer.	The importance of the choice of polymers with desirable solvent for an extrudable paste formulation, as well as extrusion pressure, speed, size and shape of syringe nozzle for extrusion-based 3D models was demonstrated.	Mohammed, et al., 2021
3D hybrid film structures	Films were fabricated using a dual-extrusion, pressure-assisted syringe, where the state-of-the-art in fabrication techniques was applied.	The study revealed that 3D Printing may be utilized to circumvent immiscibility issues associated with polymer combination in the formulation of personalized pharmaceutical products.	Elbadawi et al., 2021
Structure-Based Gastro-Retentive and Controlled Release Drug Delivery	The fabrication was under control of a pressure-assisted syringe –linked computer with a commercial pressure-assisted syringes 3D printer.	This study highlighted the future perspectives of pressure-assisted syringe, including the design, drug delivery system and flexibility compared to conventional formulation methods.	Wen et al., 2019

2.7 CONCLUSION

It may be concluded that the revolution of the 3DP technology is more advanced compared to conventional formulation processes as it also allows for formulation versatility. In the pharmaceutical industry the 3D technology enables uncomplicated fabrication of 3D pharmaceuticals with

various geometries (i.e., cube, torus, pyramid, sphere), many of which would be challenging to formulate using the conventional methods. This demonstrates the potential of 3D technology to modify drug dissolution/release profiles and aid in personalized medicine in pharmaceutics. The drug release/dissolution profiles from the different geometries showed limited dependence on the surface area but rather on surface area versus volume ratio, indicating the influence that geometrical shape (internal architecture/infill pattern) has on drug release profile. Despite the increasing amount of interest on 3D, 3D in the pharmaceutical industry is still growing and yet to be fully explored for its benefits in patients and overall healthcare system. With continuous innovation and refinement, in the near future 3D technology may be used as a potential and convenient tool for pharmaceutical industry, which would bring revolutionary in the manufacturing processes, fast-track clinical practices of more patient- oriented dosages and facilitate patient-centered health care. Up to date very few implantable 3D drugs delivery systems have been investigated and published. Therefore, novel approaches directed towards 3D implantable drug delivery systems could benefit the pharmaceutical research sector. Despite these promising results, there are still unanswered questions regarding the use of 3D in the pharmaceutical industry, such as 3D application in implants. Important aspects such as quality control/reproducibility and the cost of 3D printing need to be addressed before 3D-printing technology can be utilized.

2.8 REFERENCES

Acosta-Vélez, G.F. and Wu, B.M., 2016. 3D pharming: direct printing of personalized pharmaceutical tablets. Polymer Sciences, 2: 1:3, 1-10.

Aho, J., Bøtker, J.P., Genina, N., Edinger, M., Arnfast, L. and Rantanen, J., 2019. Roadmap to 3D-printed oral pharmaceutical dosage forms: feedstock filament properties and characterization for fused deposition modeling. Journal Pharmaceutical Sciences, 108: 26-35.

Algahtani, M.S., Mohammed, A.A. and Ahmad, J., 2018. Extrusion-based 3D printing for pharmaceuticals: Contemporary research and applications. Current Pharmaceutical Design, 24: 4991-5008.

Alhnan, M.A., Okwuosa, T.C., Sadia, M., Wan, K.W., Ahmed, W. and Arafat, B., 2016. Emergence of 3D printed dosage forms: opportunities and challenges. Pharmaceutical Research, 33: 1817-1832.

Andriotis, E.G., Eleftheriadis, G.K., Karavasili, C. and Fatouros, D.G., 2020. Development of bioactive patches based on pectin for the treatment of ulcers and wounds using 3D-bioprinting technology. Pharmaceutics, 12: 56.

Atala, A. ed., 2020. Introduction: 3D printing for biomaterials. Chemical Reviews, 120: 10545–10546

Bandyopadhyay, A., Bose, S. and Das, S., 2015. 3D printing of biomaterials. Materials Research Society Bulletin, 40: 108-115.

Barbeck, M., Serra, T., Booms, P., Stojanovic, S., Najman, S., Engel, E., Sader, R., Kirkpatrick, C.J., Navarro, M. and Ghanaati, S., 2017. Analysis of the *in-vitro* degradation and the in-vivo tissue response to bi-layered 3D-printed scaffolds combining PLA and biphasic PLA/bioglass components–Guidance of the inflammatory response as basis for osteochondral regeneration. Bioactive Materials, 2(4): 208-223.

Boehm, R.D., Miller, P.R., Daniels, J., Stafslien, S. and Narayan, R.J., 2014. Inkjet printing for pharmaceutical applications. Materials Today, 17: 247-252.

Bunea, A.I., Jakobsen, M.H., Engay, E., Bañas, A.R. and Glückstad, J., 2019. Optimization of 3D-printed microstructures for investigating the properties of the mucus biobarrier. Micro and Nano Engineering, 2: 41-47.

Cereceres, S., Lan, Z., Bryan, L., Whitely, M., Wilems, T., Greer, H., Alexander, E.R., Taylor, R.J., Bernstein, L., Cohen, N. and Whitfield-Cargile, C., 2019. Bactericidal activity of 3D-printed hydrogel dressing loaded with gallium maltolate. Applied Physics Letters Bioengineering, 3(2): 026102.

Chai, X., Chai, H., Wang, X., Yang, J., Li, J., Zhao, Y., Cai, W., Tao, T. and Xiang, X., 2017. Fused deposition modeling (FDM) 3D printed tablets for intragastric floating delivery of domperidone. Scientific Reports, 7: 1-9.

Chen, W., Xu, Y., Liu, Y., Wang, Z., Li, Y., Jiang, G., Mo, X. and Zhou, G., 2019. Three-dimensional printed electrospun fiber-based scaffold for cartilage regeneration. Materials and Designs, 179: 107886.

Chen, Y., Zhang, J., Liu, X., Wang, S., Tao, J., Huang, Y., Wu, W., Li, Y., Zhou, K., Wei, X. and Chen, S., 2020. Noninvasive *in-vivo* 3D bioprinting. Science Advances, 6(23): 7406.

Chimate, C. and Koc, B., 2014. Pressure assisted multi-syringe single nozzle deposition system for manufacturing of heterogeneous tissue scaffolds. The International Journal of Advanced Manufacturing Technology, 75(1-4): 317-330.

Cui, M., Pan, H., Fang, D., Qiao, S., Wang, S. and Pan, W., 2020. Fabrication of high drug loading levetiracetam tablets using semi-solid extrusion 3D printing. Journal of Drug Delivery Science and Technology, 57:101683.

Daly, R., Harrington, T.S., Martin, G.D. and Hutchings, I.M., 2015. Inkjet printing for pharmaceutics–a review of research and manufacturing. International Journal of Pharmaceutics, 494(2): 554-567.

Economidou, S.N., Pere, C.P.P., Reid, A., Uddin, M.J., Windmill, J.F., Lamprou, D.A. and Douroumis, D., 2019. 3D printed microneedle patches using stereolithography (SLA) for intradermal insulin delivery. Materials Science and Engineering: C, 102: 743-755.

El Aita, I., Breitkreutz, J. and Quodbach, J., 2020. Investigation of semi-solid formulations for 3D printing of drugs after prolonged storage to mimic real-life applications. European Journal of Pharmaceutical Sciences, 146:105266.

Elbadawi, M., Nikjoo, D., Gustafsson, T., Gaisford, S. and Basit, A.W., 2021. Pressure-assisted microsyringe 3D printing of oral films based on pullulan and hydroxypropyl methylcellulose. International Journal of Pharmaceutics, 595: 120197.

Fina, F., Goyanes, A., Gaisford, S. and Basit, A.W., 2017. Selective laser sintering (SLS) 3D printing of medicines. International journal of pharmaceutics, 529(1-2): 285-293.

Ghilan, A., Chiriac, A.P., Nita, L.E., Rusu, A.G., Neamtu, I. and Chiriac, V.M., 2020. Trends in 3D printing processes for biomedical field: opportunities and challenges. Journal of Polymers and the Environment, 28: 1345-1367.

Goyanes, A., Buanz, A.B., Basit, A.W. and Gaisford, S., 2014. Fused-filament 3D printing (3DP) for fabrication of tablets. International Journal of Pharmaceutics, 476(1-2): 88-92.

Goyanes, A., Det-Amornrat, U., Wang, J., Basit, A.W. and Gaisford, S., 2016. 3D scanning and 3D printing as innovative technologies for fabricating personalized topical drug delivery systems. Journal of Controlled Release, 234: 41-48.

Goyanes, A., Martinez, P.R., Buanz, A., Basit, A.W. and Gaisford, S., 2015. Effect of geometry on drug release from 3D printed tablets. International Journal of Pharmaceutics, 494: 657-663.

Goyanes, A., Wang, J., Buanz, A., Martínez-Pacheco, R., Telford, R., Gaisford, S. and Basit, A.W., 2015. 3D printing of medicines: engineering novel oral devices with unique design and drug release characteristics. Molecular Pharmaceutics, 12: 4077-4084.

Guo, Y., Patanwala, H.S., Bognet, B. and Ma, A.W., 2017. Inkjet and inkjet-based 3D printing: connecting fluid properties and printing performance. Rapid Prototyping Journal, 23: 562-76.

Holländer, J., Genina, N., Jukarainen, H., Khajeheian, M., Rosling, A., Mäkilä, E. and Sandler, N., 2016. Three-dimensional printed PCL-based implantable prototypes of medical devices for controlled drug delivery. Journal of Pharmaceutical Sciences, 105: 2665-2676.

Horst, D.J., 2018. 3D printing of pharmaceutical drug delivery systems. Archives of Organic and Inorganic Chemical Sciences, 1: 65-69.

Hsiao, W.K., Lorber, B., Reitsamer, H. and Khinast, J., 2018. 3D printing of oral drugs: a new reality or hype? Expert Opinion on Drug Delivery, 15: 1-4.

Jain, V., Haider, N. and Jain, K., 2018. 3D printing in personalized drug delivery. Current pharmaceutical design, 24: 5062-5071.

Jammalamadaka, U. and Tappa, K., 2018. Recent advances in biomaterials for 3D printing and tissue engineering. Journal of functional biomaterials, 9: 22.

Jamróz, W., Szafraniec, J., Kurek, M. and Jachowicz, R., 2018. 3D printing in pharmaceutical and medical applications–recent achievements and challenges. Pharmaceutical research, 35(9): 1-22.

Jassim-Jaboori AH, Oyewumi MO., 2015. 3D printing technology in pharmaceutical drug delivery: prospects and challenges. Journal of Biomolecular Research & Therapeutics, 4: 1-3.

Jose, P.A. and GV, P.C., 2018. 3D printing of pharmaceuticals–a potential technology in developing personalized medicine. Asian Journal of Pharmaceutical Research and Development, 6: 46-54.

Kalam, M.A., Humayun, M., Parvez, N., Yadav, S., Garg, A., Amin, S., Sultana, Y. and Ali, A., 2007. Release kinetics of modified pharmaceutical dosage forms: a review. Continental Journal Pharmaceutical Sciences, 1:30-5.

Kempin, W., Franz, C., Koster, L.C., Schneider, F., Bogdahn, M., Weitschies, W. and Seidlitz, A., 2017. Assessment of different polymers and drug loads for fused deposition modeling of drug loaded implants. European Journal of Pharmaceutics and Biopharmaceutics, 115:84-93.

Khaled, S.A., Alexander, M.R., Irvine, D.J., Wildman, R.D., Wallace, M.J., Sharpe, S., Yoo, J. and Roberts, C.J., 2018. Extrusion 3D printing of paracetamol tablets from a single formulation with tunable release profiles through control of tablet geometry. American Association of Pharmaceutical Scientists, 19(8): 3403-3413.

Kirchmajer, D.M. and Gorkin Iii, R., 2015. An overview of the suitability of hydrogel-forming polymers for extrusion-based 3D-printing. Journal of Materials Chemistry B, 3: 4105-4117.

Kjar, A. and Huang, Y., 2019. Application of micro-scale 3D printing in pharmaceutics. Pharmaceutics, 11: 390.

Konta, A.A., García-Piña, M. and Serrano, D.R., 2017. Personalised 3D printed medicines: which techniques and polymers are more successful? Bioengineering, 4(4): 79.

Krieger, K.J., Bertollo, N., Dangol, M., Sheridan, J.T., Lowery, M.M. and O'Cearbhaill, E.D., 2019. Simple and customizable method for fabrication of high-aspect ratio microneedle molds using low-cost 3D printing. Microsystems and Nanoengineering, 5: 1-14.

Lamichhane, S., Bashyal, S., Keum, T., Noh, G., Seo, J.E., Bastola, R., Choi, J., Sohn, D.H. and Lee, S., 2019. Complex formulations, simple techniques: Can 3D printing technology be the Midas touch in pharmaceutical industry? Asian Journal of Pharmaceutical sciences, 14: 465-479.

Li, Q., Wen, H., Jia, D., Guan, X., Pan, H., Yang, Y., Yu, S., Zhu, Z., Xiang, R. and Pan, W., 2017. Preparation and investigation of controlled-release glipizide novel oral device with three-dimensional printing. International Journal of Pharmaceutics, 525: 5-11.

Long, J., Etxeberria, A.E., Nand, A.V., Bunt, C.R., Ray, S. and Seyfoddin, A., 2019. A 3D printed chitosan-pectin hydrogel wound dressing for lidocaine hydrochloride delivery. Materials Science and Engineering: C, 104: 109873.

Lu, M., 2019. Novel excipients and materials used in FDM 3D printing of pharmaceutical dosage forms. 3D and 4D printing in biomedical applications: Process Engineering and Additive Manufacturing, 211-237.

Maroni, A., Melocchi, A., Parietti, F., Foppoli, A., Zema, L. and Gazzaniga, A., 2017. 3D printed multi-compartment capsular devices for two-pulse oral drug delivery. Journal of Controlled Release, 268:10-18.

Martinez, P.R., Goyanes, A., Basit, A.W. and Gaisford, S., 2018. Influence of geometry on the drug release profiles of stereolithographic (SLA) 3D-printed tablets. American Association of Pharmaceutical Scientists, 19(8): 3355-3361.

Mathew, E., Pitzanti, G., Larrañeta, E. and Lamprou, D.A., 2020. 3D printing of pharmaceuticals and drug delivery devices. Pharmaceutics, 12(3): 266.

Maulvi FA, Shah MJ, Solanki BS, Patel AS, Soni TG, Shah DO., 2017. Application of 3D printing technology in the development of novel drug delivery systems. International Journal Drug Delivery and Research. 9: 44-9.

Melocchi, A., Parietti, F., Loreti, G., Maroni, A., Gazzaniga, A. and Zema, L., 2015. 3D printing by fused deposition modeling (FDM) of a swellable/erodible capsular device for oral pulsatile release of drugs. Journal of Drug Delivery Science and Technology, 30, 360-367.

Mohammed, A.A., Algahtani, M.S., Ahmad, M.Z. and Ahmad, J., 2021. Optimization of semisolid extrusion (pressure-assisted microsyringe)-based 3D printing process for advanced drug delivery application. Annals of 3D Printed Medicine, 2: 100008.

Norman, J., Madurawe, R.D., Moore, C.M., Khan, M.A. and Khairuzzaman, A., 2017. A new chapter in pharmaceutical manufacturing: 3D-printed drug products. Advanced Drug Delivery Reviews, 108: 39-50.

Nukala, P.K., Palekar, S., Solanki, N., Fu, Y., Patki, M., Shohatee, A.A., Trombetta, L. and Patel, K., 2019. Investigating the application of FDM 3D printing pattern in preparation of patient-tailored dosage forms. Journal of 3D Printing in Medicine, 3: 23-37.

Osouli-Bostanabad, K. and Adibkia, K., 2018. Made-on-demand, complex and personalized 3D-printed drug products. Bio-Impacts, 8: 77.

Pandey, M., Choudhury, H., Fern, J.L.C., Kee, A.T.K., Kou, J., Jing, J.L.J., Her, H.C., Yong, H.S., Ming, H.C., Bhattamisra, S.K. and Gorain, B., 2020. 3D printing for oral drug delivery: a new tool to customize drug delivery. Drug Delivery and Translational Research, 10(4): 986-1001.

Park, B.J., Choi, H.J., Moon, S.J., Kim, S.J., Bajracharya, R., Min, J.Y. and Han, H.K., 2019. Pharmaceutical applications of 3D printing technology: Current understanding and future perspectives. Journal of Pharmaceutical Investigation, 49: 575-585.

Prasad, L.K. and Smyth, H., 2016. 3D Printing technologies for drug delivery: a review. Drug Development and Industrial Pharmacy, 42: 1019-1031.

Real, J.P., Barberis, M.E., Camacho, N.M., Bruni, S.S. and Palma, S.D., 2020. Design of novel oral ricobendazole formulation applying melting solidification printing process (MESO-PP): An innovative solvent-free alternative method for 3D printing using a simplified concept and low temperature. International Journal Pharmaceutics, 587: 119653.

Reddy Dumpa, N., Bandari, S. and A Repka, M., 2020. Novel gastroretentive floating pulsatile drug delivery system produced via hot-melt extrusion and fused deposition modeling 3D printing. Pharmaceutics, 12(1): 52.

Rowe, C.W., Katstra, W.E., Palazzolo, R.D., Giritlioglu, B., Teung, P. and Cima, M.J., 2000. Multimechanism oral dosage forms fabricated by three-dimensional printing™. Journal of Controlled Release, 66: 11-17.

Sadia, M., Arafat, B., Ahmed, W., Forbes, R.T. and Alhnan, M.A., 2018. Channelled tablets: An innovative approach to accelerating drug release from 3D printed tablets. Journal of Controlled Release, 269: 355-363.

Seoane-Viaño, I., Januskaite, P., Alvarez-Lorenzo, C., Basit, A.W. and Goyanes, A., 2021. Semi-solid extrusion 3D printing in drug delivery and biomedicine: Personalised solutions for healthcare challenges. Journal of Controlled Release, 332, 367-389.

Singhvi, G. and Singh, M., 2011. In-vitro drug release characterization models. International Journal Pharmacy Studies Research, 2: 77-84.

Soleymani Eil Bakhtiari, S., Bakhsheshi-Rad, H.R., Karbasi, S., Razzaghi, M., Tavakoli, M., Ismail, A.F., Sharif, S., RamaKrishna, S., Chen, X. and Berto, F., 2021. 3-Dimensional printing of hydrogel-based nanocomposites: A comprehensive review on the technology description, properties, and applications. Advanced Engineering Materials, 23(10): 2100477.

Trenfield, S.J., Awad, A., Goyanes, A., Gaisford, S. and Basit, A.W., 2018. 3D printing pharmaceuticals: drug development to frontline care. Trends in Pharmacological Sciences, 39(5): 440-451.

Trenfield, S.J., Awad, A., Madla, C.M., Hatton, G.B., Firth, J., Goyanes, A., Gaisford, S. and Basit, A.W., 2019. Shaping the future: recent advances of 3D printing in drug delivery and healthcare. Expert opinion on Drug Delivery, 16(10): 1081-1094.

Vaz, V.M. and Kumar, L., 2021. 3D printing as a promising tool in personalized medicine. American Association of Pharmaceutical Scientists, 22(1): 1-20.

Vithani, K., Goyanes, A., Jannin, V., Basit, A.W., Gaisford, S. and Boyd, B.J., 2019. An overview of 3D printing technologies for soft materials and potential opportunities for lipid-based drug delivery systems. Pharmaceutical Research, 36(1): 1-20.

Wallacec, S.S., Yood, J. and Robertsa, C.J., 2020. Extrusion 3D printing of paracetamol tablets from a single formulation with tunable release profiles through control of tablet geometry 2.

Wang, Y., Sun, L., Mei, Z., Zhang, F., He, M., Fletcher, C., Wang, F., Yang, J., Bi, D., Jiang, Y. and Liu, P., 2020. 3D printed biodegradable implants as an individualized drug delivery system for local chemotherapy of osteosarcoma. Materials and Design, 186: 108336

Wang, Z. and Yang, Y., 2021. Application of 3D Printing in Implantable Medical Devices. BioMed Research International, 2021-2021.

Wasti, S. and Adhikari, S., 2020. Use of biomaterials for 3D printing by fused deposition modeling technique: a review. Frontiers in Chemistry, 8: 315.

Water, J.J., Bohr, A., Boetker, J., Aho, J., Sandler, N., Nielsen, H.M. and Rantanen, J., 2015. Three-dimensional printing of drug-eluting im.plants: preparation of an antimicrobial polylactide feedstock material. Journal of Pharmaceutical Sciences, 104(3): 1099-1107.

Wen, H., He, B., Wang, H., Chen, F., Li, P., Cui, M., Li, Q., Pan, W. and Yang, X., 2019. Structure-based gastro-retentive and controlled-release drug delivery with novel 3D printing. American Association of Pharmaceutical Scientists, 20(2): 1-12.

Wójcik-Pastuszka, D., Krzak, J., Macikowski, B., Berkowski, R., Osiński, B. and Musiał, W., 2019. Evaluation of the release kinetics of a pharmacologically active substance from model intra-articular implants replacing the cruciate ligaments of the knee. Materials, 12: 1202.

Xu, X., Zhao, J., Wang, M., Wang, L. and Yang, J., 2019. 3D printed polyvinyl alcohol tablets with multiple release profiles. Scientific Reports, 9: 1-8.

Yang, N., Chen, H., Han, H., Shen, Y., Gu, S., He, Y. and Guo, S., 2018. 3D printing and coating to fabricate a hollow bullet-shaped implant with porous surface for controlled cytoxan release. International Journal of Pharmaceutics, 552: 91-98.

Yang, Y., Qiao, X., Huang, R., Chen, H., Shi, X., Wang, J., Tan, W. and Tan, Z., 2020. E-jet 3D printed drug delivery implants to inhibit growth and metastasis of orthotopic breast cancer. Biomaterials, 230: 119618.

Yi, H.G., Choi, Y.J., Kang, K.S., Hong, J.M., Pati, R.G., Park, M.N., Shim, I.K., Lee, C.M., Kim, S.C. and Cho, D.W., 2016. A 3D-printed local drug delivery patch for pancreatic cancer growth suppression. Journal of Controlled Release, 238: 231-241.

Zhang, J., Vo, A.Q., Feng, X., Bandari, S. and Repka, M.A., 2018. Pharmaceutical additive manufacturing: a novel tool for complex and personalized drug delivery systems. American Association of Pharmaceutical Scientists, 19(8): 3388-3402.

CHAPTER THREE
PRELIMINARY 3D PRINTED TORO-POLOIDAL PU-PEG-PLGA/HPMC DEVICES USING A 3D BIOPLOTTER

3.1 INTRODUCTION

The need for consistent daily administration of antithrombotic drugs and onus on patient compliance provides an initial outline of the research problem, viz. the development of a Drug Delivery System (DDS) that is as effective as the current development, but not as reliant on patient compliance. DDSs can be broadly described as systems that enable controlled drug release. This includes DDSs such as implants which are also referred to as Implantable Drug Delivery Devices (IDDDs). These IDDDs enable site specific and controlled drug delivery with lower drug concentrations and fewer side-effects, coupled with either increased or less reliance on patience compliance. IDDDs can be manufactured via different techniques, for example compression techniques which negate the use of solvent and heat but results in quick drug release, solvent casting which results in film formation through solvent evaporation, hot melt extrusion which requires extrusion thermoplastic polymers, injection moulding which involves thermoplastic polymers set in a mould, and 3-Dimensional Printing (3DP) techniques (Stewart et al., 2018).

The ToroPoloidal shaped 3DP IDDDs developed in this project are expected to improve the pharmacokinetics of antithrombotic drugs such as RXB, as the device will be formulated using appropriate bio-degradable polymers implanted through conventional subcutaneous methods (Stewart *et al.*, 2018). Examples of some subcutaneously implanted polymeric IDDDs include prototype polycaprolactam (PCL) film implants for HIV pre-exposure prophylaxis (Schlesinger et al., 2016), and Nexplanon® for long term delivery of contraceptives (Palomba et al., 2012). Depending on the circumstances of the patient, and reason for antithrombotic therapy, 3DP IDDDs could also be administered during surgery and inserted at the site to prevent thrombosis, for example during hip replacement surgery.

Bio-compatible polymers typically used in controlled drug delivery applications include aliphatic polyesters and polyurethanes, the application of which will also be investigated in this project. Aliphatic polyesters such as polylactide, polyglycolide, poly(ε-caprolactone), and copolymers thereof have also been applied for the manufacture of IDDDs (Stewart *et al.*, 2018), and previous

work within the WADDP research unit has also demonstrated the application thereof in novel ToroPoloidal shaped minitablets incorporating poly(lactide-co-glycolide) (PLGA), where drug release was optimized for up to 12 months (Choonara *et al.*, 2006). Since the late 1990's, bio-degradable polyurethanes (Pus) have been extensively applied for the fabrication of bio-medical devices for implants, tissue and bone engineering, wound healing, and drug delivery (Song et al., 2018). PUs is a class of condensation polymers that are characterized by the urethane group (-NHCOO-) (Lowinger et al., 2018). Amide (–NH–CO–) and ester (–COO–) moieties are generally found in peptide and lipids respectively. In this study the polymers were chosen based on previous findings as follows: polyurethane (PU) (Griffin et al., 2020), poly (lactic-co-glycolic acid) (PLGA) (Guo et al., 2017; Makadia HK, Siegel SJ., 2011; Rezvantalab et al., 2018) Polyethylene glycol (PEG) (Hutanu et al., 2014; Hoang Thi et al., 2020; D'souza and Shegokar (2016) and Hydroxypropyl methylcellulose (HPMC) (Polamaplly et al 2019; Azad et al., 2020). The novel 3D Toro-Poloidal Device was formulated with specific polymers selected based on literature searches, a combination of polymers with different properties were selected for the novelty of the device. Where 3D Toroidal refers to the direction of fill which is co-planar to the circle and poloidal refers to the direction of the fill that is perpendicular to the circle. To the best of our knowledge no one has published a study based on PU-PEG-PLGA/HPMC ink for a 3D device, this 3D Bioplotter® printed device is intended for subcutaneous implantation for extended drug delivery.

3.2 MATERIALS AND METHODS

3.2.1 Materials

Poly (D,L-lactide-co-glycolide) (PLGA, copolymer ratio 50:50, Mw=55,000g/moL) from Boehringer Ingelheim, GmbH, (Ingelheim, Germany), polyethylene Glycol (average MW 4000), polyurethane and hydroxypropyl methylcellulose (HPMC) were all purchased from Sigma-Aldrich Chemie GmbH (Steinheim, Germany). Methanol was purchased from Merck (Wadeville) and chloroform from Rochelle Chemicals (Johannesburg, South Africa). All other chemicals were of analytical grade.

3.2.2 Preliminary fabrication of the 3D printed toro-poloidal PU-PEG-PLGA/HPMC devices

The 3D printed toro-poloidal PU-PEG-PLGA/HPMC devices were fabricated using a 3D Bioplotter® (EnvisionTEC, GmBH). Firstly, the HPMC/PU-PEG-PLGA blend was formulated as a polymeric ink, where a 1:1:1 molar ratio of PU, PEG, and PLGA were formulated into a mixture then incorporated HPMC to formulate a HPMC/PU-PEG-PLGA polymeric ink. Typically, PU and PLGA

were separately dissolved in chloroform, to attain a clear yellow and white solution, respectively. PEG was added into the PU solution before the addition of PLGA solution, resulting into a clear light-yellow solution which was then stirred for two hours at room temperature. To improve the viscosity of the PU-PEG-PLGA gel like mixture, 12% w/v of HPMC in methanol was added and made into a homogenous HPMC/PU-PEG-PLGA gel blend**.**

The HPMC/PU-PEG-PLGA blend was used as a biopolymeric ink for the 3D devices, CAD was utilised to create the desired structure of the devices. The importing software of the STL data and the control of the 3D Bioplotter® consisted of two modules: (i) the 3D Bioplotter® software for STL data importation and structure (e.g., implant) slicing; and (ii) the Visual Machine software for material parameters and machine control. The scaffold was printed at room temperature (25°C) where the HPMC/PU-PEG-PLGA biopolymeric ink was fed into a 30 cm^3 cartridge and dispensed through a plastic needle (nozzle diameter 0.41mm), under a pressure of 2.0 Bar and deposition speed of 7 mm/s. The layers were deposited at 90-degree angle and layers were successively printed with the average delay time between layers of 30 seconds. The 3D printed toro-poloidal PU-PEG-PLGA/HPMC devices were printed using parameters as described in **Table 3.1.**

Table 3.1.: Parameters used for the 3D printed toro-poloidal PU-PEG-PLGA/HPMC devices

Parameter	**Value**
Temperature	25°C
Pressure	2.0 Bar
Bar Speed	7 mm/s
Platform temperature	25°C
Delay time between layers	30 sec

3.3 RESULTS AND DISCUSSION

3.3.1 Preliminary evaluation of the fabrication of the 3D printed toro-poloidal PU-PEG-PLGA/HPMC devices

As illustrated in **Figure 3.1**, the preliminary images of the novel 3D printed toro-poloidal PU-PEG-PLGA/HPMC devices was designed and printed using a 3D Bioplotter® (EnvisionTEC, GmBH). This 3D bio-printed device highlights a novel application of the PU-PEG-PLGA/HPMC polymeric ink, with the challenge being the solidification of the bio-plotted strands. Stable solidification is required to enable the next layer to be printed on top of the previous layer, which is vital for this

layer-by-layer fabrication approach of the Bioplotter®. Chloroform and methanol were the solvents of choice because they are both nontoxic as well as volatile, allowing for the fabrication of the PU-PEG-PLGA/HPMC architecture as they allowed for easy solidification of the printed strands.

Due to technical issues of the Bioplotter® the 3DP toro-poloidal PU-PEG-PLGA/HPMC device design was not optimised, **Figure 3.1** illustrates the toro-poloidal device at different stages of layering, at 7, 11 and 16 layers, to be noted is that the more layers were fabricated the thicker was the device. The 3D toroidal layering system was archived as both the co-planar and perpendicular layering directions are observed within the different layers. The poloidal direction is following a small circular ring around the surface, while the toroidal direction follows a large circular ring around the torus, encircling the central void.

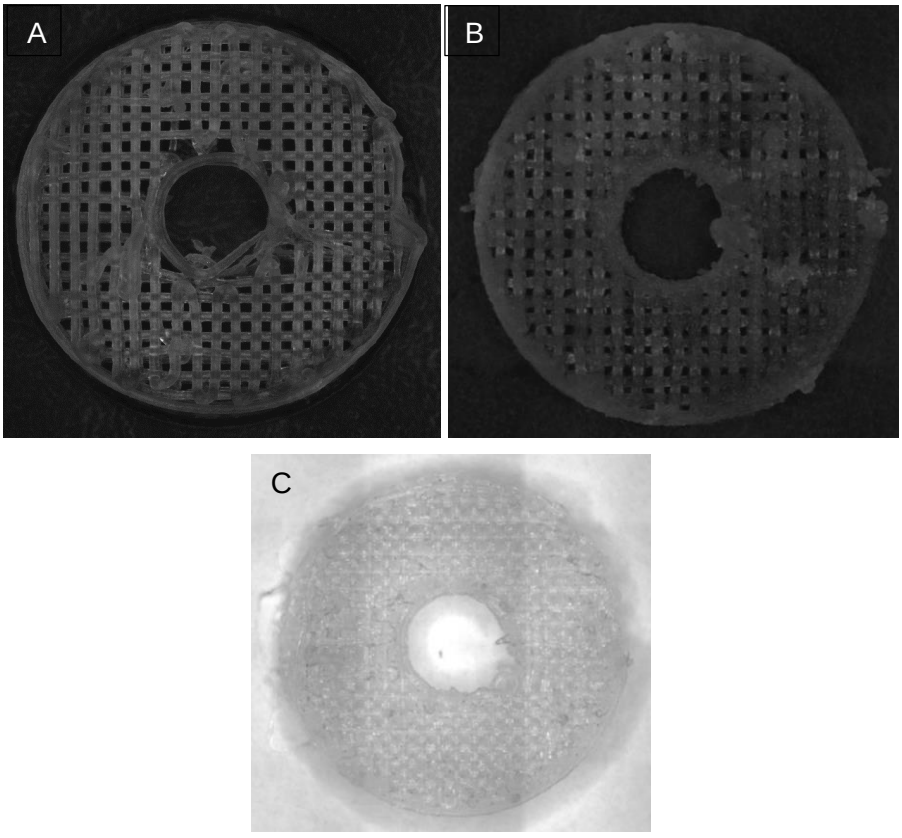

Figure 3.1. The pictorial results of the devices printed on preliminary studies, A) 7 layers with a thickness of 1.920 mm, B) 11 layers with a thickness of 3.2 mm 11 layers 3.2 mm, and C) 16 layers with a thickness of 4.800 mm**.**

3.4 CONCLUSION

In this preliminary study a polymer's ink formulation was prepared from PU, PEG, PLGA and HPMC, with chloroform and methanol as solvents. The ink formulation was then employed to print a preliminary toro-podial device via the 3D Bioplotter®, where the evaporation of chloroform and methanol showed to be an effective mechanism for solidification and fabrication of the toro-podial device. However, due to some maintenance delays on the 3D Bioplotter the study had to focus on other comparative formulation methods producing pressed tablets. The study was deviated into other methods using available equipment i.e., the extrusion-based 3D formulation using a Texture Analyzer (TA) (TA. XT plus, Stable Microsystems, Surrey, UK) and direct compressed using a Manesty F3 eccentric compressor (Oystar Manesty (Pty) Ltd., Merseyside, England). In-vitro dissolution studies were carried out for both the compressed and extruded tablets to explore the effects of the two formulation techniques as well as the shapes of the tablets.

With the PU-PEG-PLGA/HPMC polymeric ink that was used for 3D bioplotter it was noted that the TA extrusion force of up to 15 kg was not able to extrude the ink, the ink had to be diluted in chloroform to allow for extrusion using the TA. As the solidification and fabrication of the ink is directly dependent on the drying of extruded strands it became impossible to fabricate the toro-poloidal device with desired architecture using the TA independently. What was also noted was that the less viscous extruded strands were too weak/not dry enough to withhold individual strands into layers as the 3D bioplotter. The compressed tablets showed promising results when compared to the extruded tablets, resulting into the direct compression method being preferred over the extrusion-based formulations, in chapter 4 and 5 the different formulation techniques are detailed.

3.5 REFERENCES

Algahtani, M.S., Mohammed, A.A. and Ahmad, J., 2018. Extrusion-based 3D printing for pharmaceuticals: Contemporary research and applications. Current Pharmaceutical Design, 24(42): 4991-5008.

Alhnan, M.A., Okwuosa, T.C., Sadia, M., Wan, K.W., Ahmed, W. and Arafat, B., 2016. Emergence of 3D printed dosage forms: opportunities and challenges. Pharmaceutical research, 33(8): 1817-1832.

Azad MA, Olawuni D, Kimbell G, Badruddoza AZ, Hossain M, Sultana T., 2020. Polymers for Extrusion-Based 3D Printing of Pharmaceuticals: A Holistic Materials–Process Perspective. Pharmaceutics, 12(2):124.

Choonara, Y.E., Pillay, V., Carmichael, T. & Danckwerts, M.P. 2006. An in vitro study of the design and development of a novel doughnut-shaped minitablet for intraocular implantation. International Journal of Pharmaceutics, 310(1):15-24.

D'souza, A. A., & Shegokar, R., 2016. Polyethylene glycol (PEG): a versatile polymer for pharmaceutical applications. Expert Opinion on Drug Delivery, 13(9): 1257–1275.

Gao, G., Ahn, M., Cho, W.W., Kim, B.S. and Cho, D.W., 2021. 3D printing of pharmaceutical application: drug screening and drug delivery. Pharmaceutics, 13(9): 1373.

Goyanes, A., Det-Amornrat, U., Wang, J., Basit, A.W. and Gaisford, S., 2016. 3D scanning and 3D printing as innovative technologies for fabricating personalized topical drug delivery systems. Journal of Controlled Release, 234: 41-48.

Griffin, M., Castro, N., Bas, O., Saifzadeh, S., Butler, P. and Hutmacher, D.W., 2020. The current versatility of polyurethane three-dimensional printing for biomedical applications. Tissue Engineering Part B: Reviews, 26(3): 272-283.

Guo T, Holzberg TR, Lim CG, Gao F, Gargava A, Trachtenberg JE, Mikos AG, Fisher JP., 2017. 3D printing PLGA: a quantitative examination of the effects of polymer composition and printing parameters on print resolution. Biofabrication. 12; 9(2):024101.

Hoang Thi, T.T., Pilkington, E.H., Nguyen, D.H., Lee, J.S., Park, K.D. and Truong, N.P., 2020. The importance of poly (ethylene glycol) alternatives for overcoming PEG immunogenicity in drug delivery and bioconjugation. Polymers, 12(2): 298.

Hutanu, D., Frishberg, M.D., Guo, L. and Darie, C.C., 2014. Recent applications of polyethylene glycols (PEGs) and PEG derivatives. Modern Chemistry and Applications, 2(2): 1-6.

Jamróz, W., Szafraniec, J., Kurek, M. and Jachowicz, R., 2018. 3D printing in pharmaceutical and medical applications–recent achievements and challenges. Pharmaceutical Research, 35(9): 1-22.

Kimbell, G. and Azad, M.A., 2021. 3D printing: Bioinspired materials for drug delivery. In Bioinspired and Biomimetic Materials for Drug Delivery, 295-318.

Kjar, A. and Huang, Y., 2019. Application of micro-scale 3D printing in pharmaceutics. Pharmaceutics, 11(8): 390.

Lowinger, M.B., Barrett, S.E., Zhang, F. & Williams, R.O., 3rd 2018. Sustained release drug delivery applications of polyurethanes. Pharmaceutics, 10(2).

Ma, X., Liu, J., Zhu, W., Tang, M., Lawrence, N., Yu, C., Gou, M. and Chen, S., 2018. 3D bioprinting of functional tissue models for personalized drug screening and in vitro disease modeling. Advanced Drug Delivery Reviews, 132: 235-251.

Makadia HK, Siegel SJ. Poly lactic-co-glycolic acid (PLGA) as biodegradable controlled drug delivery carrier. Polymers. 20113(3):1377-97.

Maulvi, F.A., Shah, M.J., Solanki, B.S., Patel, A.S., Soni, T.G. and Shah, D.O., 2017. Application of 3D printing technology in the development of novel drug delivery systems. International Journal of Drug Development and Research, 9(1): 0-0.

Osouli-Bostanabad K, Adibkia K., 2018. Made-on-demand, complex and personalized 3D-printed drug products. Bio Impacts, 8(2):77.

Palomba, S., Falbo, A., Di Cello, A., Materazzo, C. & Zullo, F. 2012. Nexplanon: the new implant for long-term contraception. A comprehensive descriptive review. Gynecological Endocrinology, 28(9):710-721.

Park, B.J., Choi, H.J., Moon, S.J., Kim, S.J., Bajracharya, R., Min, J.Y. and Han, H.K., 2019. Pharmaceutical applications of 3D printing technology: current understanding and future perspectives. Journal of Pharmaceutical Investigation, 49(6): 575-585.

Pavan Kalyan, B.G. and Kumar, L., 2022. 3D Printing: Applications in Tissue Engineering, Medical Devices, and Drug Delivery. Pharmaceutical Sciences, 23(4):1-20.

Peng, W., Datta, P., Ayan, B., Ozbolat, V., Sosnoski, D. and Ozbolat, I.T., 2017. 3D bioprinting for drug discovery and development in pharmaceutics. Acta Biomaterialia, 57, pp.26-46.

Polamaplly, P., Cheng, Y., Shi, X., Manikandan, K., Kremer, G.E. and Qin, H., 2019. 3D printing and characterization of hydroxypropyl methylcellulose and methylcellulose for biodegradable support structures. Procedia Manufacturing, 34: 552-559.

Rezvantalab, S., Drude, N.I., Moraveji, M.K., Güvener, N., Koons, E.K., Shi, Y., Lammers, T. and Kiessling, F., 2018. PLGA-based nanoparticles in cancer treatment. Frontiers in Pharmacology, 9: 1260.

Schlesinger, E., Johengen, D., Luecke, E., Rothrock, G., McGowan, I., van der Straten, A. & Desai, T. 2016. A tunable, biodegradable, thin-film polymer device as a long-acting implant delivering tenofovir alafenamide fumarate for HIV pre-exposure prophylaxis. Pharmaceutical Research, 33(7):1649-1656.

CHAPTER FOUR
A NOVEL POLYMERIC FORMULATION FOR RIVAROXABAN LOADED 3D DEVICES

4.1 INTRODUCTION

Amongst the growing demand for customized devices combined with an expansion of technological innovation drives the major progress in personalized medicine expressed (Tappa K, Jammalamadaka U, 2018). There is a constant motivation towards new concepts in drug design, better understanding of material properties, manufacturing technology and processes that assures high quality of dosage forms (Jamróz et al., 2018). The diversity of physicochemical and biopharmaceutical characteristics of the pharmaceutical ingredients has to be considered and studied through each stage of product development (Jamróz et al., 2018; Tappa and Jammalamadaka, 2018). New 3D device approaches allow structures of significant size to be formulated in minutes and certain polymeric materials are approved for each device. Despite all these finding and developments, more studies still have to be directed towards establishing new 3D devices with excellent release systems. Currently in the pharmaceutical industry various polymer-based materials are widely implemented for 3D innovations (Tian et al., 2021).

Within many 3-Dimensional (3D) discoveries introduced into pharmaceutical and biomedical market, polymeric-based 3D structures are believed to be the most revolutionary and powerful devices for drug delivery purposes (Jamróz et al., 2018). The variety of polymeric materials have the ability to satisfy the demand for patient-personalized models, tools and devices, additionally it allows 3D devices to be formulated using different methods (Nadagouda, Rastogi, and Ginn, 2016). Various polymer-based 3D devices have been formulated to accommodate a wide array of surgical guides and other tools as well as for the production of medical model implants, abutments, crowns, bridges and CT-imaged tissue replicas (Stansbury and Idacavage, 2016). Polymeric material offers a clear environmental advantage in terms of recyclability, biocompatible hence they have become a greater choice of materials in 3D devices (Mazzanti, Malagutti, and Mollica, 2019).

Polymers play a pivotal role in the design of engineered delivery systems (Nyamweya et al., 2021). Although there are many types and classes of polymers available for the development of such systems, there is a need for better polymer properties that enable better drug loading and release outcomes. Additionally, biosafety remains a top priority, and therefore the use of new

polymers is regarded as a limiting design approach. As such the use of polymeric blends offers an alternative approach for the design of controlled release delivery systems by mitigating the limitations of individual polymers while benefiting from the combination of polymers. Blends are gaining importance in biomedical implants as they provide room for novel pharmaceutical products with improved properties, they are straightforward, time-saving (Maghsoudi et al., 2020) and blends may present with fewer side effects compared to native polyesters (Ilyés et al., 2019; Nyamweya et al., 2021). The motivation for blending in 3D devices being the ability to manipulate polyesters into customized drug delivery profiles for personalized devices.

Polymeric materials currently used in pharmaceutical products include commodities such as the polyolefin (i.e., polyethylene PE and polypropylene PP), acrylonitrile-butadiene-styrene (ABS), engineering plastics, such as polycarbonate (PC), polysulfone (PSU) or polyetherimide (PEI) and biodegradable materials like poly-(lactic acid) (PLA) (Mazzanti, Malagutti, and Mollica, 2019). In this study, four different types of polymers were each selected based on their properties. As the implant is expected to release the drug over an extended period polyurethane (PU) was selected due to their good biocompatibility, mechanical properties, and hemocompatibility in implantable medical devices (Griffin et al., 2020). PU is a polymeric material with high performance physical properties (tough, abrasion-resistant and heat-resistant) derived from a combination of amide (–NH–CO–) and ester (–COO–) groups that are present in the structure of peptides and lipids, respectively. In addition, the “segmented” structure of PU resembles the “domain” structure of a protein, hence these unique chemical and physical characteristics of PU make them suitable for 3D devices used in biomedical applications (Hung, Tseng and Hsu, 2016).

This study also used poly (lactic-co-glycolic acid) (PLGA) as the device resin, as it has been widely used for 3D devices such as scaffolds (Guo et al., 2017; Makadia HK, Siegel SJ., 2011). PLGA is a synthetic polymer that is frequently used in 3D formulated medical devices due to its biocompatibility and tunable mechanical properties (Guo et al., 2018; Rezvantalab et al., 2018)). Polyethylene glycol (PEG) was also utilized for its biomedical properties with its excellent biocompatibility, good tolerance and solubility in aqueous media (Hutanu et al., 2014; Hoang Thi et al., 2020). PEG is a hydrophilic oligomer or polymer synthesized from ethylene oxide, consisting of a repeating unit of – (O – CH2 – CH^2) – (Hutanu et al., 2014; D’souza and Shegokar (2016)), especially suitable as cross-linking agents or spacers between two chemical entities.

Additionally, Hydroxypropyl methylcellulose (HPMC) was use as a supporting material due to its gelation property, which is suitable for 3D devices (Polamaplly et al 2019). HPMC is a water-soluble polymer that enhances the sustained release capabilities, and HPMC based hydrogels have been previously used for 3D designs in pharmaceutical products (Polamaplly et al 2019; Azad et al., 2020). To the best of our knowledge no one has published a study based on PU-PEG-PLGA/HPMC hydrogel for a 3D device, hence paper focuses on the model polymeric material selected for the 3D implantable toro-poloidal devices and its characterization.

4.2 MATERIAL AND METHODS

4.2.1 Materials

Poly (D, L-lactide-co-glycolide) (PLGA, copolymer ratio 50:50, Mw=55,000g/moL) from Boehringer Ingelheim, GmbH, (Ingelheim, Germany). Polyethylene Glycol (average MW 4000), Polyurethane, Oleic acid, polysorbate-40, hydroxypropyl methylcellulose (HPMC) and sodium chloride (NaCl) were all purchased from Sigma-Aldrich Chemie GmbH (Steinheim, Germany). Buffering constituents: potassium chloride, potassium dihydrogen phosphate, disodium hydrogen phosphate, sodium chloride, sodium hydroxide pellets, and hydrochloric acid, as well as methanol, dimethyl sulfoxide (DMSO were purchased from Merck (Wadeville). Deionised water was obtained from a Milli-Q system (Milli-Q, Millipore, Johannesburg) and chloroform from Rochelle Chemicals (Johannesburg, South Africa). All other chemicals were of analytical grade.

4.2.2 Formulation of PU-PEG-PLGA/HPMC blend

The RXB loaded HPMC/PU-PEG-PLGA blend was formulated using a 1:1:1 molar ratio of PU, PEG, and PLGA, the PU-PEG-PLGA blended mixture was then incorporated into HPMC to formulate RXB loaded HPMC/PU-PEG-PLGA. Briefly, PU and PLGA were separately dissolved in chloroform, to attain a clear yellow and white solution, respectively. PEG was added into the PU solution before the addition of PLGA solution, resulting into a clear light-yellow solution which was then stirred for two hours at room temperature. Separately, RXB was solubilized as described by Xue and co-workers (2018), where a mixture of polysorbate-40 and oleic acid (50:50 v/v) was used to dissolve 40mg/ml of RXB, added into the PU-PEG-PLGA clear solution and stirred for another hour. Lastly, to improve the gelation of the RXB loaded PU-PEG-PLGA, 12% w/v of HPMC in methanol was added and made into a homogenous RXB loaded HPMC/PU-PEG-PLGA blend. For analysis the RXB loaded HPMC/PU-PEG-PLGA blend was washed (three times)

with distilled water, frozen and then lyophilized, where the samples were primarily freeze dried between -2 and -8 °C , over a period of 24 h.

For direct compression into 3D devices the lyophillised RXB loaded HPMC/PU-PEG-PLGA blend was compressed using a Manesty F3 eccentric compressor (Oystar Manesty (Pty) Ltd., Merseyside, England). This project only focuses on donut and cylinder-shaped devices. The same mold was used for both shapes, with an additional rod inserted in the middle of the mold for donut shaped devices, **Figure 4.1.** shows the compression method process in four stages. The compressor exerts pressure only on the top puncher which is opposed by the bottom puncher, resulting in tablets with desired geometry.

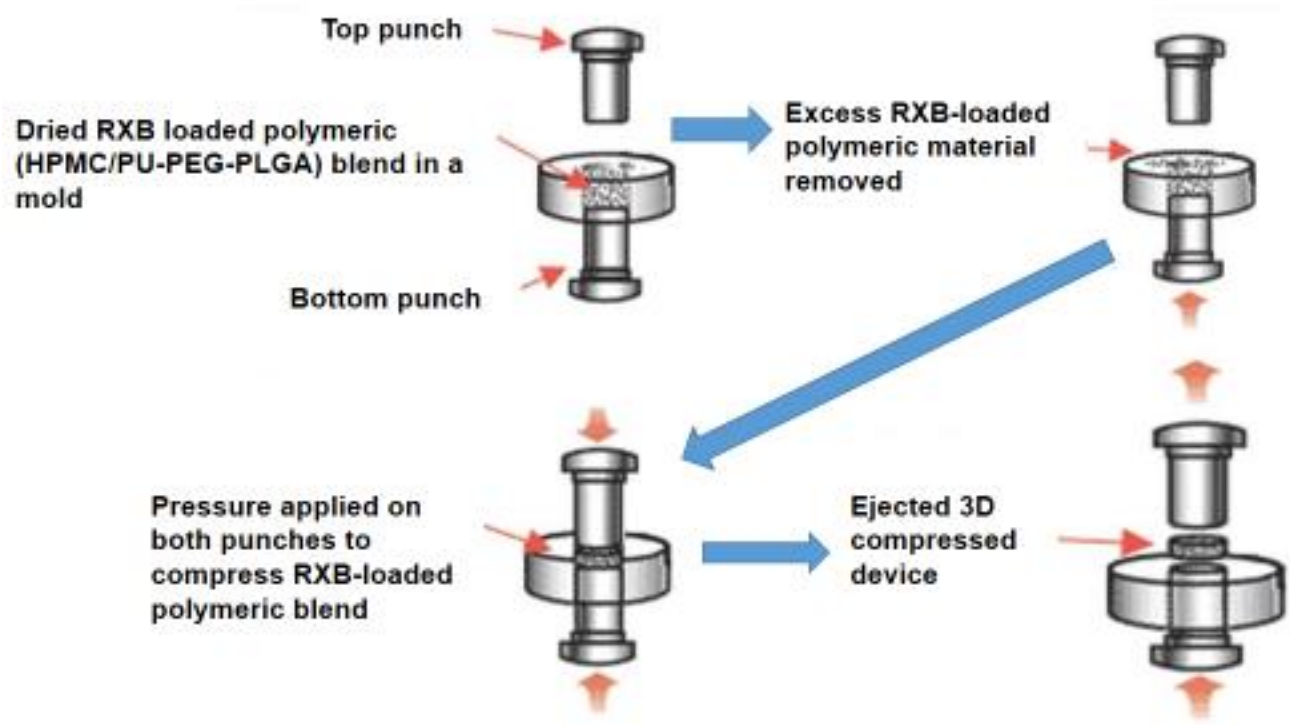

Figure 4.1. The 3D device compression process from stage 1 to 4.

Porous and non-porous donut shaped tablets were also fabricated for comparison purposes using the direct compression method. Porous 3D devices were formulated by an addition of NaCl into the PU-PEG-PLGA/HPMC mixture, where NaCl served as a pore forming or porogen agent.

The hardness, diameter, thickness and friability of the implantable tablets was obtained from Hardness tester PTB 111EP (Pharma Test Apparatebau, Germany).

4.2.3 Quantification of RXB loaded into the polymeric blend

The content of RXB loaded into the PU-PEG-PLGA/HPMC blend was determined using a UV spectrophotometric method (adapted from Kumar et al., 2015) and calibration curve was utilized as per Çelebier and co-workers (2014).

4.2.3.1 RXB calibration Standards

A stock standard solution of RXB (1000 µg/mL) was prepared by dissolving 5 mg of RXB in 5 mL of Acetonitrile, based on the quantification of RXB of on section **4.2.3** ~85 mg of the dried RXB loaded PU-PEG-PLGA/HPMC was weighed to make up the 5 mg RXB. Calibration standards (1.0, 3.0, 5.0, 10.0, 20.0, 30.0, and 50.0 µg/mL) were prepared daily from the stock standard solution by appropriate dilution using Acetonitrile /water (50:50 v/v) mixture as a dissolution buffer.

4.2.3.2 Quantity of RXB loaded in the novel polymeric blend

Weighed 10 mg of the lyophilized RXB loaded PU-PEG-PLGA in HPMC and dissolved in 2 mL DMSO (5000 µg/mL) into a clear solution, then using a 100ml volumetric flask it was filled to the mark with an acetonitrile /water (50:50 v/v) mixture. The analyte was analyzed using the UV–Vis spectrophotometer (PerkinElmer Spectrum 100, Llantrisant, Wales, UK), and recorded in 1-cm quartz cells. The absorbance was measured at 270 nm.

4.2.4. Assessment of the chemical transitions of the novel PU-PEG-PLGA/HPMC and RXB loaded PU-PEG-PLGA/HPMC

Fourier-transform infrared (FTIR) spectra were recorded in the in the range of 4000-650 cm^{1} which suitable for the observation of molecular motions of biopolymers. Comparative analysis of native polymers, novel PU-PEG-PLGA/HPMC and RXB loaded were done to provide information with regards to any changes in the chemical moieties present and this was used to infer if there were any chemical interactions present.

4.2.5 Determination of chemical interaction and crystallinity of the novel PU-PEG-PLGA/HPMC and RXB loaded PU-PEG-PLGA/HPMC

X-ray diffraction (XRD) (MiniFlex 600, Rigaku, Japan) containing nickel-filtered Cu Kα radiation (a voltage of 40 kV and a current of 30 mA) was utilized to determine the X-ray patterns of the novel PU-PEG-PLGA/HPMC and RXB loaded PU-PEG-PLGA/HPMC, compared to all the innate polymers. X-ray diffractogram was obtained at a scanning rate of 15^{o}/min to 2θ from 5-60^{o} at room temperature.

4.2.6 Determination of thermal events for the innate components, RXB loaded and non-loaded HPMC/PU-PEG-PLGA

Thermograms of the pristine polymers and the novel PU-PEG-PLGA/HPMC and RXB loaded PU-PEG-PLGA/HPMC was recorded utilizing the Differential Scanning Calorimetry (DSC) thermal analyzer to account for relative thermal changes and stability. Weighed ~10 mg of dried samples, placed them in aluminum pans and heated in a nitrogen-controlled environment at 10 ˚C/min. These results were used to assess the thermal stability of the novel PU-PEG-PLGA/HPMC and RXB loaded PU-PEG-PLGA/HPMC.

Thermogravimetric analysis (TGA) was performed using a Toledo TC15 TA controller (Mettler). It was used to measure how the changes in the chemical and physical properties of the novel PU-PEG-PLGA/HPMC and RXB loaded PU-PEG-PLGA/HPMC compared to the innate, polymer and RXB. Dried sample measurements of 5mg were analyzed after tarring the empty crucibles. The analysis was carried out from 25 to 800 °C, using a heating rate of 10 °C/min under a constant nitrogen gas flow. The percentage weight losses incurred during the heating cycle were estimated using the associated software (STARe).

4.2.7 Porosity analysis of the RXB loaded PU-PEG-PLGA/HPMC device

As changes in porosity affects the overall drug release of the device, a porositometric analysis was performed employing an ASAP 2020 Porositometer (Micromeritics Instrument Company (Pty) Ltd., Norcross, GA, USA) equipped with research grade ASAP 2020 V3.01 software. Briefly, the surface area and pore structure were analysed by degassing the RXB loaded PU-PEG-PLGA/HPMC porous compared to the non-porous device samples (mass=100 mg; density = 1g/cm^3) in order to remove sample moisture and atmospheric vapour by applying a heat gradient and evacuating with Nitrogen gas (N_2) (hard-sphere diameter = 3.860 Å; molecular cross-section

= 0.162 nm^2) that was used as a non-adsorbent gas. The overall hold pressure for the evacuation and heating phases during the degassing procedure was maintained at 100 mmHg. The sample temperature was then reduced by an adaptive rate technique (continuous) to that of liquid N_2 (-197.165 °C) for gas adsorption (maximum manifold pressure set at 925 mmHg) using an isothermal jacket surrounding a sample tube with a warm and cold free-space of 1 cm^3. The analysis was done under standard conditions of temperature and pressure (STP: 0°C and 760 torr). Adsorption isotherms representing the accumulated molar quantity of N_2 adsorbed and the gas pressure at a single constant temperature was generated. The pressure was expressed as the ratio between the relative actual N_2 pressure (P) and the vapour pressure (P_0) of N_2.

4.2.8 Dissolution Studies of RXB loaded PU-PEG-PLGA/HPMC

Dissolution studies were performed in USP 37 type II automated dissolution test apparatus (ElectrolabTDT-08L, Mumbai, India). The dissolution profiles of RXB loaded PU-PEG-PLGA/HPMC donut shaped implants were determined in triplicate using 900 mL of PBS at pH 7.4 (dissolution medium) maintained at 37±0.5°C and stirred at 50 rpm. Tableted samples RXB loaded PU-PEG-PLGA/HPMC were used with weights 170.6, 173.6 and 168.3 mg equivalent to ˜ 10 mg of RXB were added into the dissolution vessel. Samples of 1 mL were withdrawn at specific time points (0.50, 1, 2, 4, 6, 8, 10, 12, 24, 48 and 72 h) and filtered using 0.22 µm syringe filter. Equal volume of fresh dissolution medium was replenished each time immediately after the withdrawal of the aliquots to maintain the sink condition. Dissolution of 10mg RXB was done as a comparative study applying the same method. The concentration of RXB in samples was determined by UV–Vis spectrophotometer (PerkinElmer Spectrum 100, Llantrisant, Wales, UK), recorded in 1-cm quartz cells at 270 nm.

4.2.9 *In-vitro* drug release of porous and non-porous RXB loaded PU-PEG-PLGA/HPMC donut tablets

In-vitro drug release porous and non-porous RXB loaded PU-PEG-PLGA/HPMC donut tablets was performed in PBS pH 7.4 buffer at 37°C using dialysis membranes (MWCO: 1.2 kDa). Both the porous and non-porous tablets were placed in dialysis bags and immersed into 50 mL buffer solutions. At a predetermined time (0.5, 1, 2, 4, 6, 8, 12, 24 and 72 h) 1 mL of the buffer was taken out and the same amount of fresh buffer was added to make up the constant volume for the release medium. Additionally, an extended release of the RXB loaded donut tablet was done until

the RXB was all released. Absorbance was quantified using the UV-Vis spectrophotometry at 270 nm, concentration versus absorbance calibration curves were then employed to quantify RXB.

4.2.10 Statistical analysis

Data were expressed as mean ± standard deviation, where the correlations were assessed by a correlation coefficient (R^2) which was used to evaluate the accuracy of the data reported, and each value represents the mean ± SD; n = 3.

4.3. RESULTS AND DISCUSSION

4.3.1. The formulation of RXB loaded and HPMC/PU-PEG-PLGA

To evaluate the clarity, uniformity, homogeneity, and shape, all 3D devices were visually inspected**.** The PU-PEG-PLGA blend was formulated by adding PU, PEG and PLGA in equal molar ratios, resulting into a clear light-yellow gel, where a 12 % HMPC was then added to the white gel-blend for 3D formulation of the device. The blend was lyophilized to a HPMC/PU-PEG-PLGA dried powder that was used for characterisation and compressing into a white 3D donut shaped device. The formulated devices are shown on **Figure 4.2**, with an average weight of 170.8 mg (n=6), diameter of 20.54 cm with 5.04 cm thickness and an average hardness (n=6) of 14.98 Kg/cm^2, and according to Karim and co-workers (2016) the acceptable hardness for such a device is ≥5 Kg/cm^2, hence all the devices were considered to be of a desirable tensile strength. The friability of the formulated devices was below 1 % (n=6), indication a good mechanical resistance for all formulations as per Pharmacopoeia limits (Reddy et al., 2018).

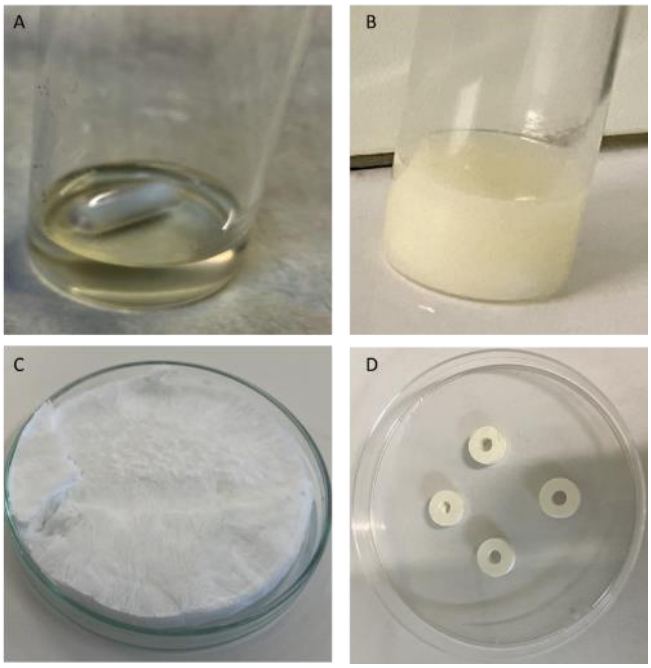

Figure 4.2. The formulated devices (A) PU-PEG-PLGA gel, (B)PU-PEG-PLGA/HPMC, (C) lyophiliised powder of PU-PEG-PLGA/HPMC and (D) PU-PEG-PLGA/HPMC 3D devices.

4.3.2 Quantity of RX loaded in the novel PU-PEG-PLGA/HPMC

To quantify the amount of drug/weight of PU-PEG-PLGA/HPMC final formulation a calibration curve was first established, see calibration curve on **Figure 4.3**. The absorbance data reported in triplicates, and $p < 0.05$.

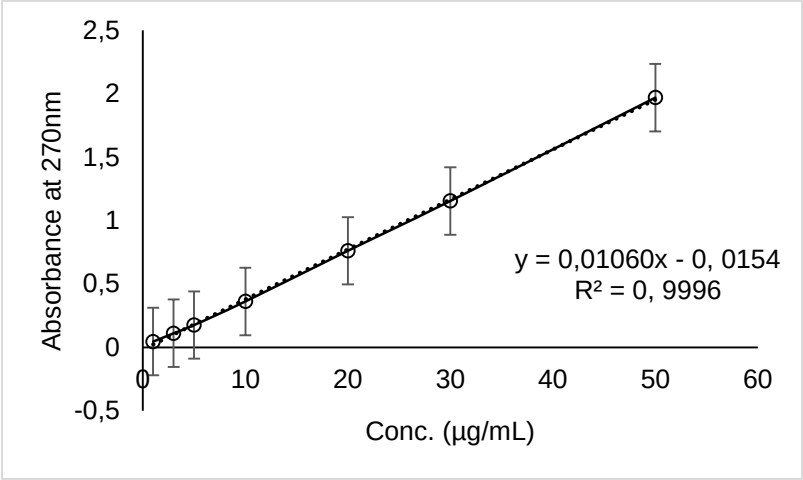

Figure 4.3. Calibration curve established by plotting the absorbance obtained from UV-Vis versus known concentrations of RXB.

The absorbance readings were done in triplicates for a 325 µg/mL RXB-loaded polymeric blend, with the following readings: 0,529, 0,532 and 0,530 with a mean of 0,530. The calibration equation was used to determine the concentration of RXB as 51,435 µg/m, which is 4.1% of the total blend formulation. This gives a total of approximately 10 mg of RXB per 3D device. The RXB content in the formulated devices was established to be within therapeutic safe index (Xue et al., 2018).

4.3.2 FTIR analysis of the innate components, RXB loaded and non-loaded HPMC/PU-PEG-PLGA

FTIR spectroscopy technique was employed to confirm the structure of PLGA, PEG, PU, HPMC and RXB in the blend, the results were consistent with the results from previous reports about PLGA-PEG and PU-PEG copolymers (Huang J, 2010; Wang et al., 2012; Gajendiran et al., 2014; Chen et al., 2017; Xu et al., 2017; Ngo et al., 2019). The peaks at 2887, 1342 and 963 cm^{-1} showed the methylene group near the oxygen atom and methyl groups in PLGA-PEG. A strong band observed at 1749 cm^{-1} corresponds to the carbonyl stretching frequency of the succinate group which is not present in the PEG spectrum (**Figure 4.4D**). A strong band appearing at 1085 cm^{-1} is due to the stretching frequency of the C–O-C group which confirms the presence of the succinate group as well as PEG.

The absorption peaks at 1749 cm^{-1} and 1560 cm^{-1} were responsible for the carbonyl groups and the C-N bonds, respectively and the peak at 1453 cm^{-1} was the symmetry bending vibration peak of -CH_2-. The 1222 cm^{-1} bond was assigned to ester C-O-C stretching in the PU fragment, **Figure 4.4E**. A band centered at about 1080cm^{-1} was clearly seen, attributed to the C-O-C stretching vibration of PEG. Meanwhile, the HPMC was characterized by the peak at 1082 - 1056 cm^{-1} due to the C–O stretch, the C=O stretch was due to the appearance the spectra between 1753 – 1600 cm^{-1} (**Figure 4.4A**). The above confirms no interaction between innate polymers and RXB in the blend matrix, as there are no observed new absorption bands. The FTIR analysis established the formation of the RXB loaded and non-loaded HPMC/PU-PEG-PLGA blend, and that the individual structures of the innate polymers were not changed just blended.

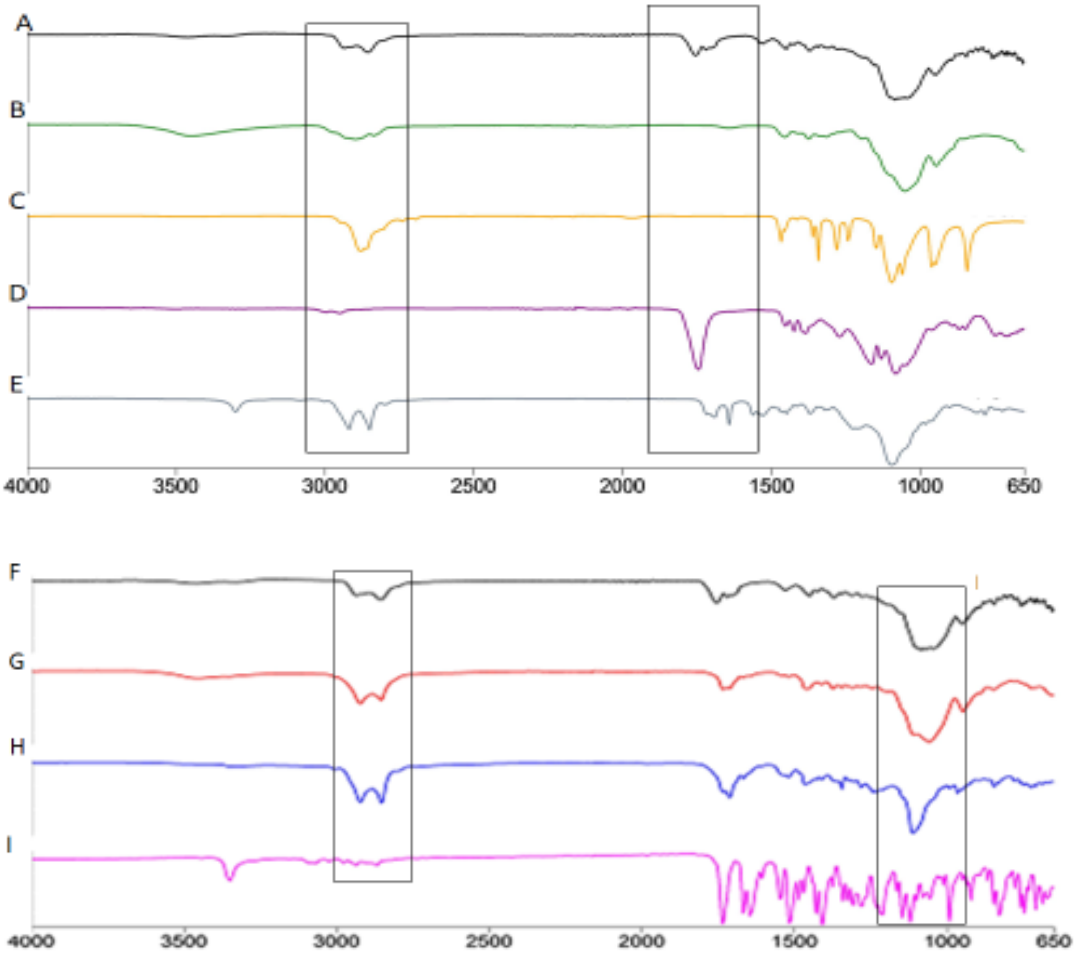

Figure 4.4. The FTIR of the innate components and the blend, (A) HPMC/PU-PEG-PLGA, (B) HPMC, (C) PLGA, (D) PEG, (E) PU, (F) HPMC/PU-PEG-PLGA, (G) RXB loaded HPMC/PU-PEG-PLGA, (H) PU-PEG-PLGA and (I) RXB

4.3.3 X-ray analysis of the innate components, RXB loaded HPMC/PU-PEG-PLGA

The nature or internal physical state of the innate polymers, the drug and the polymeric blends were also assessed by XRD, which is a great tool to assess the crystalline lattice arrangement. **Figure 4.5.** shows the crystallographic characteristics PLGA, PEG, PU, PEG, RXB and their physical mixtures. The diffractograms of RXB showed the most intensive peak at 22.44° which is one of the distinctive peaks of RXB (Xu et al., 2017), all the peaks seen on this diffractometry are evident of the pure drug's crystallinity compared to the RXB loaded blend. The PLGA, PU and HPMC showed more amorphous (less crystallinity) peaks compared to the PEG and RXB, as a number of reports have shown most polymeric material being characterised by amorphous peaks

(Wang et al., 2016; Yelles et al., 2017). The PU-PEG-PLGA and HPMC/PU-PEG- PLGA, exhibited broad peaks from 20.56° to 22.54° and 19.02° to 23.32°, respectively, with the RXB loaded and non-loaded HPMC/PU-PEG-PLGA showing even broader peaks (less crystallinity), and the RXB loaded HPMC/PU-PEG-PLGA having a better crystallinity compared to the formulation free of drug, this may be attributed to the presence of RXB. The broad peaks are indicative of the reduction in crystallinity of the innate components in the blend, which confirms the presence of numerous compounds (Liu et al., 2020), hence the success of the blend formulation. In the case of the RXB loaded and non-loaded HPMC/PU-PEG-PLGA, numerous distinct peaks are evident, indicating that crystallinity was reduced in comparison to the RXB and the innate polymers.

The fact that the XRD peaks of the innate polymers and RXB were clearly visible in the respective diffractograms compared to the blends and RXB-polymeric blend is indicative of the changes in the crystallinity, as more than one component are blended and after RXB loading. These differences show the change in components as they are blended and might affect various key properties of implantable device i.e., the swelling and disintegrating properties which ultimately controls the RXB release pattern, similar XRD changes were reported by Yelles et al. (2017). The drug peaks disappeared in the RXB loaded HPMC/PU-PEG-PLGA blend and this deduces that the drug may be present in an amorphous state.

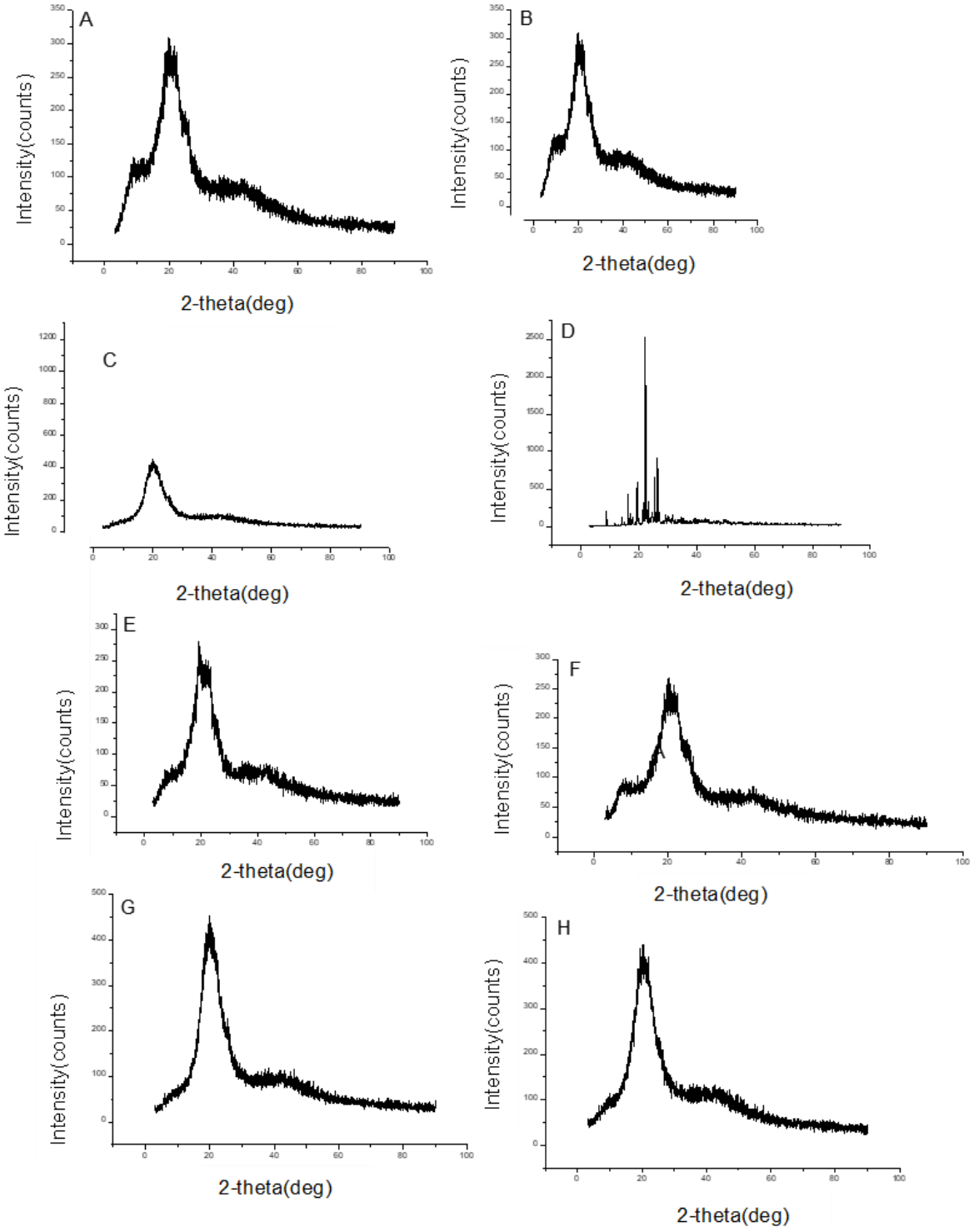

Figure 4.5. X-ray diffraction patterns of the innate polymers and RXB, physical mixtures thereof as well as RXB loaded polymeric powder blend, (A) PLGA, (B) HPMC, (C) PEG, (D) RXB, (E) PU-PEG-PLGA, (F) HPMC/PU-PEG- PLGA, (G) PU, and (H) RXB loaded HPMC/PU-PEG-PLGA.

4.3.4 Comparative evaluation of thermal events for the innate components, RXB loaded and non-loaded HPMC/PU-PEG-PLGA

According to Benhabbour and co-workers (2019), the physical state of the final device, drug and polymers i.e., molecularly dispersed and crystalline state can influence the drug release of the implantable device. **Figure 4.6** shows the DSC thermograms of PLGA, PEG, PU, PU-PEG-PLGA, HPMC, HPMC/PU-PEG-PLGA, RXB and RXB loaded HPMC/PU-PEG-PLGA. The innate polymers PLGA, PEG, PU, HPMC showing endothermic peaks generated ~48°C, ~59°C, ~105°C, ~146°C, respectively. From **Figure 4.6**, it is evident that RXB showed a distinctive endothermic peak at ~260°C, whilst the polymer combinations and blend showed more than one peaks, which was also observed in a number of previous studies where polymeric material was used to formulate a blend (Chen et al., 2015; Yelles et al., 2017; Molina et al., 2020). Additionally, the shift in temperature towards a higher degree evident with the PU-PEG-PLGA up to 107°C HPMC/PU-PEG-PLGA up to 238°C indicates that the change in viscosity of the polymeric blend with the addition of the HPMC (Xu et al., 2017). The shift of the peak from the unloaded PU-PEG-PLGA to RXB loaded HPMC/PU-PEG-PLGA proves the success of the blend, even though the RXB peak did not appear in the RXB loaded HPMC/PU-PEG-PLGA formulation, which may be due to RXB being entrapped in the polymeric material.

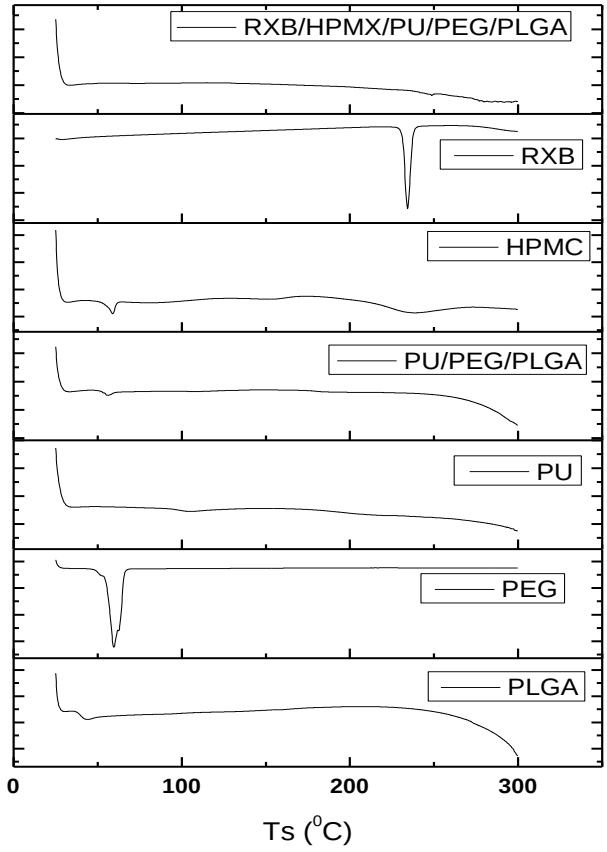

Figure 4.6. The DSC of the innate components, RXB loaded and non-loaded HPMC/PU-PEG-PLGA

The physical state of a drug in an implant has been used to account for the occurrence and the extent of the burst release (Nikkola et al., 2009; Benhabbour et al., 2019), as such TGA analysis was carried out to evaluate the physical state of the PLGA, polymers and drug in 3D implant as a function of heating.

The TGA curves shown on **Figure 4.7.** are displaying the temperature range of 35–900°C of PLGA, PEG, PU, PU-PEG-PLGA, HPMC, HPMC/PU-PEG-PLGA, RXB and RXB loaded HPMC/PU-PEG-PLGA, which all show two stages of weight loss, firstly some gradual weight loss of ±10 wt% between, which can be attributed to the decomposition of water-soluble composites, and secondly the rapid weight loss which is attributed to the curdlan decomposition. PU first weight loss of ±9 wt% between 104 – 380°C and rapidly to 100% weight loss between 380-456°C, PEG 1st weight loss of 7% 104–374°C and rapidly to 100% weight loss between 374-719°C,

PLGA 1st weight loss of ±5 wt% between 238 – 293°C and rapidly to 100% weight loss between 293-456°C, HPMC 1st weight loss of ±9 wt% between 104 – 380°C and rapidly to 100% weight loss between 380-456°C, RXB 1st weight loss of ±9 wt% between 104–380°C and rapidly to 100% weight loss between 380-456°C, HPMC/PU-PEG-PLGA 1st weight loss of ±9 wt% between 104–380°C and rapidly to 100% weight loss between 380-456°C, RXB loaded HPMC/PU-PEG-PLGA 1st weight loss of ±9 wt% between 104–374°C and rapidly to 100% weight loss between 374-719°C.

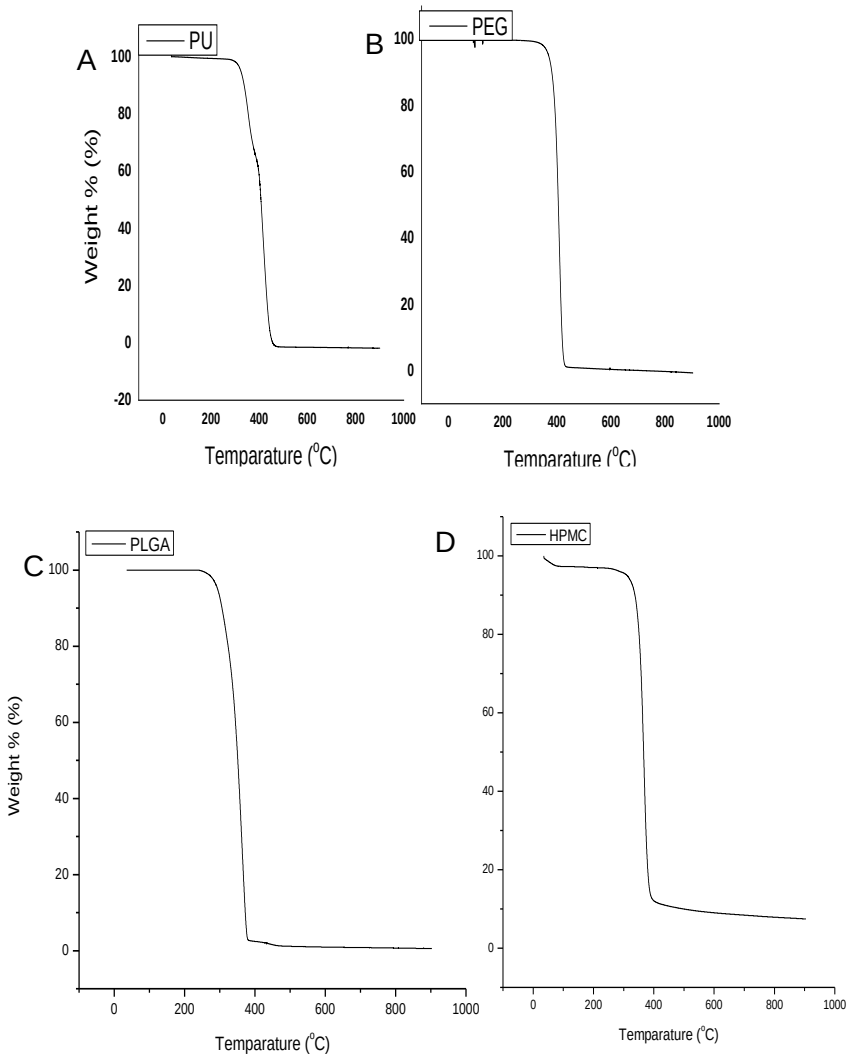

Figure 4.7. TGA of the innate components, (A) PU, (B) PEG, (C) PLGA, (D) HMPC

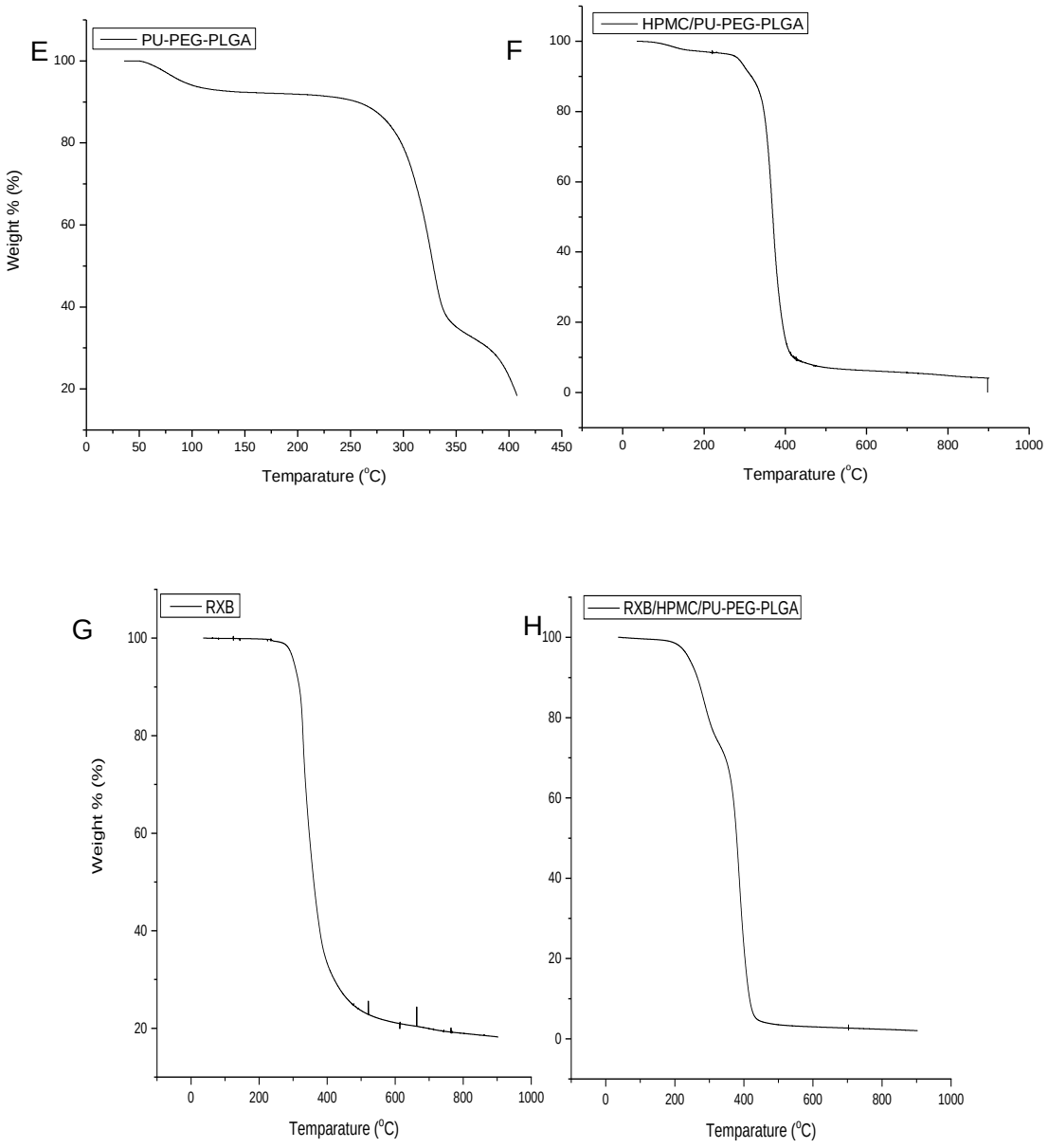

Figure 4.7(continued) TGA of the innate components, (E) HPMC/PU-PEG-PLGA, (F) RXB and (G) non-loaded HPMC/PU-PEG-PLGA

4.3.5 Porositometric analysis of the HPMC/PU-PEG-PLGA device

Porositometric analysis was carried out to establish the total surface area of the porous and non-porous HPMC/PU-PEG-PLGA particles, as well as the volume transition, pores size and distribution. The porous and non-porous HPMC/PU-PEG-PLGA particles were analyzed following the BJH method, BET surface area and the t-plot analysis (Lippens and De Boer, 1965). **Table 4.1**

shows the calculated BET surface areas, BJH pore volume and size engendered for the porous and non-porous HPMC/PU-PEG-PLGA particles. A distinct variance was noted between the porositometric values obtained for the porous and non-porous HPMC/PU-PEG-PLGA particles. The non-porous HPMC/PU-PEG-PLGA particles displayed a negative BET total surface area of -0.0189 ± 0.0164 m^2/g with R^2=0.73 compared to the porous HPMC/PU-PEG-PLGA particles which had a BET total surface area of 2.8927 ± 0.1100 m^2/g with R^2=0.99, displaying a significant increment of the pore volume. The isotherm tabular reports and isotherm log/linear plots of both the porous (**Figure 4.8 A and C**) and non-porous (**Figure 4.8 B and D)** HPMC/PU-PEG-PLGA particles show the distinctive pattern variations are displayed due to the increase in pore size/volume of porous HPMC/PU-PEG-PLGA particles**.** From these results it was evident that the NaCl significantly improved the porosity of the HPMC/PU-PEG-PLGA, thus influencing the RXB released from porous RXB loaded HPMC/PU-PEG-PLGA.

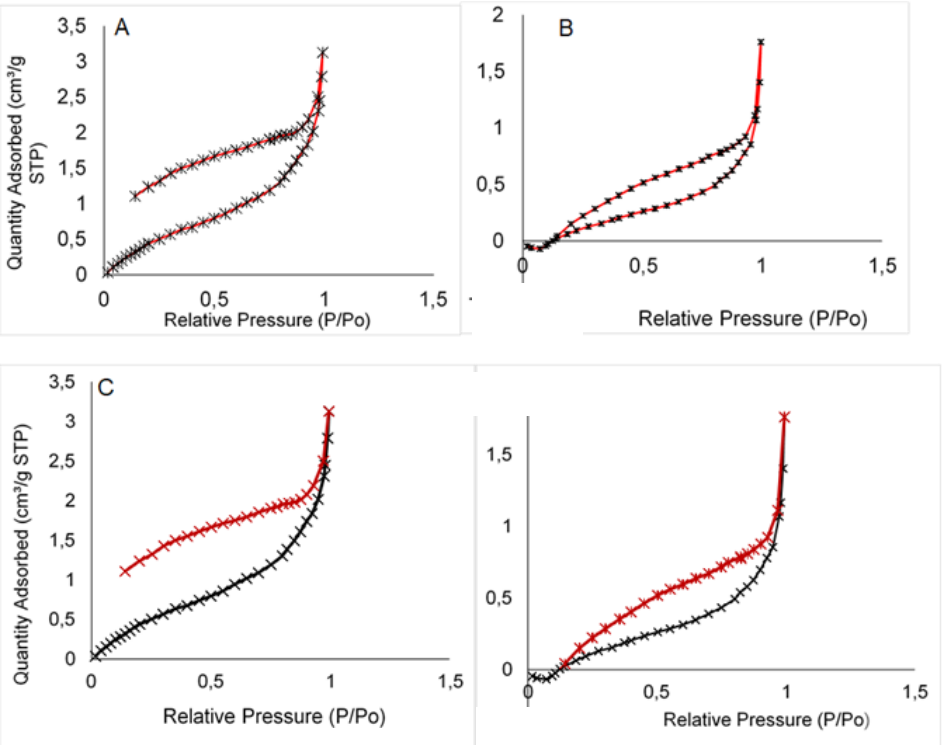

Figure 4.8. The isotherm tabular reports for: (A) porous and (B) non –porous HPMC/PU-PEG-PLGA, then the isotherm log/linear plots for: (C) porous and (D) non –porous HPMC/PU-PEG-PLGA.

Table 4.1. Summary report of the porous and non –porous HPMC/PU-PEG-PLGA

Parameter	Porous	Non-porous
Surface Area		
Single point surface area at P/Po = 0.201879924:	1.5349 m²/g	0.3137 m²/g
BET Surface Area:	2.8927 m²/g	-0.0189 m²/g
t-Plot External Surface Area:	4.0633 m²/g	
BJH Adsorption cumulative surface area of pores between 17.000 Å and 3000.000 Å diameter:	2.098 m²/g	0.763 m²/g
BJH Desorption cumulative surface area of pores between 17.000 Å and 3000.000 Å diameter:	3.6238 m²/g	1.1090 m²/g
Pore Volume		
Single point adsorption total pore volume of pores less than 798.785 Å diameter at P/Po = 0.975153565:	0.003576 cm³/g	0.001655 cm³/g
t-Plot micropore volume:	-0.001112 cm³/g	
BJH Adsorption cumulative volume of pores between 17.000 Å and 3000.000 Å diameter:	0.004645 cm³/g	0.002601 cm³/g
BJH Desorption cumulative volume of pores between 17.000 Å and 3000.000 Å diameter:	0.004575 cm³/g	1.1090 m²/g
Pore Size		
Adsorption average pore width (4V/A by BET):	49.4484 Å	-3501.6337 Å
BJH Adsorption average pore diameter (4V/A):	88.535 Å	136.469 Å
BJH Desorption average pore diameter (4V/A):	)6	′6

4.3.6 Dissolution studies of HPMC/PU-PEG-PLGA loaded with RXB

The *in-vitro* dissolution profiles of RXB from conventional tablet and HPMC/PU-PEG-PLGA device in PBS pH 7.4 buffer were investigated over a period of 72 h. By analyzing the results on **Figure 4.9.** the effects of the device on dissolution were evaluated compared to the conventional tablet, where they both had burst release from initial stage, reaching a steady state after 10 h, the main difference being that the device had a higher percentage of drug released, approximately ±17% more RX released. These findings support the notion that release kinetics are influenced by the swelling/disintegration behavior of the 3D implants when immersed in the dissolution media.

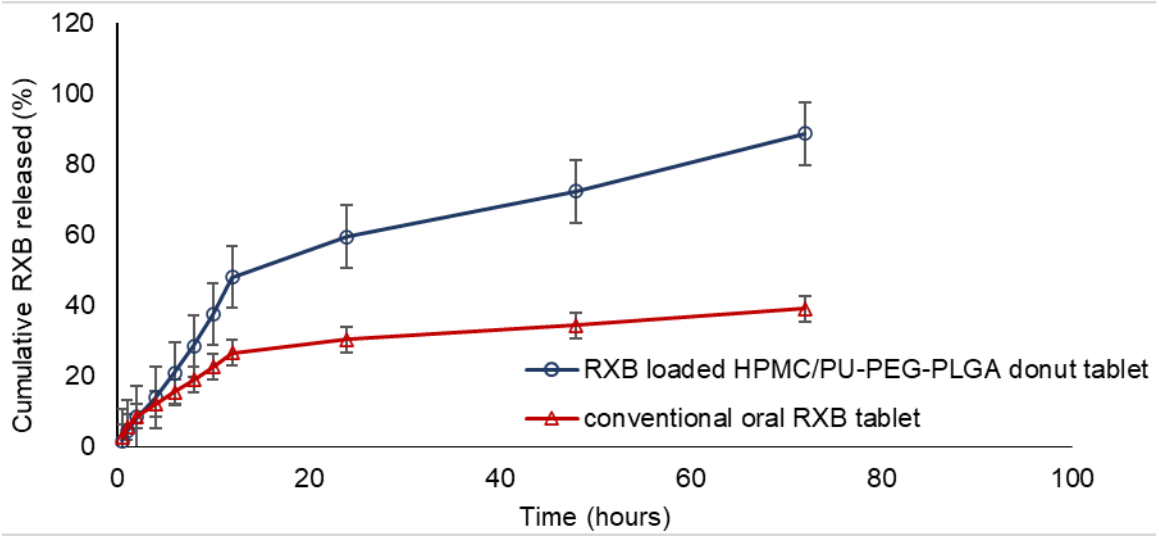

Figure 4.9. Cumulative dissolution studies of RXB loaded HPMC/PU-PEG-PLGA donut device and conventional (plain) oral RXB tablet.

The burst release of the drug from both systems may be due to the tablet and 3D device breaking after immersing in dissolution media. The 3D toro-poloidal device shows a great potential for use in long-term drug release as the conventional tablets reached a flat steady state after 24 h while the 3D toro-poloidal device was still showing a steadily increase, which is a controlled sustained drug release. The burst and controlled extended drug release characteristics from the toro-poloidal device may be attributed to the donut shape of the device and the choice of polymeric material. The presence of a HPMC and PEG (hydrophilic polymer) in microparticulate systems most likely enabled water penetration in the 3D implants, facilitating degradation, while the hydrophobic PLGA and PU slowed down the degradation of the implant and the overall RXB release (Yelles et al., 2019). The dissolution profiles of the oral RXB tablet and the RXB loaded HPMC/PU-PEG-PLGA 3D device had test values of t=0.000 and t= 0.00404, respectively, which were considered statistically significant (the mean ± SD; n = 3).

4.3.7 *In-vitro* drug release porous and non-porous RXB loaded HPMC/PU-PEG-PLGA

The *in-vitro* release profiles of porous and non-porous HPMC/PU-PEG-PLGA toro-poloidal devices simulated in PBS pH 7.4 buffer are presented in **Figure 4.10**. The studies were performed for 72 h and a higher percentage of drug release released from the porous device compared to the non-porous device, this may be attributed to the increased pore size/volume, hence the me-

dium flowing through the system better than non-porous device. The porous device released approximately ±9% more drug compared non-porous device, this could be due to the NaCl effects on the device's surface microstructure. Overall, both devices have the potential for controlled release behavior, as they displayed a similar drug release pattern, this may be due to the same polymeric material used and similar geometry. The RXB release from both the donut and cylinder implants followed a biphasic release pattern with Higuchi kinetics and was proportional to the surface area of implants, where the cylindrical shaped device released the RXB at a much slower rate compared to the donut shaped, as the donut shaped device has a greater surface area. Similar findings were reported by Bansal, Vadhanam and Gupta (2011), where polymeric implants for continuous systematic delivery of curcumin were studied.

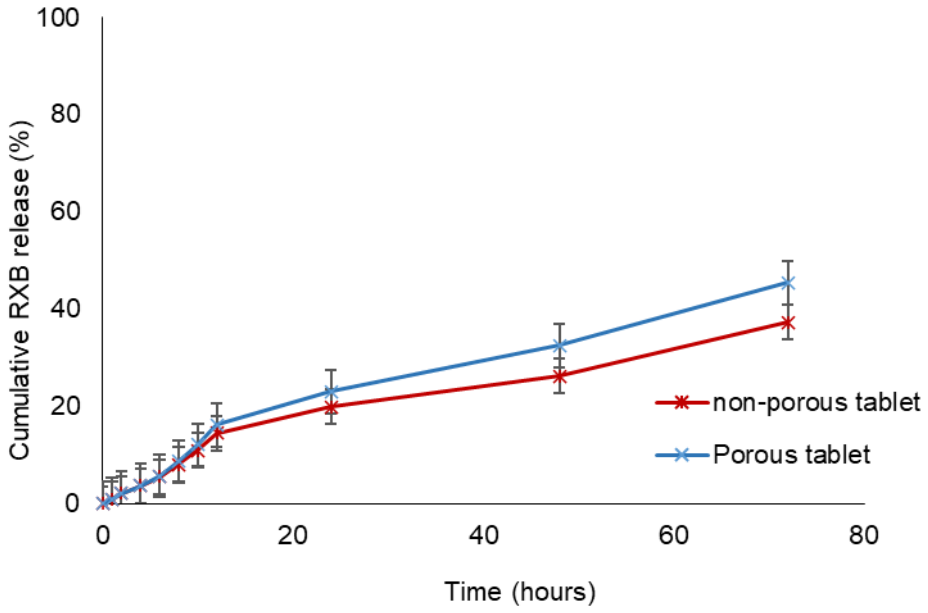

Figure 4.10. Cumulative *in-vitro* drug release from a porous and non-porous RXB loaded HPMC/PU-PEG-PLG

These results agree well with the *in-vitro* release patterns previously observed in other studies (Sivak et al., 2008; Laschke et al., 2014; Wang et al., 2020). These results suggest that the HPMC/PU-PEG-PLGA polymeric combination could be an ideal approach for applications requiring drug release over longer periods of time. The release of RXB from RXB-loaded was significantly more to the release of a P= Kruskal–Wallis test ($p < 0.0001$).

4.4 CONCLUSION

RXB sustained controlled-release was successfully achieved from the donut shaped designed device using HPMC/PU-PEG-PLGA polymeric material. Results from the *in-vitro* analysis confirmed the release characteristics predicted due to the donut shape of the device. It can then be concluded that the combination of the polymeric material and the geometry (donut shape) of the device has a great potential for an efficient delivery of drugs needed for an extended period of time. Thereby increasing patient compliance with the potential for extended drug release, as well as reducing the adverse effects as drugs could be released at a steady constant rate. Also, it can be concluded that the addition of NaCl does increase the porosity of the 3D toro-poloidal device, resulting into an increased surface area of the device's microstructures, hence affecting the release pattern of the drug between the porous and non-porous devices. The higher is the surface area, the faster is the disintegration of the device as there is increased media contact with higher surface area.

4.5 REFERENCES

Azad MA, Olawuni D, Kimbell G, Badruddoza AZ, Hossain M, Sultana T., 2020. Polymers for Extrusion-Based 3D Printing of Pharmaceuticals: A Holistic Materials–Process Perspective. Pharmaceutics, 12(2):124.

Bansal, S.S., Vadhanam, M.V. and Gupta, R.C., 2011. Development and in vitro-in vivo evaluation of polymeric implants for continuous systemic delivery of curcumin. Pharmaceutical Research, 28(5): 1121-1130.

Benhabbour, S.R., Kovarova, M., Jones, C., Copeland, D.J., Shrivastava, R., Swanson, M.D., Sykes, C., Ho, P.T., Cottrell, M.L., Sridharan, A. and Fix, S.M., 2019. Ultra-long-acting tunable biodegradable and removable controlled release implants for drug delivery. Nature Communications, 10(1), 1-12.

Çelebier, M., Kaynak, M.S., Altinoz, S. and Sahin, S., 2014. UV spectrophotometric method for determination of the dissolution profile of rivaroxaban. Dissolution Technologies, 56-58.

Chen, W.L., Peng, Y.F., Chiang, S.K. and Huang, M.H., 2015. Thermal properties and physicochemical behavior in aqueous solution of pyrene-labeled poly (ethylene glycol)-polylactide conjugate. International Journal of Nanomedicine, 10: 2815.

Chen, X., Chen, J., Li, B., Yang, X., Zeng, R., Liu, Y., Shao, J., 2017. PLGA-PEG-PLGA triblock copolymeric micelles as oral drug delivery system: In-vitro drug release and in-vivo pharmacokinetics assessment. Journal of Colloid and Interface Science, 490: 542–552.

D'souza, A. A., & Shegokar, R., 2016. Polyethylene glycol (PEG): a versatile polymer for pharmaceutical applications. Expert Opinion on Drug Delivery, 13(9): 1257–1275.

Daud, H., Ghani, A., Iqbal, D.N., Ahmad, N., Nazir, S., Muhammad, M.J., Hussain, E.A., Nazir, A. and Iqbal, M., 2021. Preparation and characterization of guar gum based biopolymeric hydrogels for controlled release of antihypertensive drug. Arabian Journal of Chemistry, 14(5): 103111.

Gajendiran, M., Jainuddin Yousuf, S. M., Elangovan, V., & Balasubramanian, S., 2014. Gold nanoparticle conjugated PLGA–PEG–SA–PEG–PLGA multiblock copolymer nanoparticles: synthesis, characterization, *in-vivo* release of rifampicin. Journal of Materials Chemistry B, 2(4): 418–427.

Griffin, M., Castro, N., Bas, O., Saifzadeh, S., Butler, P. and Hutmacher, D.W., 2020. The current versatility of polyurethane three-dimensional printing for biomedical applications. Tissue Engineering Part B: Reviews, 26(3): 272-283.

Guo T, Holzberg TR, Lim CG, Gao F, Gargava A, Trachtenberg JE, Mikos AG, Fisher JP., 2017. 3D printing PLGA: a quantitative examination of the effects of polymer composition and printing parameters on print resolution. Biofabrication. 12; 9(2):024101.

Guo, T., Lim, C., Noshin, M., Ringel, J. P., & Fisher, J. P., 2018. 3D printing bioactive PLGA scaffolds using DMSO as a removable solvent. Bioprinting, 10; e0038

Hoang Thi, T.T., Pilkington, E.H., Nguyen, D.H., Lee, J.S., Park, K.D. and Truong, N.P., 2020. The importance of poly (ethylene glycol) alternatives for overcoming PEG immunogenicity in drug delivery and bioconjugation. Polymers, 12(2): 298.

Huang J, Xu W. Zwitterionic monomer graft copolymerization onto polyurethane surface through a PEG spacer. Applied Surface Science. 2010 Apr 1; 256(12):3921-7.

Hung, K.C., Tseng, C.S. and Hsu, S.H., 2016. 3D printing of polyurethane biomaterials. In Advances in Polyurethane Biomaterials, 149-170.

Hutanu, D., Frishberg, M.D., Guo, L. and Darie, C.C., 2014. Recent applications of polyethylene glycols (PEGs) and PEG derivatives. Modern Chemistry and Applications, 2(2): 1-6.

Ilyés, K., Kovács, N.K., Balogh, A., Borbás, E., Farkas, B., Casian, T., Marosi, G., Tomuță, I. and Nagy, Z.K., 2019. The applicability of pharmaceutical polymeric blends for the fused deposition modelling (FDM) 3D technique: Material considerations–printability–process modulation, with consecutive effects on *in-vitro* release, stability and degradation. European Journal of Pharmaceutical Sciences, 129: 110-123.

Jamróz, W., Szafraniec, J., Kurek, M. and Jachowicz, R., 2018. 3D printing in pharmaceutical and medical applications–recent achievements and challenges. Pharmaceutical Research, 35(9): 1-22.

Jusu, S.M., Obayemi, J.D., Salifu, A.A., Nwazojie, C.C., Uzonwanne, V., Odusanya, O.S. and Soboyejo, W.O., 2020. Drug-encapsulated blend of PLGA-PEG microspheres: In vitro and in vivo study of the effects of localized/targeted drug delivery on the treatment of triple-negative breast cancer. Scientific Reports, 10(1): 1-23.

Karim, S., Hossain, F., Uddin, J., Bhuiyan, M.A. And Harun-Or-Rashid, M.D., 2016. Formulation and *in-vitro* evaluation of aspirin sustained release tablets using hydrophilic polymers. World, 3(3): 39-45.

Kumar, P., Ganure, A.L., Subudhi, B.B. and Shukla, S., 2015. Design and comparative evaluation of in-vitro drug release, pharmacokinetics and gamma scintigraphic analysis of controlled release tablets using novel pH sensitive starch and modified starch-acrylate graft copolymer matrices. Iranian Journal of Pharmaceutical Research, 14(3): 677.59.

Laschke, M.W., Schank, T.E., Scheuer, C., Kleer, S., Shadmanov, T., Eglin, D., Alini, M. and Menger, M.D., 2014. *In-vitro* osteogenic differentiation of adipose-derived mesenchymal stem cell spheroids impairs their *in-vivo* vascularization capacity inside implanted porous polyurethane scaffolds. Acta Biomaterialia, 10(10): 4226-4235.

Lippens, B.C. and De Boer, J.H., 1965. Studies on pore systems in catalysts: V. The t method. Journal of Catalysis, 4(3): 319-323.

Maghsoudi, S., Shahraki, B.T., Rabiee, N., Fatahi, Y., Dinarvand, R., Tavakolizadeh, M., Ahmadi, S., Rabiee, M., Bagherzadeh, M., Pourjavadi, A. and Farhadnejad, H., 2020. Burgeoning polymer nano blends for improved controlled drug release: a review. International Journal of Nanomedicine, 15: 4363.

Makadia HK, Siegel SJ. Poly lactic-co-glycolic acid (PLGA) as biodegradable controlled drug delivery carrier. Polymers. 20113(3):1377-97.

Mazzanti, V., Malagutti, L. and Mollica, F., 2019. FDM 3D printing of polymers containing natural fillers: A review of their mechanical properties. Polymers, 11(7): 1094.

Metre, S., Mukesh, S., Samal, S. K., Chand, M., & Sangamwar, A. T., 2018. Enhanced biopharmaceutical performance of Rivaroxaban through polymeric amorphous solid dispersion. Molecular Pharmaceutics, 15(2), 652–668.

Molina, G.A., Elizalde-Mata, A., Hernández-Martínez, Á.R., Fonseca, G., Cruz Soto, M., Rodríguez-Morales, Á.L. and Estevez, M., 2020. Synthesis and characterization of inulin-based responsive polyurethanes for breast cancer applications. Polymers, 12(4): 865.

Nadagouda, M.N., Rastogi, V. and Ginn, M., 2020. A review on 3D printing techniques for medical applications. Current Opinion in Chemical Engineering, 28: 152-157.

Ngo, H. V., Tran, P. H. L., Lee, B.-J., & Tran, T. T. D. (2019). The roles of a surfactant in zein-HPMC blend solid dispersions for improving drug delivery. International Journal of Pharmaceutics. 263:169-173.

Nikkola, L., Viitanen, P. and Ashammakhi, N., 2009. Temporal control of drug release from biodegradable polymer: multicomponent diclofenac sodium releasing PLGA 80/20 rod. Journal of Biomedical Materials Research Part B: Applied Biomaterials: An Official Journal of The Society for Biomaterials, The Japanese Society for Biomaterials, and The Australian Society for Biomaterials and the Korean Society for Biomaterials, 89(2): 518-526.

Nyamweya, N.N., 2021. Applications of polymer blends in drug delivery. Future Journal of Pharmaceutical Sciences, 7(1): 1-15.

Patel P, Patel R, and Patel Y., 2017. Formulation, development and evaluation of Rivaroxaban tablets by using solubility enhancement technique. International Journal of Pharmaceutical Sciences and Research**,** 3:3, 51-55.

Polamaplly, P., Cheng, Y., Shi, X., Manikandan, K., Kremer, G.E. and Qin, H., 2019. 3D printing and characterization of hydroxypropyl methylcellulose and methylcellulose for biodegradable support structures. Procedia Manufacturing, 34: 552-559.

Reddy, B.B.K., Nagoji, K.E.V. and Sahoo, S., 2018. Preparation and in-vitro & in-vivo evaluation of cephalexin matrix tablets. Brazilian Journal of Pharmaceutical Sciences, 54.

Rezvantalab, S., Drude, N.I., Moraveji, M.K., Güvener, N., Koons, E.K., Shi, Y., Lammers, T. and Kiessling, F., 2018. PLGA-based nanoparticles in cancer treatment. Frontiers in Pharmacology, 9: 1260.

Sivak, W.N., Pollack, I.F., Petoud, S., Zamboni, W.C., Zhang, J. and Beckman, E.J., 2008. LDI–glycerol polyurethane implants exhibit controlled release of DB-67 and anti-tumor activity *in-vitro* against malignant gliomas. Acta Biomaterialia, 4(4): 852-862.

Stansbury, J.W. and Idacavage, M.J., 2016. 3D printing with polymers: Challenges among expanding options and opportunities. Dental Materials, 32(1): 54-64.

Tappa K, Jammalamadaka U. Novel biomaterials used in medical 3D printing techniques. Journal of Functional Biomaterials. 2018; 9(1):17.

Tian, Y., Chen, C., Xu, X., Wang, J., Hou, X., Li, K., Lu, X., Shi, H., Lee, E.S. and Jiang, H.B., 2021. A review of 3D printing in dentistry: Technologies, affecting factors, and applications. Scanning, 2021- 4.

Wang, H., Feng, Y., Fang, Z., Yuan, W. and Khan, M., 2012. Co-electrospun blends of PU and PEG as potential biocompatible scaffolds for small-diameter vascular tissue engineering. Materials Science and Engineering*: C*, *32*(8): 2306-2315.

Wang, Y., Sun, L., Mei, Z., Zhang, F., He, M., Fletcher, C., Wang, F., Yang, J., Bi, D., Jiang, Y. and Liu, P., 2020. 3D printed biodegradable implants as an individualized drug delivery system for local chemotherapy of osteosarcoma. Materials and Design, 186:108336.

Xu, Y., Wu, S.P., Liu, X.J., Zhang, L.J. and Lu, J., 2017. Crystal characterization and transformation of the forms I and II of anticoagulant drug rivaroxaban. Crystal Research and Technology, 52(3): 1600379.

Xue, X., Cao, M., Ren, L., Qian, Y. and Chen, G., 2018. Preparation and optimization of rivaroxaban by self-nanoemulsifying drug delivery system (SNEDDS) for enhanced oral bioavailability and no food effect. American Association of Pharmaceutical Scientists, 19(4): 1847-1859.

Yelles, M.H.B., Tan, V.T., Danede, F., Willart, J.F. and Siepmann, J., 2017. PLGA implants: How Poloxamer/PEO addition slows down or accelerates polymer degradation and drug release. Journal of Controlled Release, 253: 19-29.

CHAPTER FIVE

3D TORO-POLOIDAL IMPLANTABLE DEVICE FOR CONTROLLED DELIVERY OF RIVAROXABAN

5.1 INTRODUCTION

Implantable drug delivery devices offer advantages over other routes of drug delivery, as they are designed to release drugs for a defined period at a definite rate. They may deliver lower drug concentrations to achieve required therapeutic effects over an extended period of time (Stewart et al., 2020), thus reducing systemic adverse effects and subsequently replacing the daily oral or injections required on daily basis for chronic use or any other extended use of a specific drug (Santos et al., 2014). Additionally, these devices allow for increased compliance, personalised medicine and are cost-effective compared to other conventional routes of drug delivery (Wolfe et al., 2021).

Recently, an exponential growth has been experienced in the drug delivery sector, where the role played by the delivery system's geometry (i.e., size and shape) in its function such as drug loading and release, stability and, ultimately, delivery properties has been an area of interest for researchers. 3D devices may be designed in various odd geometries (size and shape of the 3D products) and the geometrical properties of pharmaceutical products are very important to consider when it comes to personalized medication, as they affect the overall biological performance of pharmaceutical products (i.e., drug release profiles) (Martinez et al., 2018: Goyanes et al., 2015). There are two critical factors that affect the geometry of a 3D devices: the selection of biomaterial and the fabrication method (Jammalamadaka and Tappa, 2018).

As the implant is expected to release the drug over an extended period polyurethane (PU) was selected due to their good biocompatibility, mechanical properties, and hemocompatibility in implantable medical devices (Griffin et al., 2020). This study also used poly (lactic-co-glycolic acid) (PLGA) as the 3D device resin, as it has been widely used on devices such as scaffolds (Guo et al., 2017; Makadia HK, Siegel SJ., 2011). Polyethylene glycol (PEG) was utilized due to its PEGylation property (Hutanu et al., 2014; Veronese and Pasut, 2005) and in this study it was used as a spacer between the two chemical entities PLGA and PU to produce PU-PEG-PLGA. Additionally, Hydroxypropyl methylcellulose (HPMC) was used as a supporting material due to its gelation property, which is required for 3D formulations (Polamaplly et al 2019). Rivaroxaban

(RXB) was used as the model drug. RXB directly inhibits both free and clot-bound Factor Xa and prevents the formation of new clots and the extension of existing clots (Turpie, 2014; Curto, 2017; Antoniou and Amara, 2018). RXB is one of the preferred antithrombotic agents (Paikin et al., 2012), currently administered via oral drug delivery for the primary prevention of stroke and systemic embolism in the general population of patients with thromboembolic disorders (Laube et al., 2012). Even though RXB is preferred it is associated with some degree of gastrointestinal (GI) bleeding, which is the most common extracranial haemorrhagic complication in patients on oral RXB (Ammar et al., 2006; Lewalter et al., 2014). Hence the 3D implant being proposed will offer an alternative route that will bypasses the gut system.

Even though correlation of medicine drug release characteristics with their complex microstructures is one of the mostly explored novelty, there are still some gaps requiring more research directed towards designing formulations with various release profiles such as sustained and delayed release due to changes in polymers, densities and shape. This chapter demonstrated the correlation of the geometrical properties with its drug release profiles. The 3D implant formulated in this study will offer an alternative route that will bypasses the gut, be more convenient and safer for RXB delivery especially during long-term use, this device may be widely applied over a range of diseases requiring long-term use of a specific drug. In this study toro-poloidal, 3D devices were formulated to study their effects on drug release.

5.2 MATERIALS AND METHODS

5.2.1 Materials

Poly (D,L-lactide-co-glycolide) (PLGA, copolymer ratio 50:50), Polyethylene Glycol (average MW 4000), Polyurethane, Oleic acid, Tween-40, hydroxypropyl methylcellulose (HPMC) were all purchased from Sigma-Aldrich Chemie GmbH (Steinheim, Germany). Factor Xa (FXa) assay kit (Sigma-Aldrich Chemical Corp., St. Louise, MO, USA). 3T3 fibroblast cell line (Merck KGaA, Darmstadt, Germany), MTT assay, DMEM/F-12 media, foetal bovine serum (Gibco), penicillin (100 units/mL) and streptomycin (Sigma Chemical Corp., St. Louise, MO, USA). All other chemicals were of analytical grade.

5.2.2 Preparation of RXB loaded PU-PEG-PLGA/HPMC 3D toro-poloidal device

The blend for 3D device was prepared as described in section 3.2.2. To optimise the formulation method two different methods were explored for formulation of the 3D devices. One method was

an extrusion-based Texture Analyzer (TA) (TA. XT plus, Stable Microsystems, Surrey, UK), where RXB loaded PU-PEG-PLGA/HPMC blend was extruded into donut and cylindrical shaped tablet molds and dried under fume hood. **Figure 5.1** demonstrates a TA and functioning during extrusion. The polymeric material is loaded into the needle and connected to the extrusion probe, the probe is then controlled by the arm which exerts its force by moving up and down while extruding the material into the mold. The parameters used for TA compression are shown in **Table 5.1.** The other method employed was direct compression, where the dried (lyophilised) RXB loaded PU-PEG-PLGA/HPMC blend was compressed into tablet molds using a Manesty F3 eccentric (single punch) tableting press (Oystar Manesty (Pty) Ltd., Merseyside, England). The dried powder blends of RXB loaded PU-PEG-PLGA/HPMC were directly compressed into the desired donut and cylinder-shaped devices.

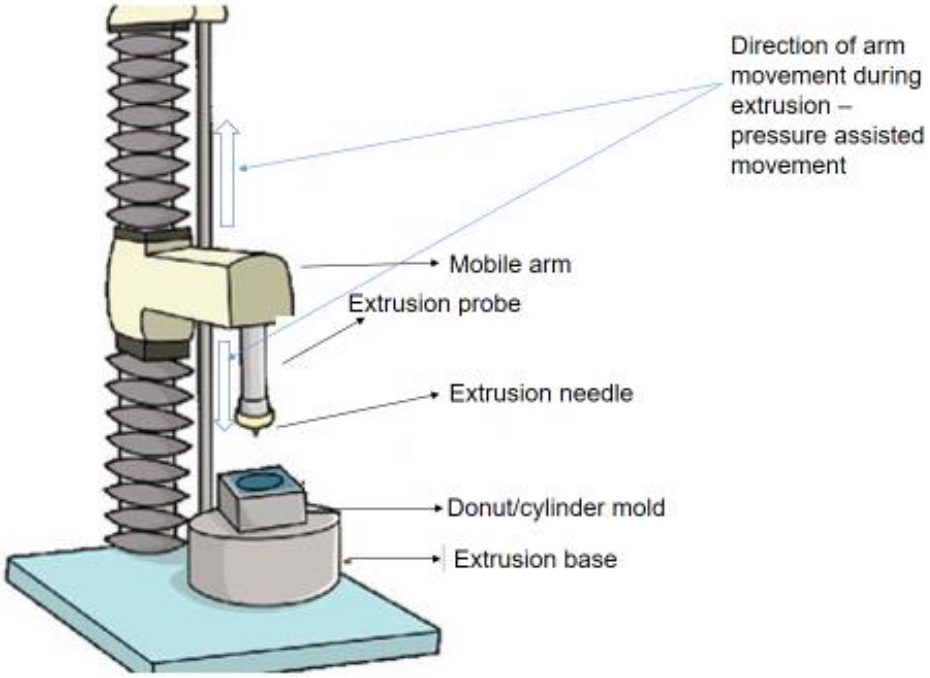

Figure 5.1. Graphic representation of 3D extrusion using a texture analyser

Table 5.1.TA compression parameters

Compression caption	Compression values
Pre-Test Speed	1.00 mm/sec
Test speed	1.00 mm/sec
Post-Test Speed	1.00 mm/sec
Target Mode	Distance
Distance	5.00 mm
Delay between compressions	5 s
Trigger Type	Auto Force
Trigger Force	0.049 N

5.2.3 *In-vitro* Factor Xa (FXa) assay of the RXB loaded PU-PEG-PLGA/HPMC

FXa Activity was determined using an FXa Activity Fluorometric Assay Kit (sigma Aldrich, St. Louis, MO63103 USA). FXa is the activated form of the coagulation factor X, which plays an important role at several stages of the coagulation pathway (Turpie, 2014). It acts by converting prothrombin into active thrombin by complexing with activated co-factor V in the prothrombinase complex (Curto, 2017). RXB functions binding to plasma cofactor antithrombin to inactivate several coagulation factors including factor Xa (Antoniou and Amara, 2018), hence this Factor Xa activity assay kit utilizes the ability of Factor Xa to cleave a synthetic substrate thereby releasing a fluorophore, which can be quantified by fluorescence readers. All samples were prepared in small quantities into a 96 well flat-bottom plate as the kit can detect activity from as low as 1 ng of Factor Xa.

Firstly, a standard curve was prepared using FXa Enzyme Standard diluted with an FXa Dilution Buffer to 5 ng/μL and FXa Enzyme stock solution (100 ng/μL). Diluted FXa Enzyme Standard (5 ng/μL) was mixed with FXa Enzyme stock solution (100 ng/μL) and prepared into a series of concentrations in a well plate 0, 20, 40, 60, 80 and 100 ng/well, final concentrations were adjusted using FXa Dilution Buffer. Then RXB samples were prepared by adding 2–50 μL of 100 ng/μL RXB per well of 96 well plate and the volume was adjusted to 50 μL with FXa Assay Buffer.

Thereafter a Master Reaction Mix was added into the sample and standard wells. The Master Reaction Mix was formulated as below:

(i) Reagents Volume FXa Assay Buffer 48 μL

(ii) FXa Substrate 2 μL

Both the standard curve and the sample with master reaction mix were measured after an hour using a fluorescence multi-well plate reader (FilterMax™ F5 Multi-Mode Microplate Reader, Molecular Devices, US) at t 37 °C (λ_{ex} = 350 nm/λ_{em} = 470 nm). A standard curve was plotted on both wavelengths, FXa activity versus change in area under curve (ΔRFU) was determined using the FXa standard curve.

5.2.4 *In-vitro* cytotoxicity analysis of the RXB loaded PU-PEG-PLGA/HPMC

Fibroblast 3T3 cell lines (Cell Applications Inc. (CAI), San Diego, USA) were seeded in culture flasks with complete media consisting of GIBCO®-Dulbecco's Modified Eagle Medium (DMEM) supplemented with 10% fetal bovine serum and 100U/ml penicillin/streptomycin (Sigma-Aldrich; St. Louise, MO, USA). The flasks used for the culturing were coated with poly-l-lysine (Sigma-Aldrich; St. Louise, MO, USA) 24h before cell culture was initiated. During cell culture the cells were then maintained in an incubator (RS Biotech Galaxy, Irvine, UK) with a humidified atmosphere of 5 % CO_2 at 37 °C.

Cultured Fibroblast 3T3 cells were seeded at a concentration of 15000 cells/well. After culturing for 48 h in complete media, HPMC/PU-PEG-PLGA and RXB loaded HPMC/PU-PEG-PLGA dissolved in 0.1 % DMSO were added at a concentration of 0.1, 1 and 100 µg/ml drug (RXB) equivalent concentrations and the cells were further incubated for 48 h. At the end of the incubation the medium was removed and 100µL of MTT (3-(4,5-dimethylthiazol-2-yl)-2,5-diphenyltetrazolium bromide) solution (diluted in a culture media with a final concentration of 0.5 mg/mL) was added and incubated for another 4 h, 0.1 and 100 % DMSO were also incubated as controls for the study. Following incubation, the medium was removed through centrifuging (Optima® LE-80 K, Beckman, California, USA) at 3000 rpm for 5 min. Next the remaining formazan crystals were dissolved by incubation for 30 min in 100µL of dimethyl sulfoxide (DMSO) and analysed with microplate reader (FilterMax™ F5 Multi-Mode Microplate Reader, Molecular Devices, US). The number of viable cells is directly proportional to the quantity of formazan product formed as quantified by absorbance at 570 nm (Mohanty et al., 2012), using a microplate reader. Results are

presented as %cell viability (CV) (mean ± standard deviation), the percentage of viable cells was calculated using the following equation:

$$\%\ \text{Cell viability} = \frac{(A_{\text{treatment}} - A_{\text{blank}})}{(A_{\text{control}} - A_{\text{blank}})} \times 100\%$$

Where, A = absorbance.

Equation 5.1. % Cell viability

To ensure that devices were sterile before its application in the *in-vitro* cytotoxicity the novel RXB loaded HPMC/PU-PEG-PLGA device was sterilized under UV light overnight (Karunakaran et al., 2011; Luo et al., 2008) and the sterility of the device was validated by streaking the sterilised HPMC/PU-PEG-PLGA elements in an alga plate and incubating at 37°C for 24h.

5.2.5 *In-vitro* degradation studies of the donut and cylinder RXB loaded PU-PEG-PLGA/HPMC

Donut and cylindrical RXB loaded PU-PEG-PLGA/HPMC samples were immersed in a closed petri dish containing 15 ml Phosphate Buffered Saline (PBS, pH 7.4). PBS was prepared by dissolving PBS tablets (1 tablets per 200 mL deionized water). All samples were done in triplicates were incubated at 37 °C in an orbital shaker throughout the study. The buffer was refreshed every week and degradation of the devices was monitored by device diameter/circumference and for donut the inner circumference was also measured, all measurements were done using the Leica Microscope scale bar (Wetzlar, Germany).

5.2.6 *In-vitro* release studies of the donut and cylindrical RXB loaded PU-PEG-PLGA/HPMC

In-vitro RXB release from the donut and cylindrical RXB loaded PU-PEG-PLGA/HPMC was carried out in PBS (pH 7.4) at 37 °C using dialysis membranes (MWCO: 1.2 kDa), samples were left in an orbital shaker. Three donut and cylindrical shaped devices were placed in dialysis bags and immersed in 20 mL of buffer medium. At predetermined time intervals (0.5, 1, 2, 4, 6, 10, 12, 24 and 48 h, thereafter on day 7, 14, 21, 28, 35, 42), 0.5 mL of the buffer medium was removed for analysis and replaced with the same quantity of fresh buffer medium, to maintain sink conditions. Samples were filtered and analysed using a UV-Vis spectrophotometer (PerkinElmer Spectrum 100, Llantrisant, Wales, UK), set to 270 nm wavelength for RXB. The results were then inserted

to a previously plotted standard curve, to obtain the concentrations and thereby the amount of drug released.

5.2.7 Comparison of *in-vitro* RXB release studies

To optimise the formulation method two different methods as described in **4.2.** and **5.2**., they were both explored for the formulation of the 3D devices. Both methods were used to formulate the donut and cylindrical devices, release profiles were drawn out and compared, and release studies were carried out in **Section 5.2.6**.

5.3 RESULTS AND DISCUSSIONS

5.3.1 Formulated RXB loaded PU-PEG-PLGA/HPMC 3D toro-poloidal devices

The RXB loaded PU-PEG-PLGA/HPMC was extruded into uniform filaments using the TA (**Figure 5.2.**), the filaments were subsequently utilized as feed material for the both the donut and cylinder molds. The RXB loaded PU-PEG-PLGA/HPMC filaments were directly compressed into 3D devices as shown on **Figure 5.1.** Then, **Figure 5.2** shows the resulting toro-poloidal, cylindrical and donut shaped 3D devices, both the compressed and extruded devices were similar, their release profiles were studied to further compare the 3D formulation methods. The layers of the extruded material (filaments) were not strong enough to withhold the weight of subsequent layers, as a results extruded filament layers were collapsing on each other, forming a smooth end-product comparable to compressed devices, and a similar observation was reported by Vaz and Kumar (2021). Previously it was highlighted that mitigating the main extrusion challenge which is the drying of extruded layers is by extruding the polymeric material directly into capsules, which allows indirect handling during drying, and increasing the overall drying time (Melnyk and Oyewumi, 2021). The same principle was applied in this study where extrusion was done directly into a tablet mold, however the extruded strands were still not strong enough to form visible layers as donut or cylindrical shaped devices. Additionally, increasing the viscosity of the blend in attempt to circumvent collapsing of the extruded layers resulted in no extrusion as extrusion-based 3D devices are strongly dependent on material used and applied pressure (Pandey et al., 2020).

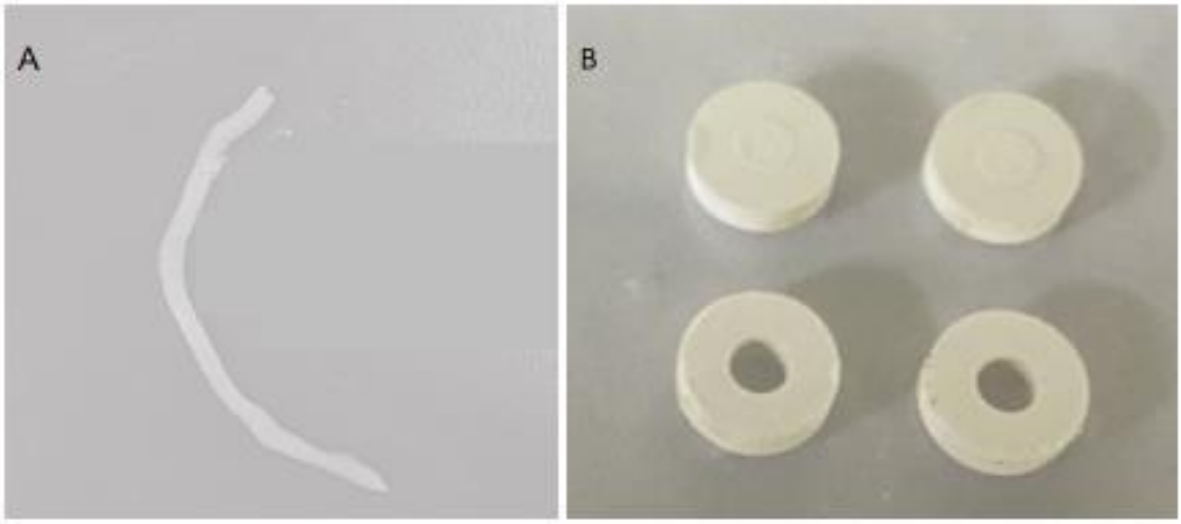

Figure 5.2. Extruded filaments and formulated model geometries. A) Extruded feed material (RXB loaded PU-PEG-PLGA/HPMC filaments) B) 3D devices (donut and cylinder) geometries.

5.3.2 *In-vitro* Factor Xa (FXa) assay of the RXB loaded PU-PEG-PLGA/HPMC

As RXB directly inhibits both free and clot-bound FXa and prevents the formation of new clots and the extension of existing clots (Turpie, 2014; Curto, 2017; Antoniou and Amara, 2018), the FXa Activity Fluorometric Assay Kit was utilised to assess the FXa activity of the formulated RXB loaded PU-PEG PLGA/HPMC 3D toro-poloidal3D device. **Figure 5.3**. shows the standard curves at both 350 and 470 nm where a standard FXa enzyme, and on **Figure 5.4.** the direct FXa-inhibition is demonstrated using different concentrations of the RXB loaded on the 3D toro-poloidal3D device. An excellent correlation between the anti-FXa activity and concentrations of RXB was observed as the anti-FXa activity increased together with the concentration (the higher the concentration was the higher the ΔRFU), similar results were reported by Margetić and co-workers (2020) where anti-FXa activity changed with different concentrations of RXB, hence the FXa activity of the RXB based on FXa-inhibition increased with the rivaroxaban concentration, another similar observation was reported by Hillarp et al. (2011). **Figure 5.4.** Show how the FXa inhibition was dependent on the concentration, a linear graph was obtained. The anti-Fax activity shown by the RXB loaded PU-PEG-PLGA/HPMC demonstrates the great potential for use of this device in chronic anticoagulant management.

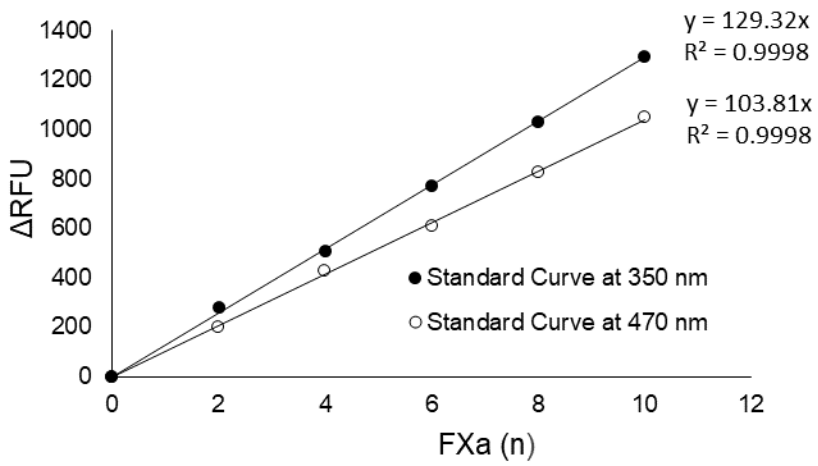

Figure 5.3.FXa enzyme activity assay's standard curve

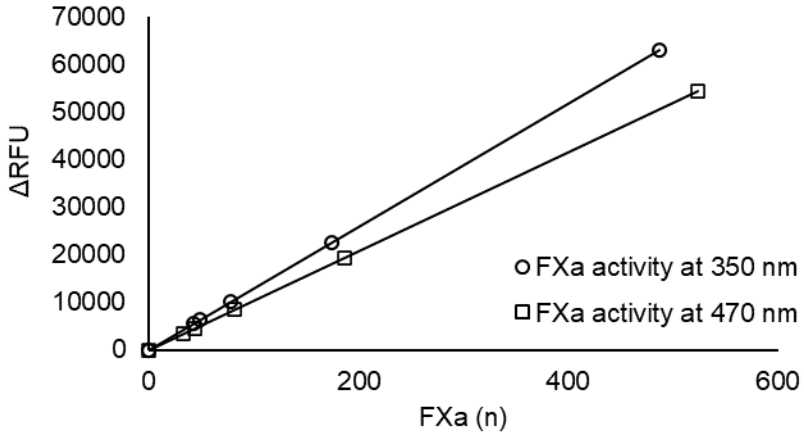

Figure 5.4. RXB loaded PU-PEG-PLGA/HPMC *in-vitro* FXa activity assay, FXa versus change in area under curve

5.3.3 Degradation of RXB loaded PU-PEG-PLGA/HPMC devices

The degradation studies revelled that the devices undergo bulk degradation as the polymeric material degrades uniformly, where the dissolution medium penetrates the polymeric material matrix, resulting into two phases of degradation. Firstly, the devices absorb the dissolution medium, swell then disintegrate slowly, and resulting into an initial burst release then sustained controlled release. The device absorbs media creating a passage for drug to be released by diffusion and erosion until the drug has reached complete solubilisation and polymer has completely disintegrated (Makadia, and Siegel, 2011). **Figure 5.5.** and **5.6.** shows both the donut and cylinder

devices at 0 h with same diameter, at 2 h they started swelling/absorbing dissolution media at the same rate both with a diameter of 20.54 mm. It was then observed at 24 h that the donut was slightly absorbing more media with an increase diameter of 24.62 mm and a reduced inner cycle diameter of 4.64 mm compared to the 22.66 mm diameter of the cylinder. Also observed at 24 h are small fragments of polymeric material as disintegration started occurring.

According to Yu and co-workers (2017) the swelling and absorption at pH 7.4 of polymeric material is due to the carboxyl groups readily available on polymers such as PLGA, PEG and HPMC used in this study. This difference is media absorption of the two geometries is due to their shapes, attributed to the exposed surface area/volume (SA/V) ratio, the donut having a higher SA/V ratio compared to the cylinder (Goyanes et al., 2015; Martinez et al., 2018). **Figure 5.5 (G) and 5.6 (D)** shows the continued swelling of the donut and cylinder, respectively, where more visible disintegration was seen at 72 h. The shape of the donut started being distorted with inner cycler becoming oval as it degraded. Disintegration of the donut was evident from both the inner and outer part of the donut, while with the cylinder it was only observed from the outer par. This degradation pattern suggests that more drug is released from donut compared to the cylinder at the same time point. Overall,both geometries do suggest the potential for a sustained controlled drug release, where the donut finishes releasing the drug before the cylinder. As the bioavailability characteristics can be predicted based on the *in-vitro* and *in-vivo* drug release pattern (Kastellorizios and Burgess, 2012), where the increased drug release is associated with a high bioavailability. The donut shaped device was preferred over the cylinder due to its increased bioavailability compared to the cylindrical shaped device. And with the personalised medication era even the cylinder could be preferred in other instances where the drug is released over extended period of time in smaller quantities, hence the deduction that 3D devices have such a great potential for personalised medicine. Both degradation patterns suggest a biphasic release profile where there is a sudden burst initially and then a sustainable controlled release. These results seem to be consistent with the expectancy based on the theories previously described by a number of researchers as per geometric influence on drug release (Goyanes et al., 2015; Domsta and Seidlitz, 2021; Martinez et al., 2018).

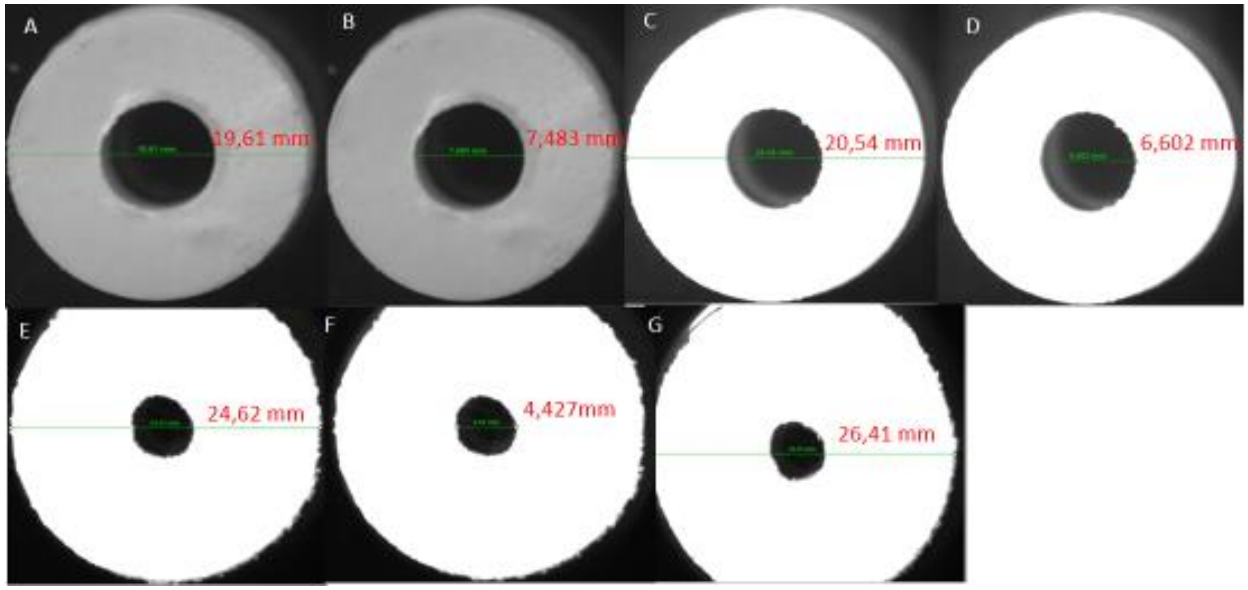

Figure 5.5. The microscope images of the donut device after immersion in PBS buffer pH 7.4 at lowest magnification 0.8 (A) and (B) at 0 h, (C) and (D) 2 h (E) and (F) 24 h and (G) 72 h (green dimensions are visibly transcribed in red).

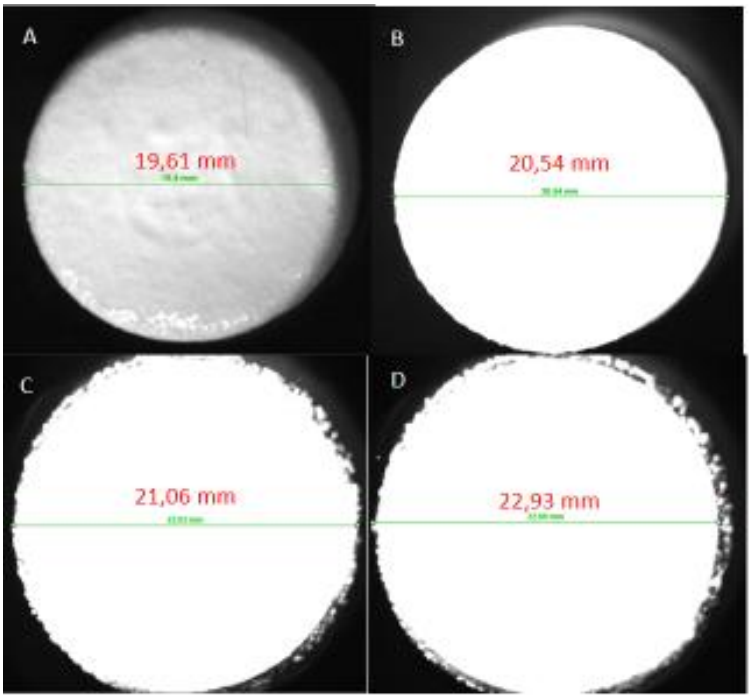

Figure 5.6. The cylindrical device after immersion in PBS buffer pH 7.4 at PBS buffer pH 7.4 at (A) 0 h, (B) 2 h, (C) 24 h and (D) 72 h (green dimensions are visibly transcribed in red).

5.3.4 *In-vitro* release studies of the donut and cylinder RXB loaded PU-PEG-PLGA/HPMC

The effect of drug release properties from the two geometrical 3D implants was investigated by comparing the release profiles of compressed donut, compressed cylinder, extruded donut and extruded cylinder. The summary of the release profiles of the 3D implants is shown in **Figure 5.7.**, where the release rate of RXB from donut shaped implants was significantly increased compared to cylindrical shaped implants from the same polymeric material. Complete RXB release was achieved after 49 days for donut 3D implants, whereas, the cylindrical shaped implants were still releasing more drug after 49 days. A similar drug release pattern was seen with all four devices, these results are in agreement with degradation studies done, where biphasic type of release was observed, the initial bust release and sustained release from 72 h. Approximately 97% and 89 % RXB was released on day 49 for donut implants, while only 61.3 % and 66.1 % of the RXB was released from the cylinder, the release was from compressed and extruded 3D implants, respectively. These results show the obvious effect of geometry on 3D devices when it comes to it release properties, and to some extent also there was a slight difference in release with extruded and compressed devices. These data were considered statistically significant ($p < 0.05$).

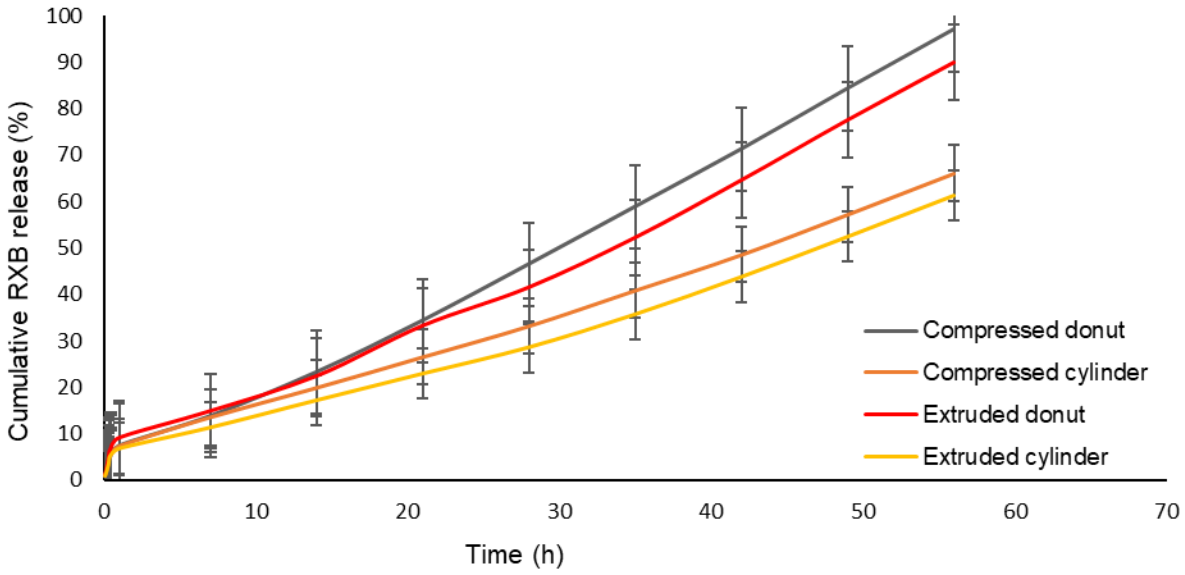

Figure 5.7. *In-vitro* drug release of the compressed and extruded devices compared.

Table 5.2 The summary of *in-vitro* drug release of the compressed and extruded devices compared.

	Compressed donut		Compressed cylinder		Extruded donut		Extruded cylinder	
Time (hours)	**Conc. (µg/mL)**	**Cum. Release**	**Conc. (µg/mL)**	**Cum. Release**	**Conc. (µg/mL)**	**Cum. Release**	**Conc. (µg/mL)**	**Cum. Release**
0,08	2,95	2,95	2,8	2,8	3,97	3,97	3,08	3,08
0,17	3,29	6,24	3,55	6,35	4,34	8,31	3,13	6,21
0,25	3,62	9,85	3,87	10,23	4,98	13,29	3,21	9,41
0,33	3,75	13,6	4,1	14,33	5,23	18,52	3,78	13,19
0,42	3,74	17,35	3,85	18,17	4,5	23,02	5,09	18,28
1	8,53	25,87	7,1	25,27	8,81	31,82	5,45	23,73
7	22,32	48,19	21,69	46,96	20,2	52,02	15,85	39,58
14	33,09	81,28	22,33	69,29	26,31	78,33	20,54	60,12
21	38,91	120,19	23,26	92,55	38,05	116,38	20,11	80,24
28	42,53	162,72	23,36	115,91	28,96	145,34	19,86	100,1
35	43,28	206	26,95	142,85	37,5	182,84	24,85	124,95
42	43,37	249,37	26,98	169,83	43,38	226,21	28,26	153,21
49	45,68	295,04	30,43	200,26	45,39	271,6	30,26	183,48
56	44,49	339,53	31,01	231,27	43,35	314,95	30,98	214,46

5.3.5 *In-vitro* cytotoxicity analysis of RXB loaded and un-loaded HPMC/PU-PEG-PLGA

The potential cytotoxicity of the RXB loaded and un-loaded HPMC/PU-PEG-PLGA assessed by exposing cultured cells to different concentrations of these compounds, and by evaluating and comparing the change in the mitochondrial metabolic activity of those cells using the MTT assay. The results obtained from the MTT assays are presented in **Figure 5.8.** The result show that RXB loaded and un-loaded HPMC/PU-PEG-PLGA don't significantly reduce the viability of the when compared to the control (untreated cells). Hence it can be established that RXB loaded and un-loaded HPMC/PU-PEG-PLGA is non-toxic and the results confirm the findings of Solayar et al. (2011) where RXB treatment did not affect cell viability. Additionally, as toxicity was only observed slightly with the higher concentration of the formulation it can be concluded that using UV-VIS as a form of sterilization was efficient for the formulation. As the incubated plate with a streak of the sterilized device revealed that there was no bacterial growth from the device, hence it was established that the device was sterile before its application in the in-vitro cytotoxicity.

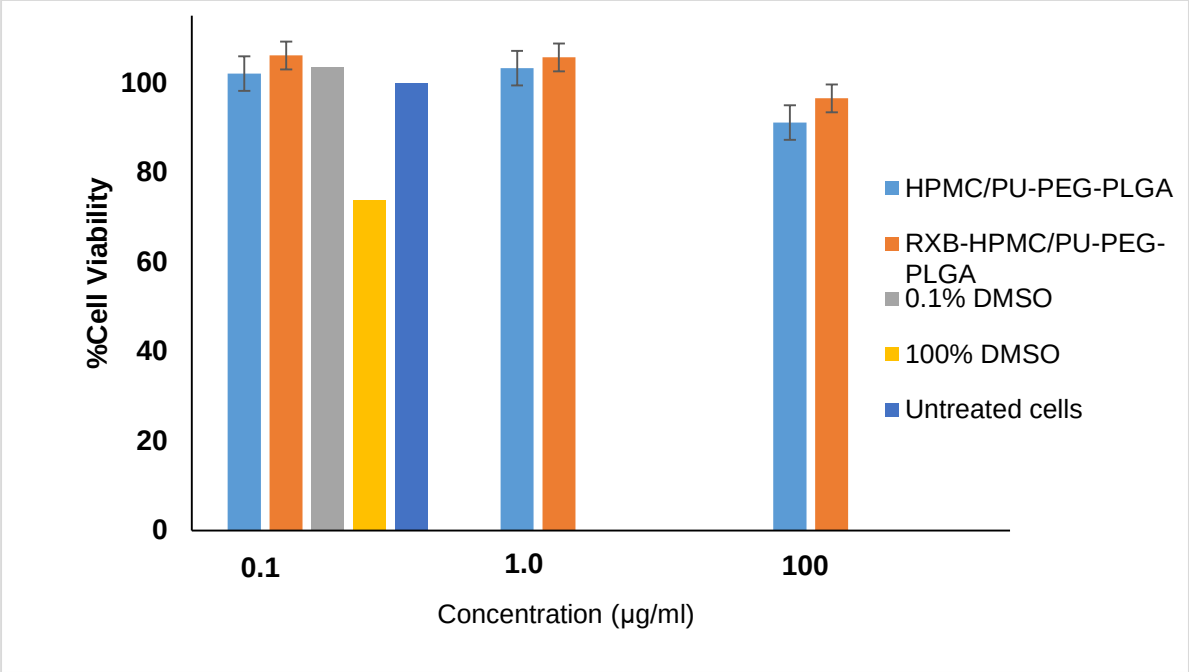

Figure 5.8. The cytotoxicity of RXB loaded and un-loaded HPMC/PU-PEG-PLGA as % cell viability

5.4 CONCLUSION

In this work, two 3D geometrical structures were successfully formulated for implantation, two different techniques were used resulting into similar release patterns, while the compressed technique showed better release compared to the TA extrusion-based method. Hence it was concluded that the compressed method had more potential for the formulation of the 3D implants. This work has shown the potential for personalised as these devices can be modified by changing implant geometry and formulation technique. The results described on this work show the simplicity of 3D technology, where it can easily be transferred to clinical trials and implemented for chronic drug delivery, the toro-poloidal, 3D implantable devices may be applied for both systematic and local drug delivery while avoiding the gut system.

5.5 REFERENCES

Ammar, H.O., Ghorab, M., El-Nahhas, S.A. and Kamel, R., 2006. Design of a transdermal delivery system for aspirin as an antithrombotic drug. International Journal of Pharmaceutics, 327(1-2), 81-88.

Antoniou, S. and Amara, W., 2016. Once-daily rivaroxaban for long-term stroke prevention in patients with atrial fibrillation. European Heart Journal Supplements, 18(suppl_D): D7-D15.

Brown, J.Q., Vishwanath, K., Palmer, G.M. and Ramanujam, N., 2009. Advances in quantitative UV–visible spectroscopy for clinical and pre-clinical application in cancer. Current Opinion in Biotechnology, 20(1): 19-131.

Curto, A., 2017. Management of patients taking rivaroxaban for dental treatments. European Journal of General Dentistry, 6(1): 1.

Domsta, V. and Seidlitz, A., 2021. 3D-Printing of Drug-eluting implants: an overview of the current developments described in the literature. Molecules, 26(13): 4066.

Goyanes, A., Martinez, P.R., Buanz, A., Basit, A.W. and Gaisford, S., 2015. Effect of geometry on drug release from 3D printed tablets. International Journal of Pharmaceutics, 494(2): 657-663.

Griffin, M., Castro, N., Bas, O., Saifzadeh, S., Butler, P., & Hutmacher, D. W. (2020). The current versatility of polyurethane 3D-printing for biomedical applications. Tissue Engineering Part B: Reviews. 26(3):272-283.

Guo T, Holzberg TR, Lim CG, Gao F, Gargava A, Trachtenberg JE, Mikos AG, Fisher JP. 3D printing PLGA: a quantitative examination of the effects of polymer composition and printing parameters on print resolution. Biofabrication. 2017 12 ;9(2): 024101.

Hutanu D, Frishberg MD, Guo L, Darie CC. Recent applications of polyethylene glycols (PEGs) and PEG derivatives. Modern Chemistry and Applications 2014 26; 2(2):1-6.

Ishigaki, M., Meksiarun, P., Kitahama, Y., Zhang, L., Hashimoto, H., Genkawa, T. and Ozaki, Y., 2017. Unveiling the aggregation of lycopene *in-vitro* and *in-vivo*: UV–Vis, resonance raman, and raman imaging studies. The Journal of Physical Chemistry B, 121(34): 8046-8057.

Karunakaran, C., Vijayabalan, A., Manikandan, G. and Gomathisankar, P., 2011. Visible light photocatalytic disinfection of bacteria by Cd–TiO2. Catalysis Communications, 12(9): 826-829.

Kastellorizios, M. and Burgess, D.J., 2012. In vitro drug release testing and in vivo/in vitro correlation for long-acting implants and injections. In Long-Acting Injections and Implants. 475-503.

Laube, E.S., Yu, A., Gupta, D., Miao, Y., Samedy, P., Wills, J., Harnicar, S., Soff, G.A. and Mantha, S., 2017. Rivaroxaban for stroke prevention in patients with nonvalvular atrial fibrillation and active cancer. The American Journal of Cardiology, 120(2): 213-217.

Lewalter T, Kanagaratnam P, Schmidt B, Rosenqvist M, Nielsen-Kudsk JE, Ibrahim R, Albers BA, Camm AJ., 2014. Ischaemic stroke prevention in patients with atrial fibrillation and high bleeding risk: opportunities and challenges for percutaneous left atrial appendage occlusion. Europace, 1; 16 (5):626-30.

Luo L., Miao L., Tanemura S., Tanemura M., 2008. Photocatalytic sterilization of TiO2 films coated on Al fibe. Materials Science and Engineering: B, 148 (1–3): 183–186.

Makadia HK, Siegel SJ. Poly lactic-co-glycolic acid (PLGA) as biodegradable controlled drug delivery carrier. Polymers. 20113(3):1377-97.

Makadia, H.K. and Siegel, S.J., 2011. Poly lactic-co-glycolic acid (PLGA) as biodegradable controlled drug delivery carrier. Polymers, 3(3): 1377-1397.

Margetić, S., Ćelap, I., Delić Brkljačić, D., Pavlović, N., Šupraha Goreta, S., Kobasić, I., Lovrenčić-Huzjan, A. and Bašić Kes, V., 2020. Chromogenic anti-FXa assay calibrated with low molecular weight heparin in patients treated with rivaroxaban and apixaban: possibilities and limitations. Biochemia Medica, 30(1): 74-82.

Martinez, P.R., Goyanes, A., Basit, A.W. and Gaisford, S., 2018. Influence of geometry on the drug release profiles of stereolithographic (SLA) 3D-printed tablets. merican Association of Pharmaceutical Scientists, 19(8): 3355-3361.

Paikin, J.S., Manolakos, J.J. and Eikelboom, J.W., 2012. Rivaroxaban for stroke prevention in atrial fibrillation: a critical review of the ROCKET AF trial. Expert Review of Cardiovascular Therapy, 10(8): 965-972.

Pandey, M., Choudhury, H., Fern, J.L.C., Kee, A.T.K., Kou, J., Jing, J.L.J., Her, H.C., Yong, H.S., Ming, H.C., Bhattamisra, S.K. and Gorain, B., 2020. 3D printing for oral drug delivery: a new tool to customize drug delivery. Drug delivery and Translational Research, 10(4): 986-1001.

Polamaplly, P., Cheng, Y., Shi, X., Manikandan, K., Kremer, G.E. and Qin, H., 2019. 3D printing and characterization of hydroxypropyl methylcellulose and methylcellulose for biodegradable support structures. Procedia Manufacturing, 34: 552-559.

Santos, A., Aw, M.S., Bariana, M., Kumeria, T., Wang, Y. and Losic, D., 2014. Drug-releasing implants: current progress, challenges and perspectives. Journal of Materials Chemistry B, 2(37): 6157-6182.

Solayar, G.N., Walsh, P.M. and Mulhall, K.J., 2011. The effect of a new direct Factor Xa inhibitor on human osteoblasts: an in-vitro study comparing the effect of rivaroxaban with enoxaparin. BMC Mmusculoskeletal Disorders, 12(1): 1-8.

Stewart M.W., 2010. Optimal management of cytomegalovirus retinitis in patients with AIDS. Clinical Ophthalmology (Auckland, NZ), 4:285-99

Turpie A.G., 2014. Rivaroxaban as an oral anticoagulant for stroke prevention in atrial fibrillation. Therapeutics and Clinical Risk Management, 10:197.

Vaz, V.M. and Kumar, L., 2021. 3D printing as a promising tool in personalized medicine. Journal of the American Association of Pharmaceutical Scientists, 22(1)1-20.

Veronese, F.M. and Pasut, G., 2005. PEGylation, successful approach to drug delivery. Drug Discovery Today, 10(21): 1451-1458.

Yu, S., Zhang, X., Tan, G., Tian, L., Liu, D., Liu, Y., Yang, X. and Pan, W., 2017. A novel pH-induced thermosensitive hydrogel composed of carboxymethyl chitosan and poloxamer cross-linked by glutaraldehyde for ophthalmic drug delivery. Carbohydrate Polymers, 155, 208-217.

CHAPTER SIX

IN-VIVO STUDY OF A 3D TORO-POLOIDAL IMPLANTABLE DEVICE FOR THE CONTROLLED DELIVERY OF RIVAROXABAN ON NEW ZEALAND WHITE ALBINO RABBITS

6.1 INTRODUCTION

According to Connelly and co-workers (2016) the estimated morbidity and mortality incidence of patients who do not receive appropriate thromboprophylaxis is as high as 20% to 58%. Patients prone to thromboembolic disorders are given antithrombotic drugs for prophylactic purposes, as these drugs function by preventing thrombus formation (thrombosis) (Acosta et al., 2016). Oral rivaroxaban (RXB) has been an attractive alternative drug compared with other antithrombotic agents (Paikin et al., 2012), several studies have proved oral RXB to be more efficacious and associated with decreased major bleeding risks (Krothapalli and Bhave, 2014; Lewalter et al., 2014). Even though RXB is preferred it is associated with some degree of gastrointestinal (GI) bleeding, which is the most common extracranial haemorrhagic complication in patients on oral RXB (Krothapalli and Bhave, 2014; Ammar et al., 2016). Hence the 3D implant formulated in this study will offer an alternative route by passing the gut system, more convenient and safer, especially for long-term use.

3D is a technology that forms a physical version by fusing different materials into a 3D structure (Li et al., 2018). This technology has been around for a number of years predominately used in manufacturing, however due to its properties, it presents opportunities for pharmaceutical innovation (Li et al., 2018; Maulvi et al., 2017). In this study a novel 3D, toro-poloidal device for implantation will be evaluated. With the 3D toro-poloidal device referring to a 3D toro-poloidal structured device (donut shaped-like device) with a specific direction of fill. This project focuses on designing a 3D implantable drug delivery device for controlled release of RXB, this 3D approach is anticipated to tremendously surpass in the area of personalized medicines by tailoring the shape of the implant to control drug release (Li et al., 2018). In addition, controlled drug delivery can be achieved by the toro-poloidal shape of the device. This toro-poloidal 3D is anticipated to deliver the drug at a constant and predetermined rate over a period longer than one month, however this *in-vivo* study was designed for 28 days. This 3D implantable device has great potential in minimising frequent dosing and potential systemic side effects.

In this study, the *in-vivo* drug delivery on the New Zealand White Albino male rabbits was undertaken to complement the *in-vitro* drug release, and cell viability studies performed on Albino Swiss Mouse Embryo Fibroblasts (3T3 Line). The *in-vivo* studies were essential to determine the outcomes of the toro-poloidal 3D implantable device over a 28 days period that are otherwise not possible with *in-vitro* models. A number of *in-vitro* and *in-vivo* studies where oral RXB was formulated have been established (Perzborn et al., 2014), however to the best of my knowledge no RXB implant *in-vivo* studies have been established, hence the need for these studies. The efficacy and safety of oral RXB in the prevention of thrombosis has been established (Haas, 2009). The size of rabbits permits the ready sampling of blood, more blood samples from a single animal, a longer life span than that of rodents, and the immune system genes of rabbits are apparently more similar to those of the human immune system than are rodent genes (Esteves et al., 2018). In animal models of both venous and arterial thrombosis, RXB has shown potent antithrombotic efficacy (Perzborn, Heitmeier and Laux, 2015) and it has been pointed out to be associated with some degree of gastrointestinal bleeding, which is the most common extracranial haemorrhagic complication in patients on oral RXB (Ammar et al., 2006; Lewalter et al., 2014). Hence the 3D implant being proposed will offer an alternative route that will bypasses the gut, be more convenient and safer for RXB delivery especially during long-term use. Rabbits were chosen as they are indicated for long-term studies in subcutaneous tissue (Anderson and Schoen, 2013).

6.2 MATERIALS AND METHODS

6.2.1 Materials

Poly (D,L-lactide-co-glycolide) (PLGA, copolymer ratio 50:50, Mw=55,000 g/moL), rivaroxaban (RXB) from Boehringer Ingelheim, GmbH, (Ingelheim, Germany). Polyethylene Glycol (average MW 4000), Polyurethane, Oleic acid, Tween-40, hydroxypropyl methylcellulose (HPMC) and sodium chloride (NaCl) were all purchased from Sigma-Aldrich Chemie GmbH (Steinheim, Germany). All other chemicals were of analytical grade

6.2.2 Formulation of toro-poloidal, 3D implantable devices

The devices were formulated as described 4.2.2 and 5.2.2.

6.2.3 *In-vivo* study of the 3D toro-poloidal implantable devices on New Zealand White Albino rabbits

6.2.3.1 Experimental Design

Ethical approval was obtained for the *in-vivo* studies from Wits Research Animal Facility (WRAF) and Animal Ethics Committee (2021/08/08/C). A total of 21 rabbits aged between 3-8 months, with a weight of 2.5 - 3.5kg were utilized in study, 3 rabbits allocated to the pilot study. The pilot study was used to evaluate the implantation procedure, and to ensure the efficacy of the pain management. The remaining 18 rabbits were used for the experimental study, where the treatment groups were divided into one control group, one experimental group and one comparative group. Before the surgery of the 12 rabbits (for Group 1 and 2), the animals were randomly separated (n=6/group) and each group was assigned to the relevant treatment groups as described below. The animals were then observed over a period of 28 days.

Pilot study:

Group A: Evaluation of the RXB loaded toro-poloidal 3D device implantation procedure
Group B: Evaluation of the no drug loaded toro-poloidal 3D implant implantation procedure
Group C: Evaluation of oral RXB administration

Treatment groups:

Group 1: Control group: Plain non-drug loaded toro-poloidal 3D device
Group 2: Experimental group: RXB loaded toro-poloidal 3D device
Group 3: Comparative group: Conventional system (oral RXB)

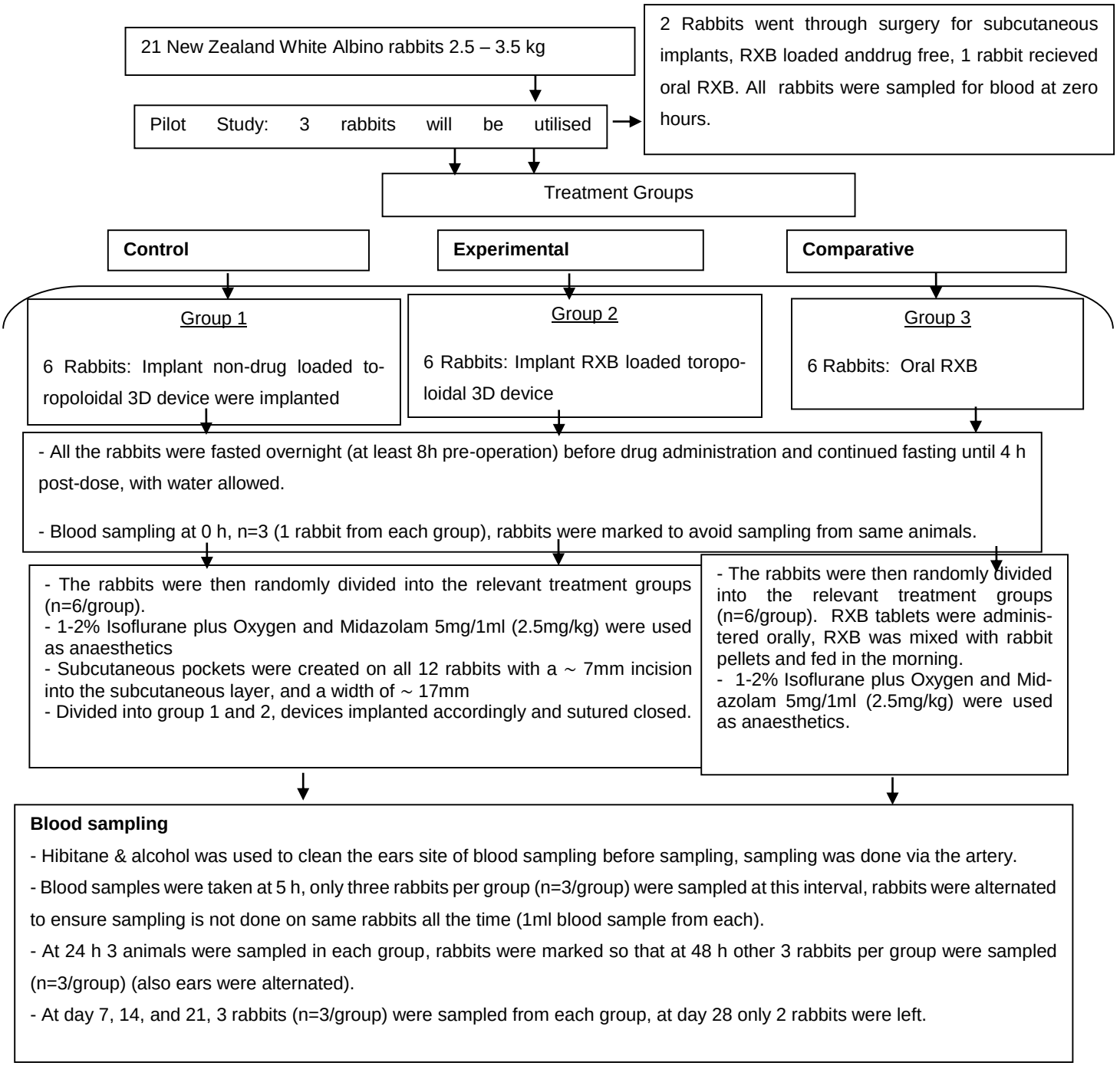

Figure 6.1. Schematic representation of *in-vivo* animal studies to be conducted on the rabbit model with depiction of assigned experimental and control groups.

6.2.3.2 Sequence and timing

The pilot study was performed prior to the experimental study and the sequence was as follows. The pilot was perfumed 28 days prior to the main study, where the implantation site (subcutaneous pocket) was prepared, and the device implanted as described under “Surgical procedures with recovery”. The response of the animals to the implantation and pain management was closely monitored.

For the main study rabbits were randomly divided into the relevant treatment groups (n=6/group). Subcutaneous pockets created on 12 rabbits, divided into group 1 and 2, devices implanted accordingly and sutured closed. Each device was loaded with RXB, releasing the RXB slowly within the safe range of 0.001 – 0.1 mg/mL into the blood stream as determined by the *ex vivo* (cytotoxicity) and *in-vitro* studies already done as part of this study at the Wits Advanced Drug Delivery laboratories, also previous studies have shown the dose to be safe for use in rabbit models given (Brown, 2010; Godier et al., 2012).

RXB tablets were administered daily orally with rabbit pellets on the group 3 animals, 3 mg/Kg RXB dose was given every 24 h (Biemond et al., 2007; Yin et al., 2022). According to *ex vivo* (cytotoxicity) and *in-vitro* studies already done as part of this study at the Wits Advanced Drug Delivery laboratories it was established that the concentration of the drug that enters the blood system were within the safe range of 0.001 – 0.1 mg/mL. All the rabbits were fasted overnight (at least 8h pre-operation) before oral drug administration and continued fasting until 4 h post-dose, with water allowed.

Day 0 - 28:

On each of the four intervals photographs of the implantation site was taken on the anterior abdomen of the remaining rabbits from each group. Blood samples were taken on intervals for the first 48 h (0, 5, 24 and 48 h) then weekly (day 7, 14, 21 and 28) from three rabbits in each group (n = 3/ group), one rabbit from each group was then be euthanized on days 1, 7, 14, 21 and 28 and tissue samples from the superior dorsal (implantation site) were surgically removed for histological evaluation. Within the first 48 h blood sampling were rotated amongst all the rabbits in each group and then alternate both ears for blood collection (as a form of refinement). Blood samples were collected from the rabbits, centrifuged to collect the plasma and stored at -70 °C.

The plasma was used to quantify the concentration of the RXB in the blood and GI bleeding was evaluated using Faecal Occult Blood Test (FOBT).

6.2.3.3 Surgery and recovery

After 8 h of a preoperative fasting period, the rabbits were anesthetized with 1-2 % Isoflurane plus Oxygen and Midazolam 5 mg/1 mL (2.5 mg/kg) (Su et al., 2020). Additionally, 1 mL of local anaesthetic (Lidocaine and Epinephrine) was subcutaneously injected at the site of surgery to improve analgesia and control bleeding (Gehrker et al., 2019). After the animals have been adequately anaesthetized, the anterior abdominal wall was shaved using a hair clipper, cleaned with cleaned povidone–iodine solution and a sterile cloth (Su et al., 2020 Gehrker et al., 2019). A midline subcutaneous pocket was created with a ~ 7mm incision into the subcutaneous layer, and a width of ~ 22 mm on the rabbit skin (Sharma and Lewis, 2019; Gehrker et al., 2019). Ultraviolent sterilized RXB loaded and non-loaded 3D toro-poloidal devices with a width of ~20 mm and 5 mm thickness, were then be inserted into the subcutaneous pocket using forceps and the wounds were sutured closed. Analgesia butorphanol (0.25–0.4 mg/kg) was used throughout post-surgery to prevent any pain (Peng et al., 2011).

6.2.3.4 Histological examination

The use of histology on the subcutaneous tissue (hypodermis) of implanted and non-implanted rabbits' skin was used to evaluate the effects of the implantation (i.e., any signs of adverse reactions such as inflammation), while the currently available histological rabbit studies allowed for comparative studies as well as translation of the results to humans (Allan, Giare-Patel and Olson, 2012). As per Qin (2015) the duration of implantation studies is dictated by the clinical exposure time of the test and for a permanent implant, a minimum short term of 1–4 weeks, hence this study was conducted of a 28-day period. Tissue samples on the implantation site were collected, fixed and embedded in paraffin. Paraffin-embedded specimens were stained with haematoxylin and eosin. Stained tissue sections were evaluated for signs of the presence and severity of inflammation. Tissue samples from the comparative group of rabbits were used as controls. Samples were blinded and scored by a trained pathologist.

6.2.3.5 Faecal Occult Blood Test (FOBT)

FOBT were done at every time interval as blood sampling up to 28 days. Rectal swabs were obtained by inserting a sterile cotton swab 20–30 mm into the rectum and rotating the swab

against the bowel wall. The FOBT samples were taken at 5 h, only three rabbits per group (n = 3/ group) were sampled at this interval, rabbits were alternated to ensure sampling is not done on same rabbits all the time. At 24 h 3 animals were sampled in each group, rabbits were marked so that at 48 h other 3 rabbits per group were sampled (n=3/group). At day 7, 14, and 21, 3 rabbits (n = 3/ group) were sampled from each group, at day 28 only 2 rabbits were left for sampling. The faecal samples were collected into clean Eppendorf tubes and stored at −20°C until further processing. An FOBT kit was used for the analysis.

6.2.4 Estimation of RXB in rabbit plasma

Ultra violet-visible spectrophotometric method was used to determine RXB in rabbit plasma levels, similar method was described by Bhavyasri, Dhanalakshmi and Sumakanth (2020). The advantage of using UV-Vis nanophotometer is that it does not require the elaborate treatment and procedures usually associated with chromatographic methods. It is less time consuming and economical. And according to Dhole, Amnerkar, and Khedekar (2012) it was indicated that UV Vis methods are adequate to quantify drug released and there are a number of reported quantitative *in-vivo* analysis where UV-Vis was used (; Brown et al., 2009; Ishigaki et al., 2017).

6.2.4.1 Preparation of standard calibration curve

To prepare a standard solution 10mg RXB was weighed into a 100ml volumetric flask, dissolved with acetonitrile: water (60:40), then sonicated for 2 min and made up to the mark with acetonitrile: water (60:40). The standard solution was used to determine the maxima absorption of the RXB where a scan was done between 200-900 nm range of the UV spectroscopy and the absorption was found at 252 nm. The same standard solution was also used to dilute the RXB into 6 solutions to establish a standard calibration curve. A blank plasma was used for the calibration curve.

6.2.4.2 Extraction of plasma from blood

Blood was collected into an EDTA containing tube, centrifuged for 15 min at 5000 rpm, the supernatant (blood plasma) was collected and stored at −20 °C until further processing. For plasma extraction, the frozen plasma was thawed, vortexed and ready for preparation. The plasma solution was deprotonated by adding 0.5 mL plasma, 1 mL of RXB solution (spiked with 1 mL similar concentration for main study and different concentration in 1 mL used for calibration curve) and the mixture was vortexed for a minute before adding 1 mL of acetonitrile, vortexed again and filtered using 0.25 µm filters. Then the filtered mixture was collected and analysed at absorbance

250 nm using a nanophotometer (IMPLEN Nanophotometer™, Implen GmbH, Munchen Germany).

6.3 RESULTS AND DISCUSSION

6.3.1 *In-vivo* study of the 3D toro-poloidal, implantable devices on New Zealand White Albino rabbits

The study was successfully carried out using New Zealand White Albino rabbits, see **Figure 6.2.**

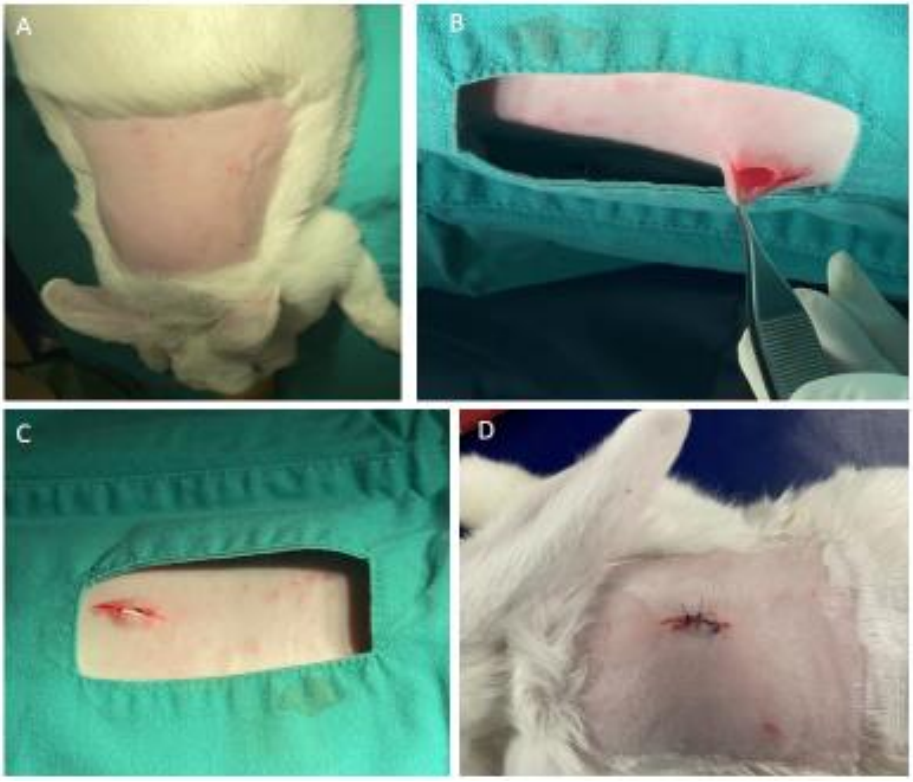

Figure 6.2. Images from *in-vivo* study using New Zealand White Albino rabbits where: (A) was after the rabbit has been shaved, (B) a subcutaneous pocket created for implant insertion, (C) the device inside the subcutaneous pocket and (D) after the implant was inserted the pocket was sutured.

Figure 6.3 shows the healing of the sutured wound after implantation, where the sutured area was healed on day 7 (**Figure 6.3A**), stitches started coming out, **Figure 6.3B** shows complete healing and hair growing back on the implantation site.

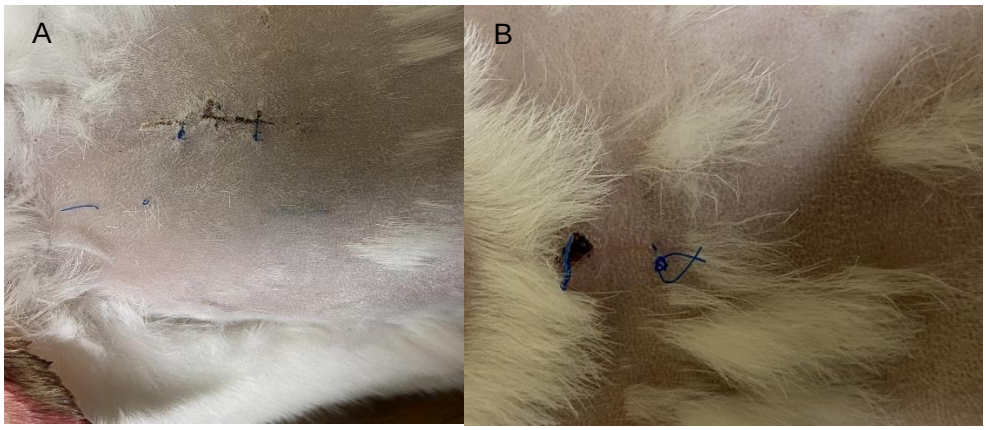

Figure 6.3. The visual recovery of the subcutaneneous incision (A) The implantation site on day 7, and (B) day 14.

In addition to the *in-vitro* tests, physical and histological toxicity and inflammatory response of the novel 3D toro-poloidal implantable device was assessed. The animals in the test groups 1 and 2 (who received the RXB loaded and drug free devices) had normal body weight growth. The body weight of all the rabbits in all groups was generally increasing throughout the study, and there was no significant difference from all the groups. No animals died throughout the study, and the animals that received implantation showed excellent healing and recovery, see **Figure 6.3**. where the recovery of the animals was visually monitored.

6.3.2 Histology analysis

All samples from the individuals in group 3 that did not have implant surgery yielded presence of normal skin structures as would be expected in a normal animal without invasive surgery **Figure 6.4.** (C, F, I, L). The two individuals' skins evaluated at day 1 show acute changes involving the surgically-induced subcutaneous pocket/cyst. These include haemorrhage with fibrin deposition and mild acute necrosis of traumatized tissues around/lining the pocket. Acute heterophilic infiltrates would be the first inflammatory cell type expected to invade at this point, and are mild to moderate only.

After 7 days the cyst/pocket has developed early mild to moderate peripheral macrophage infiltration with granulomatous inflammation, and granulation tissue formation in the form of a capsular type of structure. The lesion thus represents a pseudocyst. Macrophage infiltration would be

indicative of an early foreign body reaction. There is not much difference between the reaction noted on day 7 between the 2 individuals in groups 1 and 2.

At 14 days the cystic space is reduced in size and devoid of exudate. Surrounding fibrosis, in the formation of granulation tissue (pseudo-capsule) has become thicker than noted in earlier samples (moderate to severe). Inflammation is granulomatous and mild in G (group 1), while moderate in H (group 2). Few heterophils are still present in G. Foreign material is present in G, but not clearly in H.

The samples from day 28 in group 1 reveal absence of, or a very small remaining central space in samples D, G and J. The sub-cutis in these 3 samples contain varying degrees of interstitial presence of foamy macrophages, accompanied by small amounts of haphazard fibroblasts. A capsule is not visible. The subcutaneous tissue is also mildly oedematous and no foreign material is evident.

The samples from day 28 in group 2 show remaining cystic spaces (K) and they are surrounded by moderate to severe granulomatous inflammation which includes macrophages and multinucleate giant cells. The inflammation is associated with moderate to large amounts of refractory crystalline foreign material (3D device), unlike group 1 where foreign crystalline material is not visible histologically. The granulomas are surrounded by mild to moderate encircling fibrosis. In group 1 the 28-day inflammation is milder in general, mostly consisting of a homogenous infiltrate of disseminate/interstitial macrophages without a cystic space or capsule and without foreign material.

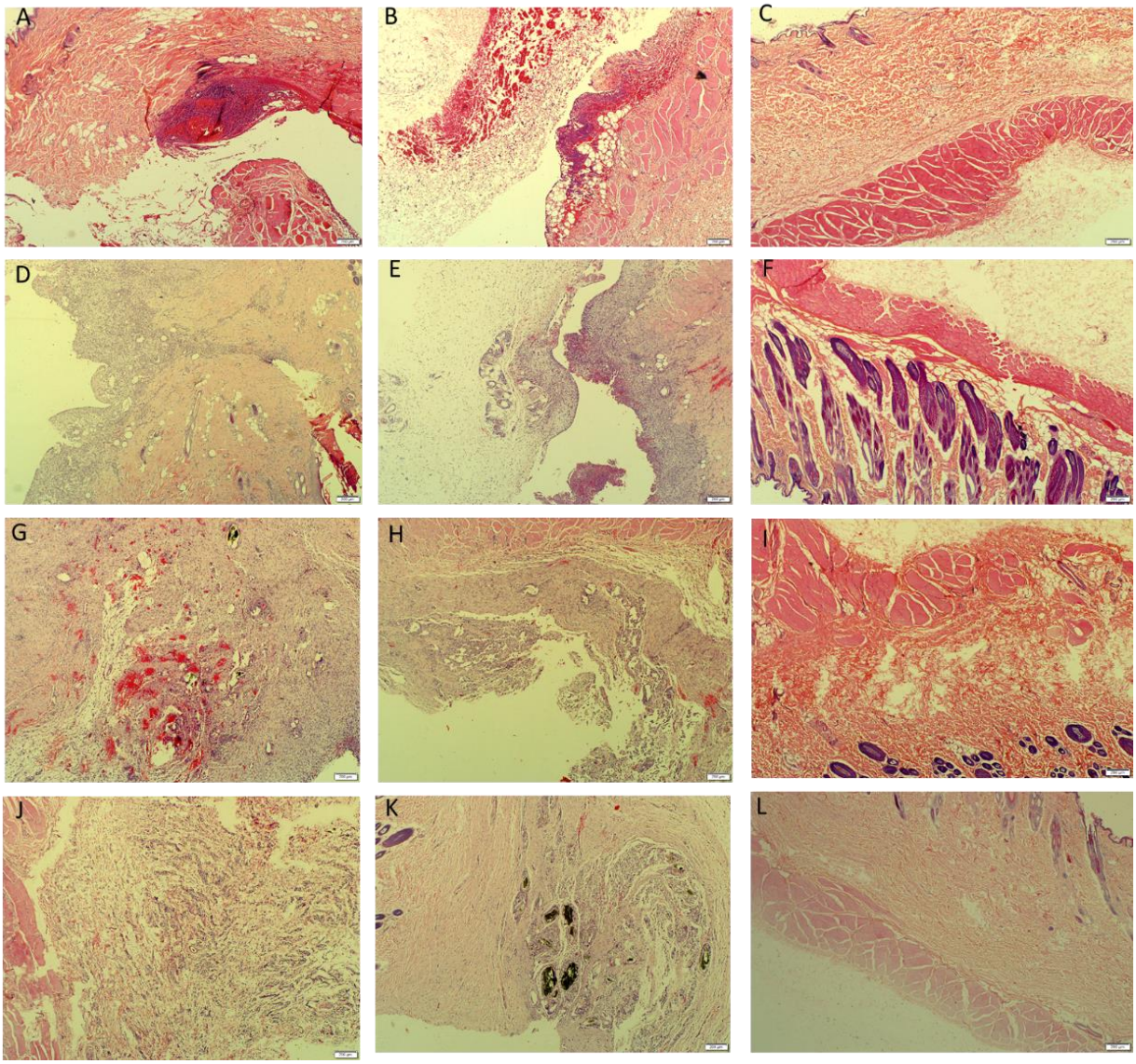

Figure 6.4. The H&E-stained histological analysis of the tissue surrounding the implantation site. A-C at day 2, D-F at day 7, G-I at day 14 and J-L at day 28, all with group 1, 2 and 3, respectively.

6.3.3 Faecal Occult Blood Test (FOBT) analysis

The faecal Occult Blood Test (FOBT) analysis kits only showed positive and negative results, see **Figure 6.5**. According to the samples total samples collected from the rabbits for each group, it was shown that ~83 %of the results collected from the oral RXB group showed either a faint or a strong T line, indicating the presence of blood, which is indicative of abnormal bleeding occurring somewhere within the GI system. In this study it was concluded that the oral RXB that increase the chances of GI bleeding compared to the implantation of the 3D toro-poloidal device for the

delivery of RXB, where only ~17 % of the faecal samples showed a faint T line indicating the slight presence of GI bleeding after receiving the RXB loaded implants, this could be due to reduced tolerance of the drug by the specific rabbit. The non-RXB loaded control group showed no indication of GI bleeding.

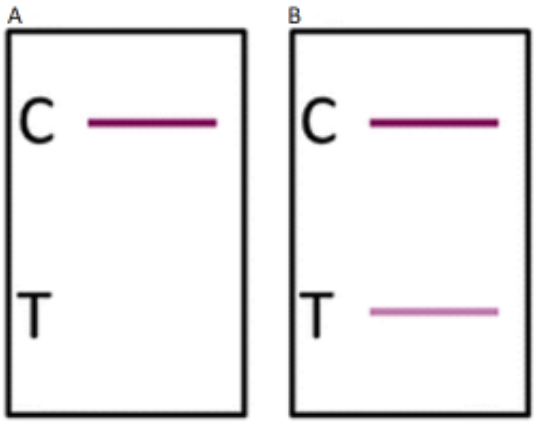

Figure 6.5. A) The negative FOBT, where C shows the present control line and T the absent test line, and B) The positive FOBT, where C shows the present control line and T the present test line.

Table 6.1 The summarised outcome of the FOBT from the main study rabbits

Time (days)	Implant RXB loaded toro-poloidal 3D device	Implant with no RXB loaded toro-poloidal 3D device	Oral RXB
1	negative FOBT	negative FOBT	negative FOBT
2	negative FOBT	negative FOBT	positive FOBT
7	negative FOBT	negative FOBT	positive FOB
14	negative FOBT	negative FOBT	positive FOB
21	positive FOBT	negative FOBT	positive FOB
28	negative FOBT	negative FOBT	positive FOB

6.3.4 *In-vivo* RXB released using New Zealand White Albino rabbits

6.3.4.1 RXB quantification using a nanophotometer

The calibration curve of the RXB using blank plank plasma was successfully achieved using a nanophotometer, where all analysis was done in triplicates and the correlation coefficient (R^2) was

0.99. **Figure 6.6** shows the summarised outcome of the RXB calibration curve using blank plasma.

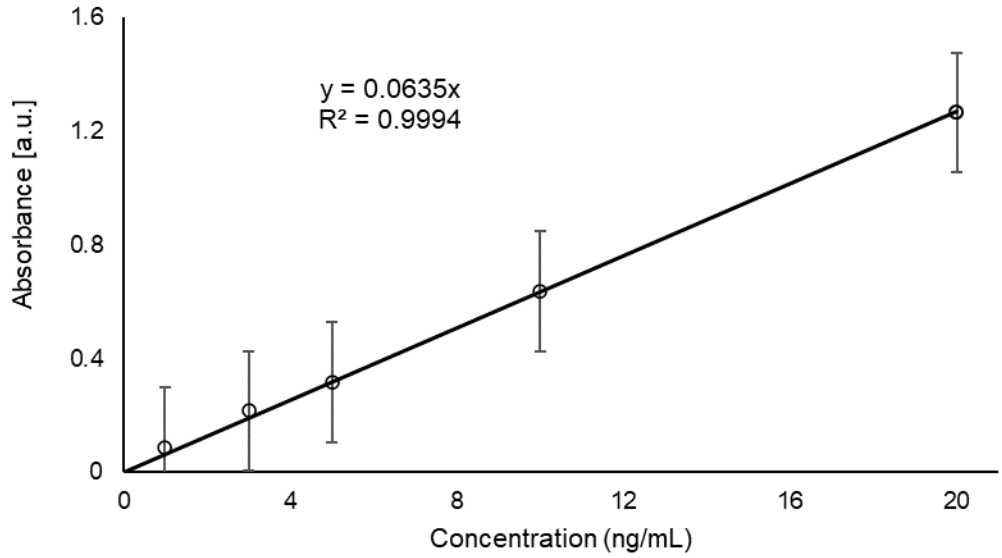

Figure 6.6. The calibration curve of the RXB using the nanophotometer at 252 nm

6.3.5 *In-vivo* RXB release of the 3D toro-poloidal implantable devices

The drug release profiles of the 3D toro-poloidal, implantable devices were examined in rabbit models. The plasma samples obtained from the rabbits treated by oral and subcutaneous implant were evaluated using a nanophotometer UV/Vis, in order to analyse the RXB release from the blood plasma the samples were subjected to extraction suing the liquid-liquid extraction principle. The concentrations of RXB released from both the oral administered and subcutaneous implanted devices are shown on **Table 6.1**, also shown on the table are the cumulative concentrations which were then used to plot the RXB release on **Figure 6.7** over the period of 28 days. The RXB released from the implantable devices show a two-step release mechanism where a burst release is initially observed with the first day, then a slight decrease in RXB released leading to increased and sustained RXB release plasma concentrations, where it's shown that the RXB release had not reached its completion stage on day 28, it looks like it was still increasing. Looking at the oral conventional RXB release studies a steady increase of the RXB released was observed where the bioavailability was approximately 32 % lower compared to the implantable RXB device, also the steady increase of the oral RXB released showed to some extent that full elimination of the

RXB was not achieved for RXB as it was dosed daily the same quantity, yet the drug concentration was increasing.

Judging from the release data, the implantable device drug release did not reach the peak value of the RXB released, this suggests the potential for use the 3D toro-poloidal, implantable devices over extend period of time. This device may be used for both local and systemic drug delivery, as it has shown the potential for maintaining a high drug concentration systematically for an extended period of time, this also shows that fewer side effects of the drug may be experienced as it bypass the gut system. Also improved patient compliance and personalised medicine may be achieved using the novel 3D toro-poloidal, implantable device.

Table 6.1. The summary of the plasma concentration of RXB and cumulative RXB released after subcutaneous implantation of the 3D toro-poloidal, implantable device and oral RXB administration

Time (days)	Oral RXB		RXB loaded device	
	Conc. RB released (µg/mL)	Cum. RXB released (µg/mL)	Conc. RXB released (µg/mL)	Cum. RXB release (µg/mL)
0.21	1.04	1.04	3.43	3.43
1	1.65	2.68	2.77	6.21
2	1.76	4.45	3.05	9.26
7	2.75	7.20	3.41	12.67
14	3.73	10.93	4.21	16.88
21	4.04	14.97	4.00	20.88
28	4.68	19.65	7.26	28.15

*Where Conc. is the plasma concentration of RXB (µg/mL) and Cum. is the cumulative RXB released.

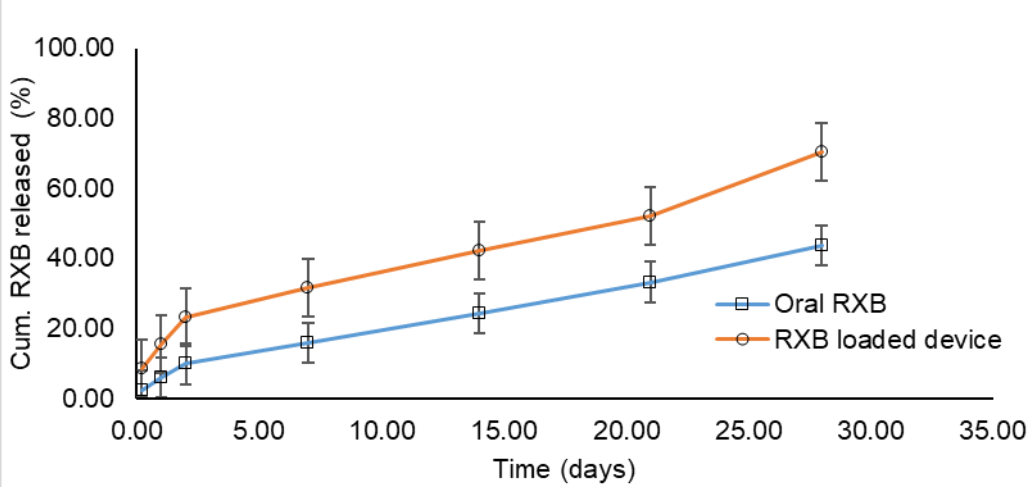

Figure 6.7. The plasma cumulative RXB concentrations in rabbits after subcutaneous implantation of the 3D toro-poloidal, implantable device and oral RXB administration.

6.3.6 Correlation of the *in-vivo* and *in-vitro* RXB release from the 3D toro-poloidal implantable devices

In **chapter 4** and **5**, *in-vitro* release studies were carried out, where *in-vitro* release conditions closely mimicked *in-vivo* conditions. The similarity between *in-vitro* dissolution/ release studies with the *in-vivo* release on models can be considered a validation approach of the in vitro–in vivo correlation (Shleghm et al., 2021). One particular study to be noted (Le Guellec, Ehrmann, and Vecellio, 2021) where the *in-vitro* and *in-vivo* correlation described was based on deposition pattern of the drug in the in vitro and in vivo studies (Le Guellec, Ehrmann, and Vecellio, 2021).

Considering the *in-vitro* release studies covered in chapter 3/4 and the *in-vivo* release studies in this chapter for the RXB released from the 3D toro-poloidal, implantable devices, it is indicated that even though the release rates were higher in the in-vitro studies there is still some correlation in the release pattern. In the literature*, in-vivo-in-vitro* correlations performed on other drugs and animal model showed a generally poor correlation between in-vitro and *in-vivo*, where the *in-vitro* studies gave higher rates than *in-vivo* results (Kararli et al., 1995). Both the *in-vitro* and *in-vivo* studies are showing a biphasic release mechanism where there is an initial burst release followed by a consistent RXB release. The *in-vivo* RXB further proved that the drug release from the model has the potential of being released for longer than a month as the animals' studies were only carried out over a period of 28 days, which is correlating to the *in-vitro* studies where the release

was observed over a period of six weeks. It can therefore be concluded that the correlation perceived in this study is considered to be scientifically significant, as the relationship observed between the *in-vivo* and *in-vitro* studies is showing some consistency.

6.4 CONCLUSION

In conclusion, the *in-vitro* and *in-vivo* correlation was observed in this chapter, indicating that the use of the 3D toro-poloidal, implantable device may enhance the delivery of RXB over an extended period of time. The novel 3D toro-poloidal, implantable device designed and studied in this project is capable of circumventing the known shortcomings of the oral administration of RXB, such as high low bioavailability and GI associated bleeding. This novel device demonstrated its potential in its ability to deliver the required therapeutic dose, increasing RXB blood bioavailability, while reducing the expected adverse effects as the device by passes the gut system. According to this study it was established that the 3D toro-poloidal, implantable device may be a promising 3D device for long term delivery of potent drugs like RXB. Collectively, the data observed under *in-vitro* and *in-vivo* studies, as well as the lack of toxicity demonstrate the potential for the use of the 3D device to achieve controlled release kinetics via the subcutaneous route. To our knowledge, this is the first report on an RXB-loaded HPMC/PU-PEG-PLGA, 3D toro-poloidal implant that can be administered for both local or systemic drug delivery, and that can provide sustained drug delivery *in-vivo.* Furthermore, follow up clinical studies may be formulated this study, as this concept can also be extended to other pharmaceutical fields for controlled release of materials. All 3D devices were well-accepted by the rabbits on the *in-vivo* studies with no signs of local inflammation or change in body weight. Collectively, the *in-vitro, in-vivo* and absence of toxicity prove the potential of the novel a RXB-loaded HPMC/PU-PEG-PLGA, 3D toro-poloidal device for use in chronic conditions.

6.5 REFERENCES

Acosta, R.D., Abraham, N.S., Chandrasekhara, V., Chathadi, K.V., Early, D.S., Eloubeidi, M.A., Evans, J.A., Faulx, A.L., Fisher, D.A., Fonkalsrud, L. and Hwang, J.H., 2016. The management of antithrombotic agents for patients undergoing GI endoscopy. Gastrointestinal Endoscopy, 83(1): 3-16.

Alhnan, M.A., Okwuosa, T.C., Sadia, M., Wan, K.W., Ahmed, W. and Arafat, B., 2016. Emergence of 3D printed dosage forms: opportunities and challenges. Pharmaceutical Research, 33(8): 1817-1832

Allan, N.D., Giare-Patel, K. and Olson, M.E., 2012. An in-vivo rabbit model for the evaluation of antimicrobial peripherally inserted central catheter to reduce microbial migration and colonization as compared to an uncoated PICC. Journal of Biomedicine and Biotechnology, 2012.

Ammar, H.O., Ghorab, M., El-Nahhas, S.A. and Kamel, R., 2006. Design of a transdermal delivery system for aspirin as an antithrombotic drug. International Journal of Pharmaceutics, 327(1-2): 81-88.

Anderson, J.M., Schoen, F.J. and Ziats, N.P., 2020. *In-vivo* assessment of tissue compatibility. In Biomaterials Science: 869-877.

Bhavyasri, K., Dhanalakshmi, C. and Sumakanth, M., 2020. Development and validation of ultra violet-visible spectrophotometric method for estimation of rivaroxaban in spiked human plasma. Journal of Pharmaceutical Sciences and Research, 12(9): 1215-1219.

Biemond, B.J., Perzborn, E., Friederich, P.W., Levi, M., Buetehorn, U. and Büller, H.R., 2007. Prevention and treatment of experimental thrombosis in rabbits with rivaroxaban (BAY 597939)–an oral, direct factor Xa inhibitor. Thrombosis and Haemostasis, 97(03): 471-477.

Connelly, C.R., Laird, A., Barton, J.S., Fischer, P.E., Krishnaswami, S., Schreiber, M.A., Zonies, D.H. and Watters, J.M., 2016. A clinical tool for the prediction of venous thromboembolism in pediatric trauma patients. JAMA Surgery, 151(1): 50-57

Dhole, S.M., Amnerkar, N.D. and Khedekar, P.B., 2012. Comparison of UV spectrophotometry and high-performance liquid chromatography methods for the determination of repaglinide in tablets. Pharmaceutical Methods, 3(2): 68-72.

Esteves, P.J., Abrantes, J., Baldauf, H.M., BenMohamed, L., Chen, Y., Christensen, N., González-Gallego, J., Giacani, L., Hu, J., Kaplan, G. and Keppler, O.T., 2018. The wide utility of rabbits as models of human diseases. Experimental & Molecular Medicine, 50(5): 1-10.

Godier, A., Miclot, A., Le Bonniec, B., Durand, M., Fischer, A.M., Emmerich, J., Marchand-Leroux, C., Lecompte, T. and Samama, C.M., 2012. Evaluation of prothrombin complex concentrate and recombinant activated factor VII to reverse rivaroxaban in a rabbit model. The Journal of the American Society of Anesthesiologists, 116(1): 94-102.

Goole J, Amighi K., 2016. 3D printing in pharmaceutics: A new tool for designing customized drug delivery systems. International Journal of Pharmaceutics 499(1-2):376-94.

Haas, S., 2009. Rivaroxaban–an oral, direct Factor Xa inhibitor–lessons from a broad clinical study programme. European journal of haematology, 82(5): 339-349.

Jassim-Jaboori AH, Oyewumi MO., 2015. 3D Printing technology in pharmaceutical drug delivery: Prospects and challenges. Journal of Biomolecular Research & Therapeutics. 4:4: 1000e141.

Krothapalli S, Bhave PD., 2014. My patient taking a novel oral anticoagulant needs surgery, device implantation, or ablation. Journal of Atrial Fibrillation, 7(3).

Le Guellec, S., Ehrmann, S. and Vecellio, L., 2021. In vitro–in vivo correlation of intranasal drug deposition. Advanced Drug Delivery Reviews, 170: 340-352.

Lewalter T, Kanagaratnam P, Schmidt B, Rosenqvist M, Nielsen-Kudsk JE, Ibrahim R, Albers BA, Camm AJ., 2014. Ischaemic stroke prevention in patients with atrial fibrillation and high bleeding risk: opportunities and challenges for percutaneous left atrial appendage occlusion. Europace, 1; 16 (5): 626-30.

Li, Q., Guan, X., Cui, M., Zhu, Z., Chen, K., Wen, H., Jia, D., Hou, J., Xu, W., Yang, X. and Pan, W., 2018. Preparation and investigation of novel gastro-floating tablets with 3D extrusion-based printing. International Journal of Pharmaceutics, 535(1-2): 325-332

Maulvi, F.A., Shah, M.J., Solanki, B.S., Patel, A.S., Soni, T.G. and Shah, D.O., 2017. Application of 3D printing technology in the development of novel drug delivery systems. International Journal of Drug Development & Research, 9(1): 44-9.

Paikin JS, Manolakos JJ, Eikelboom JW., 2012. Rivaroxaban for stroke prevention in atrial fibrillation: a critical review of the rocket AF trial. Expert review of cardiovascular therapy, 10(8): 965-72

Peng, W., Datta, P., Ayan, B., Ozbolat, V., Sosnoski, D. and Ozbolat, I.T., 2017. 3D bioprinting for drug discovery and development in pharmaceutics. Acta biomaterialia, 57: 26-46.

Perzborn, E., Heitmeier, S. and Laux, V., 2015. Effects of rivaroxaban on platelet activation and platelet–coagulation pathway interaction: *in-vitro* and *in-vivo* studies. Journal of cardiovascular pharmacology and therapeutics, 20(6): 554-562.

Perzborn, E., Heitmeier, S., Buetehorn, U. and Laux, V., 2014. Direct thrombin inhibitors, but not the direct factor Xa inhibitor rivaroxaban, increase tissue factor-induced hypercoagulability in-vitro and in-vivo. Journal of Thrombosis and Haemostasis, 12(7):1054-1065.

Qin, Y. ed., 2015. Medical textile materials. Woodhead Publishing, 24-36.

Shleghm, M.R., Mircioiu, C., Voicu, V.A., Mircioiu, I. and Anuta, V., 2021. Estimation of the in vivo release of amiodarone from the pharmacokinetics of its active metabolite and correlation with its in vitro release. Frontiers in Pharmacology, 11: 621667.

Tagami, T., Fukushige, K., Ogawa, E., Hayashi, N. and Ozeki, T., 2017. 3D printing factors important for the fabrication of polyvinylalcohol filament-based tablets. Biological and Pharmaceutical Bulletin, 40(3): 357-364

Yin, L., Qi, Y., Ge, Z. and Li, J., 2022. Effects of direct oral anticoagulants dabigatran and rivaroxaban on the blood coagulation function in rabbits. Open Life Sciences, 17(1): 1-9.

CHAPTER SEVEN
CONCLUSIONS, RECOMMENDATIONS AND FUTURE PERSPECTIVES

7.1 CONCLUSION

Developing a polymeric implant that can provide controlled drug delivery over weeks or months after a single administration is of great importance in a wide range of medical conditions requiring frequent drug dosing routines. Generally, a polymeric implant in drug delivery may be referred to as a drug reservoir where a drug is either surrounded or mixed with polymeric material, implanted on the desired area of the body, where the drug is released at a predetermined rate when the polymer degrades. In this study, a 3D implant for the delivery of RXB was formulated using polymeric material, where the *in-vitro* RXB was release over a period of six weeks, while the *in-vivo* RXB delivery was carried out over 4 weeks, where it was observed that complete RXB release was not achieved.

The novel 3D toro-poloidal, implantable device was formulated using a novel polymer combination, where polyurethane (PU), poly (lactic-co-glycolic acid) (PLGA), hydroxypropyl methylcellulose (HPMC) and polyethylene glycol (PEG) were made into a blend, and RXB loaded. The RXB loaded blend was characterised using different physicochemical properties, where it was confirmed that the blend was successfully formulated. Porous and non-porous *in-vitro* studies of the RXB loaded HPMC/PU-PEG-PLGA were also compared. It can be concluded that the addition of NaCl does increase the porosity of the 3D toro-poloidal device, resulting into an increased surface area on the device's microstructures, hence affecting the release pattern of the drug.

Further *in-vitro* RXB release studies were carried out using the RXB loaded HPMC/PU-PEG-PLGA, and cytotoxicity studies determined as well as *in-vivo* studies. Where the 3D toro-poloidal, implantable device was implanted on New Zealand White Albino rabbits and the *in-vivo* drug delivery pattern was determined. The *in-vivo* drug delivery study was undertaken to complement the *in-vitro* drug release and cell viability (cytotoxicity) studies performed on Albino Swiss Mouse Embryo Fibroblasts (3T3 Line), where major correlation was observed as the animals showed no irritation or inflammation due to any toxicity from the device constituents, and also the release of the RXB was in a consistent manner throughout the study (day 1 to day 28 of the study). Moreover, histology results showed the healing process of the incision used for implantation, no additional signs of inflammation were observed due to the devices.

Due to the positive outcomes observed in this study with the 3D toro-poloidal, implantable device, the devices have a great potential for medical application as personalised medication. The study showed how the change in the geometry of the device greatly influences the release pattern of the drug, hence the diversity of 3D devices may be expanded and translated into various clinical approaches as well as surgical procedures. Even though the complete development and introduction of 3D devices into the clinical phase is not fully devised, a number of 3D models and devices have shown major efficacy in the pharmaceutical industry.

7.2 RECOMMENDATIONS AND FUTURE PERSPECTIVES

RXB is an anticoagulation agent that functions by inhibiting the coagulation FXa, approved for the prevention of venous thromboembolism for patients undergoing knee/hip replacement surgery, stroke, systemic embolism in non-valvular atrial fibrillation, and for and for both the treatment and prevention of pulmonary embolism (PE) and deep vein thrombosis (DVT) (Bratsos, 2019). In all these conditions RXB is required for long-term usage, patient compliance is a major issue as well as the GI associated bleeding, the novel implant designed in this study is a potential drug delivery system circumventing the major challenges associated with the drug. For patients undergoing knee/hip replacement surgery the implant can easily be inserted on the wound after the surgery with no need for another incision and there would be no need for patient to be taking tablets daily. The medical application of this device has the potential of being expanded into other clinical conditions to deliver different types of drugs required for long-term usage. As this study has proved the efficacy of the novel 3D toro-poloidal, implantable device over an extended period of time. Also, *in-vivo* studies may be carried over a period longer than 4 weeks as the completion of drug release was not achieved within the 28 days done in this study.

In future work, investigating microstructure using the 3D extrusion printing might prove important to further optimising the release profile, this may be due to that computer aided design of the inner microstructure of the device. As 3D printers have the ability to precisely control both the internal and external structures of 3D devices by using different computer aided designs, hence controlling the release properties of the device because of the release link with the structure of the device (Zhu et al., 2020).

7.3 REFERENCES

Bratsos, S., 2019. Pharmacokinetic properties of rivaroxaban in healthy human subjects. Cureus, 11(8): e5484.

Zhu, X., Li, H., Huang, L., Zhang, M., Fan, W. and Cui, L., 2020. 3D printing promotes the development of drugs. Biomedicine Pharmacotherapy, 131:110644.

APPENDIX A

ANIMALS RESEARCH ETHICS COMMITTEE (AREC)

STRICTLY CONFIDENTIAL

CLEARANCE CERTIFICATE NUMBER: 2021/08/08/C

APPLICANT: Ms S Mavuso

School: School of Therapeutic Sciences; Department: N/A; Location: WRAF

PROJECT TITLE: *In-vivo* study of an architecturally variant, 3D printed, implantable toropoloidal device on New Zealand White Albino male rabbits

Category: C; Species and Numbers involved: *21X, 3-8 months old/2.5 - 3.5 kg, male, New Zealand White Albino Rabbits*

Approval is hereby given for the use of animals for the research project named above and described in the application reviewed by a quorate meeting of the AREC held on 31 Aug 2021. This approval remains valid until 10 Oct 2023 and is conditional to the following (if blank there are no special conditions):

Condition 1	Condition 2	Condition 3	Condition 4

All material changes to the approved research must be reported to the AREC before they are implemented. Failure to do so will invalidate this clearance certificate.

An annual progress report must be provided to the AREC.

The use of these animals is subject to AREC guidelines on the use and care of laboratory animals, is limited to the procedures described in the application and is subject to additional conditions listed below:

I, the Chair of the AREC (or my designated representative) am satisfied that the proposed research is ethical as judged by local law, international standards and University policy.

Signed: _____ _____ Date: ___11/10/2021___

(Chairperson of the AREC)

I am satisfied that the persons listed in this application are competent to perform the procedures described in the application, in the context of Section 23 (1) (c) of the veterinary and Para-veterinary Professions Act (19 of 1982).

Signed:  _____ Date: _11 October 2021_____

CC: Student supervisor: «Title1» «Initials1» «Supervisor_surname»
Director Wits Research Animal Facility (WRAF): Dr Kim Jardine

(Registered Veterinarian)

APPENDIX B

Please note that only typewritten applications will be accepted.

UNIVERSITY OF THE WITWATERSRAND

ANIMAL ETHICS SCREENING COMMITTEE
MODIFICATIONS AND EXTENSIONS TO EXPERIMENTS

a. Name: Simphiwe Mavuso
b. Department: Pharmacy and Pharmacology
c. Experiment to be modified / extended

	AESC NO		
Original AESC number	**2021**	**08**	**08C**
Other M&Es :			

d. Project Title: *In-vivo* study of an architecturally variant, 3D implantable toropoloidal device on New Zealand White Albino rabbits

		No.	Species
e.	Number and species of animals originally approved:	21	
f.	Number of additional animals previously allocated on M&Es:		
g.	Total number of animals allocated to the experiment to date:	21	
h.	Number of animals used to date:	3	

i. Specific modification / extension requested:
Request to add my colleague from pharmacy department Nombeko Sikhosana, student number 551945, Qualifications MSc. (Med). Honours BHSc, BSc (MCB)

j. Motivation for modification / extension:
To assist with the day-to-day procedures of my study.

Date: 08/11/2021

Signature: 

RECOMMENDATIONS
Addition of a co-worker (Nombeko Sikhosana, student number 551945). Condition: the co-worker has to attend the WRAF induction course.

Date:15/11/2021

Signature: 

Chairman, AESC

APPENDIX C

AESC 2012 M&E

Please note that only typewritten applications will be accepted.

UNIVERSITY OF THE WITWATERSRAND

ANIMAL ETHICS SCREENING COMMITTEE MODIFICATIONS AND EXTENSIONS TO EXPERIMENTS

a. Name: Simphiwe Mavuso
b. Department: Pharmacy and Pharmacology
C. Experiment to be modified / extended Department: Pharmacy and Pharmacology

	AESC NO		
Original AESC number	**2021**	**08**	**08C**
Other M&Es :			

d. Project Title: *In-vivo* study of an architecturally variant, 3D implantable toropoloidal device on New Zealand White Albino rabbits

		No.	Species
e.	Number and species of animals originally approved:	21	
f.	Number of additional animals previously allocated on M&Es:		
g.	Total number of animals allocated to the experiment to date:	21	
h.	Number of animals used to date:	3	

i. Specific modification / extension requested:

Change of implant position on the rabbits from anterior abdomen to dorsal (superior).
Change from nasal intubation to oral administration, where drug is mixed with pellets and group 3 rabbits will be fed the exact dose daily over the 28 day period of study. Animals will only be fed in the morning by researcher.

j. Motivation for modification / extension:

Rabbits were removing the implants on the anterior abdomen.
The nasal intubation procedure was too complex and was found to irritate the rabbit in the pilot study. Oral drug administration represents a simplified route of delivery.

Date: 08/11/2021 Signature: 

RECOMMENDATIONS

Approval for the change in implant position and route of drug administration as detailed above.

Date:10 November 2021 Signature:  Chairman, AESC

APPENDIX D

Please note that only typewritten applications will be accepted.

UNIVERSITY OF THE WITWATERSRAND

ANIMAL ETHICS SCREENING COMMITTEE
MODIFICATIONS AND EXTENSIONS TO EXPERIMENTS

a. Name: Simphiwe Mavuso
b. Department: Pharmacy and Pharmacology
c. Experiment to be modified / extended

	AESC NO		
Original AESC number	**2021**	**08**	**08C**
Other M&Es :			

d. Project Title: *In-vivo* study of an architecturally variant, 3D implantable toropoloidal device on New Zealand White Albino rabbits

	No.	**Species**
e. Number and species of animals originally approved:	21	
f. Number of additional animals previously allocated on M&Es:		
g. Total number of animals allocated to the experiment to date:	21	
h. Number of animals used to date:	3	

ii. Specific modification / extension requested:
To change title to: *In-vitro* study of architecturally variant, 3D implantable toro-poloidal device on New Zealand White Albino rabbits
To include New Zealand White female Albino rabbits

j. Motivation for modification / extension:
PhD title was changed with Faculty
There is currently a short supply of Male New Zealand White Albino rabbits, the study is not gender dependent, data should not be affected by gender of the animals.
To assist with the day-to-day procedures of my study.

Date: 08/11/2021

Signature: 

RECOMMENDATIONS
Addition of a co-worker (Nombeko Sikhosana, student number 551945). Condition: the co-worker has to attend the WRAF induction course.

Date:15/11/2021

Signature: 

Chairman, AESC

APPENDIX E

Simphiwe Mavuso, Thashree Marimuthu, Pradeep Kumar, Viness Pillay Yahya E. Choonara*
Wits Advanced Drug Delivery Platform Research Unit, Department of Pharmacy and Pharmacology, School of Therapeutic Science, Faculty of Health Sciences, University of the Witwatersrand, Johannesburg, South Africa**.**

Correspondence: Professor Yahya Choonara

Email Address: yahya.choonara@wits.ac.za

Tel: +27 11 717 2052

A Review on 3D Printed microstructures, their geometry and biological performance in drug delivery

Abstract: The use of three-dimensional printing (3DP) technology is increasing within various industries including the pharmaceutical industry where it is used to fabricate pharmaceuticals (drug delivery systems and other drug products) In pharmaceutics the main benefits of the 3DP technology are mostly generated from its unique manufacturing abilities, and these abilities enable time saving methods, good flexibility of the designs and personalized pharmaceutical products. Personalised medicine products are often dependent on the geometry of the product, which may be easily manipulated to suite individuals needs using the different 3DP technological methods.

The correlation of geometrical properties of various 3D printed products with their biological performances, wherein it has been envisaged that changing the geometry (shape) of a specific drug delivery system modifies drug release rates, and with the optimum shape a precise release profile could be premeditated for personalised medicine.

As 3D printing methods enable the fabrication of personalised medicine, this review focuses on the dependency 3D printed devices on the geometry for specific drug delivery system outcomes, which holds a great potential in the future perspective of 3D printing in the overall healthcare systems.

APPENDIX F

Simphiwe Mavuso, Thashree Marimuthu, Pradeep Kumar, Viness Pillay Yahya E. Choonara*

Wits Advanced Drug Delivery Platform Research Unit, Department of Pharmacy and Pharmacology, School of Therapeutic Science, Faculty of Health Sciences, University of the Witwatersrand, Johannesburg, South Africa**.**

Correspondence: Professor Yahya Choonara

Email Address: yahya.choonara@wits.ac.za

Tel: +27 11 717 2052

3D Toro-Poloidal Implantable Device for Controlled Delivery of Rivaroxaban

Abstract: This study demonstrates the correlation of the geometrical properties with its drug release profiles. The 3D implant formulated in this study will offer an alternative route that will bypasses the gut, be more convenient and safer for RXB delivery especially during long-term use, this device may be widely applied over a range of diseases requiring long-term use of a specific drug. In this study toro-poloidal, 3D devices were formulated to study their effects on drug release. The effect of drug release properties from the two geometrical 3D implants was investigated by comparing the release profiles of compressed donut, compressed cylinder, extruded donut and extruded cylinder.

Approximately 97% and 89 % RXB was released on day 49 for donut implants, while only 61.3 % and 66.1 % of the RXB was released from the cylinder, the release was from compressed and extruded 3D implants, respectively. These results show the obvious effect of geometry on 3D devices when it comes to it release properties, and to some extent also there was a slight difference in release with extruded and compressed devices.

APPENDIX G

Simphiwe Mavuso, Thashree Marimuthu, Pradeep Kumar, Viness Pillay Yahya E. Choonara*

Wits Advanced Drug Delivery Platform Research Unit, Department of Pharmacy and Pharmacology, School of Therapeutic Science, Faculty of Health Sciences, University of the Witwatersrand, Johannesburg, South Africa

Correspondence: Professor Yahya Choonara

Email Address: yahya.choonara@wits.ac.za

Tel: +27 11 717 2052

In-vivo study of a 3D toro-poloidal implantable device for the controlled delivery of rivaroxaban on New Zealand White Albino rabbits

Abstract

A rivaroxaban (RXB) 3D implantable toro-poloidal device was formulated utilising the functions of polyurethane (PU), poly (lactic-co-glycolic acid) (PLGA) polyethylene glycol (PEG), Hydroxypropyl methylcellulose (HPMC) polymers for controlled, sustained release profiles of RXB. The RXB loaded devices were evaluated by *in-vivo* studies over a period of 28 days using New Zealand White Albino rabbits. 3D implantable devices with sustained release profiles are the novel preferred drug delivery method as they conveniently implanted to efficiently release the drug for both systematic and local delivery in a controlled manner. This novel drug delivery devices may increase patient compliance and work well as personalised drug delivery systems, suitable for all kinds of diseases/drugs and patients. Using UV-Vis nanophotometer, the blood release of the RXB over 28 days was studied and analysed, histological analysis was also carried out. According to the release kinetics obtained the *in-vitro* and *in-vivo* RXB release profiles displayed consistent results suggesting that RXB release from the device was mainly affected by the composition and geometry of the device, hence the potential for use of device in personalised medicine as device could be manipulated during the development phase.

APPENDIX H

IDEXX LABORATORIES

UNIV. OF WITS MEDICAL SCHOOL
7 YORK STREET, 1ST FLOOR - ANIMAL UNIT
JOHANNESBURG
2050

2022/02/18 For attention: DR JARDINE

OUR REF: JB650455, MAVUSO, SIMPHIWE RABBIT 3D PRINTED IMPLANTABLE TOROPOILODAL DEVICE

SPECIMEN
Skin samples from 18 rabbits.

STUDY: *IN-VIVO* STUDY OF AN ARCHITECTURALLY VARIANT, 3D PRINTED, IMPLANTABLE TOROPOLOIDAL DEVICE ON NEW ZEALAND ALBINO RABBITS

HISTOLOGY

Day 1:

A (247):
The subcutis contains a large cystic space containing localised loose red blood cells admixed with fibrin. The cystic space is lined by a thin inflammatory layer containing a moderate number of intact heterophils and some fibrillar eosinophilic degenerate material (collagen/elastic fibres). Haemorrhage also extends into the surrounding subcutaneous connective and adipose tissue, accompanied by scattered small numbers of interstitial heterophils lymphocytes and plasma cells. Mild oedema is evident. There is a focal area of overlying epidermal ulceration and dermal necrosis extending to the subcutis.

B (559):
The cystic irregular space in the subcutis multifocally contains moderate amounts of loose red blood cells and scant fibrinous material. The cyst is lined by degenerate connective tissue fibres, mostly in situ collagen fibres, accompanied by few infiltrating heterophils. Few areas also show early calcification of the wall. Peripheral oedema and haemorrhage are moderate in the surrounding subcutis.

C (239):
No abnormalities in skin structure are visible and there are no signs of inflammation.

Day 7:

D (891):

The subcutaneous cystic space contains few epitheloid macrophages, single loose red blood cells and scant fibrillar material. The surrounding wall of the cyst consists of granulation tissue, consisting of haphazardly arranged or encircling fibroblast, accompanied by thin perpendicular capillaries. This pseudocyst capsule is moderately infiltrated by macrophages many of which appear foamy and some multinucleate cells. Single scattered lymphocytes and plasma cells are present. The involved muscle layer shows multifocal fibroplasia around muscle fibres and the surrounding subcutis is moderately oedematous.

E (776):

The cystic space contains luminal material consisting of loose red blood cells, fibrin deposition and degenerate leukocytes, mostly heterophils. Scant refractory crystalline structures are present embedded in the luminal material. Surrounding haphazard and mildly oedematous fibroplasia forms a capsule around the cyst and it is associated with small haphazard or perpendicular capillaries and peripherally oedema. Foamy macrophages are moderate in number within the wall accompanied by single scattered lymphoplasmacytic cells. The overlying epidermis is moderately hyperplastic with serocellular crusting on the skin surface. Superficial dermal fibrosis is irregular and vertical linear, and extends to the cyst.

F (836):

Normal histological appearance of the structures of the skin, including the subcutis. Inflammation is not visible.

14 days:

G (267):

The subcutaneous cystic space is small and does not clearly contain luminal material. The surrounding capsule is thick with haphazard to encircling fibrosis accompanied by perpendicular capillaries (granulation tissue). Few small aggregates of macrophages and multinucleate cells as well as odd heterophils are visible in the wall. Fibrosis also extends up to the dermoepidermal junction accompanied by areas of necrosis. Multifocal haemorrhage is evident adjacent to the cyst wall and few small aggregates of refractory foreign material are embedded in the capsule. The surrounding subcutis contains small amounts of macrophages lymphocytes and plasma cells.

H (469):

The cystic space contains few loose red blood cells, and is surrounded by moderate granulation tissue accompanied by moderate inflammation composed of foamy macrophages some multinucleate giant cells, as well as fewer lymphoplasmacytic cells and odd heterophils. Fibrosis extends from the capsular structure into the surrounding tissue and also to the dermoepidermal junction in a linear pattern. The overlying epidermis is hyperplastic.

I (853):

Normal histological appearance of the skin including epidermal dermal adnexal and subcutaneous structures and the cutaneous trunci muscle.

Day 28:

J (460):

Almost no cystic space remains in the subcutis and there is extensive surrounding mildly oedematous cell poor fibroplasia with haphazard collagen/elastic fibres accompanied by moderate aggregates of disseminate foamy macrophages and few heterophils. It does not form a capsule. This stromal reaction also extends through the overlying muscle layer into the superficial subcutis and it is associated with a linear area of fibrosis in the overlying dermis.

K (748):
The sample shows superficial subcutaneous haphazard fibroplasia that is poorly cellular and the fibroblasts are accompanied by collagen fibres. Beneath the cutaneous trunci muscle interstitial small numbers of foamy macrophages and few lymphocytes are present scattered throughout the oedematous stroma.

L (495):
The deep subcutis contains scattered small aggregates of foamy macrophages throughout the subcutis of the samples. Few multinucleate giant cells are present as well, and also single lymphocytes. Mild fibroplasia and oedema is also evident. The overlying muscle shows mild fibroplasia in the perimysium and a thin linear vertical band of fibrosis extends in the overlying dermis up to the dermoepidermal junction.

M (393):
A large expansile granuloma is present in the subcutis. It contains multiple small irregular cystic spaces interspersed by bands of granulomatous inflammation consisting of foamy macrophages many of which are multinucleate, as well as scattered single lymphocytes. Occasional peripheral encircling fibroblasts are present in small bundles. Few areas within the granuloma contain refractory foreign material encircled by multinucleate giant cells.

N (036):
The subcutis contains variable but mostly moderate granulomatous inflammation consisting of foamy macrophages and multinucleate giant cells. Occasional refractory foreign material are embedded in the subcutis and surrounded by small granulomasconsisting of similar foamy macrophages and multinucleate giant cells. More peripherally small numbers of macrophages heterophils and lymphoplasmacytic cells extend into the surrounding subcutis in an interstitial pattern with mild oedema. Mild collagen-rich fibroblastic tissue surrounds/encircles the inflammation.

O (849):
In this sample the discreet granuloma within the subcutis shows central eosinophilic fibrillar material filling a cyst lumen which is surrounded by multiple layers of foamy and epitheloid macrophages and multinucleate giant cells in which numerous refractory foreign material crystalline structures are embedded. Peripheral encircling fibrosis is mild to moderate and extends haphazardly and mildly into the surrounding subcutis. Mild oedema is also present in the surrounding tissue.

P (634):
The superficial dermis multifocally contains few interstitial and perivascular lymphoplasmacytic and heterophilic cells. The rest of the structures appear normal.

Q (827):
All skin structures appear normal, including the epidermis, dermis, adnexal structures, subcutis and cutaneous trunci muscle.

R (864):
Normal appearance of the skin structures.

COMMENT

All samples from the individuals in group 3 that did not have implant surgery yielded presence of normal skin structures as would be expected in a normal animal without invasive surgery (C, F, I, P, Q, R).

The 2 individuals' skins evaluated at day 1 show acute changes involving the surgically-induced subcutaneous pocket/cyst. These include haemorrhage with fibrin deposition and mild acute necrosis of traumatized tissues around/lining the pocket. Acute heterophilic infiltrates would be the first inflammatory cell type expected to invade at this point, and are mild to moderate only. The foreign material is not clearly evident.

After 7 days the cyst/pocket has developed early mild to moderate peripheral macrophage infiltration with granulomatous inflammation, and granulation tissue formation in the form of a capsular type structure. The lesion thus represents a pseudocyst. Macrophage infiltration would be indicative of an early foreign body reaction. There is not much difference between the reaction noted on day 7 between the 2 individuals in groups 1 and 2.

At 14 days the cystic space is reduced in size and devoid of exudate. Surrounding fibrosis, in the formation of granulation tissue (pseudocapsule) has become thicker than noted in earlier samples (moderate to severe). Inflammation is granulomatous and mild in G (group 1), while moderate in H (group 2). Few heterophils are still present in G. Foreign material is present in G, but not clearly in H.

The samples from day 28 in group 1 reveal absence of, or a very small remaining central space in samples J, K and L. The subcutis in these 3 samples contain varying degrees of interstitial presence of foamy macrophages, accompanied by small amounts of haphazard fibroblasts. A capsule is not visible. The subcutaneous tissue is also mildly oedematous and no foreign material is evident.

The samples from day 28 in group 2 show remaining cystic spaces (M and O) or no space (N), and they are surrounded by moderate to severe granulomatous inflammation which includes macrophages and multinucleate giant cells. The inflammation is associated with moderate to large amounts of refractory crystalline foreign material (3D printed device), unlike group 1 where foreign crystalline material is not visible histologically. The granulomas are surrounded by mild to moderate encircling fibrosis.

In group 1 the 28 day inflammation is milder in general, mostly consisting of a homogenous infiltrate of disseminate/interstitial macrophages without a cystic space or capsule and without foreign material. Inflammation and capsule formation with remaining cyst presence (except in N) are more prominent at 28 days in the individuals in group 2, thus a more notable foreign body reaction against the devices, and the foreign material (3D printed device) is also prominent in this group at 28 days.

Yours faithfully

Dr. Liza du Plessis
BVSc, Mmed Vet (Path)
Veterinary Anatomical Pathologist e-mail: liza-duplessis@idexx.com
Mob: +27(0)82 873 0193
Tel: +27(0)11 691 8200

2022/02/21 15:09:39

The link to the photos are:
https://drive.google.com/drive/folders/1uOE_Wzj4ZNitlmKwydxv6MlWu6CflJFo?usp=sharing

-

FINALISED LABORATORY REPORT version 1/1

Univ. of Wits Medical School
ACCOUNTS PAYABLE DEPARTMENT
WITS University
7 York Street, 1st Floor - Animal Unit
Johannesburg 2050
Telephone: 011 717 1300
Fax: 086 517 0742 Account: 223

Owner: MAVUSO, SIMPHIWE
Patient: 3D PRINTED IMPLANTABLE TOROPOILODAL DEVICE Gender:
Specie: Rabbit
Age: 0Y 0M 0W
Breed: NEW ZEALAND WHITE

Lab number: JB650455
Received: 19 January 2022
Printed: 21 February 2022
Referring vet: DR JARDINE
Your reference:

CLINICAL HISTORY:

Testname	Test value	Units	Flag	Range	Low Normal High
Sample	-				
Handling					
Histopathology Tumours & Skin Biopsies (max. 2 sites)					
Histopathology Tumours & Skin Biopsies - Additional (per 30min, minimum)				Sites (max. 2 sites) Photography	

LABORATORY OPERATIONS: Address: Idexx Laboratories (Pty) Ltd, 57 Forssman Close, Unit 8, Kyalami Village, Barbeque Downs, Johannesburg
Tel: (011) 691-8200 Option 2, Email: lab-sa@idexx.com

Disclaimer: Please note that we provide this report and relevant services in a professional manner and we warrant the accuracy of test results for the sample as submitted. Diagnosis (if any) is provided without warranty of any kind, either expressed or implied, including but not limited to, the accuracy of a diagnosis and the use of this diagnosis for any particular purpose. We expressly exclude warranties relating to merchantability or satisfactory quality, fitness for a particular purpose, care and skill. We do not assume, nor do we authorize any employee, agent or other person to assume for us, any other liability in connection with our services. And we accept no legal responsibility for the purposes for which you use our diagnosis, reports or other services.

Policy for allocation of pathology work: IDEXX
Laboratories currently employs multiple qualified pathologists, and it is the policy of the laboratory to allocate work on a non-selective basis to the next available pathologist to optimize workflow and ensure that turnaround times are met. As part of delivering a quality service, clients have the option to contact any IDEXX pathologist for additional clarification of results or comments